FEMTOSECOND FIBER LASERS AT 1550 NM FOR HIGH REPETITION RATES AND LOW TIMING JITTER

by

JONATHAN LEE MORSE

B.S. (Biological Systems Engineering)
University of Nebraska, Lincoln (2003)

M.S. (Biological Systems Engineering)
University of Nebraska, Lincoln (2005)

SUBMITTED TO THE DEPARTMENT OF ELECTRICAL ENGINEERING AND COMPUTER SCIENCE
IN PARTIAL FULFILLMENT OF THE REQUIREMENTS FOR THE DEGREE OF

DOCTOR OF PHILOSOPHY IN ELECTRICAL ENGINEERING
AT THE
MASSACHUSETTS INSTITUTE OF TECHNOLOGY

JUNE 2013

Signature of Author: _____
Department of Electrical Engineering and Computer Science
May 22, 2013

Certified by: _____
Erich P. Ippen
Elihu Thomson Professor of Electrical Engineering
Professor of Physics
Thesis Supervisor

Accepted by: _____
Leslie A. Kolodziejski
Professor of Electrical Engineering
Chairman, Department Committee on Graduate Students

Femtosecond Fiber Lasers at 1550 nm for High Repetition Rates and Low Timing Jitter

by

Jonathan Lee Morse

Submitted to the Department of Electrical Engineering and Computer Science
On May 22, 2013, in partial fulfillment of the requirements for the degree of
Doctor of Philosophy in Electrical Engineering

Abstract

Femtosecond fiber lasers have become an important enabling technology for advances in many areas including: frequency combs, precise timing distribution, optical arbitrary waveform generation, and high bit rate sampling for analog to digital conversion. Experiments and applications like these put demanding requirements on the source laser oscillator; such as operating near 1550 nm in wavelength, multi-gigahertz repetition rates, sub 100 femtosecond pulse widths, and sub 10 femtosecond timing jitters.

This thesis describes the design, fabrication, and characterization of three different iterations of mode-locked laser sources utilizing erbium doped fibers and semiconductor saturable absorbing mirrors to form pulse trains in the 1550 nm wavelength band. The first systems took advantage of a highly doped erbium fiber in a sigma cavity configuration to generate 100 fs pulses at up to a 300 MHz repetition rate through polarization additive pulse mode-locking. At the time, this was the highest fundamental repetition rate to be reported for a fiber cavity in a ring configuration.

The next two systems are variations on a linear cavity fiber laser design. In the first, the fiber coupling was achieved through free space optics and the saturable absorbing mirror was also imaged through lenses. Once mode-locked, repetition rates of just beyond 1 GHz were demonstrated with this design; however the laser output was relatively low power. The second version coupled the input and output light through fiber components and coupled the fiber directly to the saturable absorbing mirror. This laser mode-locked in several different states and a study to characterize and understand these states was undertaken.

Ultimately, it was understood which conditions minimized the cavity noise and pulse widths thus allowing for the achievement of a 1550 nm, 1 GHz, sub 10 fs jitter, femtosecond fiber laser. This laser is more compact than competing technologies and could be constructed with relatively low cost.

Thesis Supervisor: Erich P. Ippen

Title: Elihu Thomson Professor of Electrical Engineering and Computer Science, Professor of Physics

Acknowledgements

The journey to this point, the day one submits a Ph.D. thesis, is long and arduous. Yet, along the way so many wonderful things are learned and experiences had to make the adventure worth it. I find that writing this fills me with an interesting superposition of joy and sadness. One the one hand, my chapter as a student at MIT is closing and my first real employment is waiting for me to find it. On the other hand, my chapter as a student at MIT is closing, and all of the wonderful people and experiences that brought me will be in the past. Speaking of people, I'd like to acknowledge a few for being a part of my life and providing help and encouragement along the way:

The defining relationship of a Ph.D. program is the one you have with your thesis advisor. Professor Ippen is the best advisor one could hope for. His experimental and technical intuition is vast and impressive and his research guiding style encourages exploration and learning. Thank you for the freedom to fully experience all that MIT had to offer during my time learning about our applied fiber lasers and their applications.

Research collaborations and classes brought me in contact with many excellent Professors. Thank you to Prof. Franz Kärtner for always having time to talk, and an optimistic suggestion or two for how to proceed in the experiment. Thank you for being essentially a second advisor to me and for serving on my thesis committee. Thanks to Prof. Leslie Kolodziejski for not only providing our lasers with the excellent mirrors grown in your labs but also for your advice over the years and for serving on my RQE and Ph.D. thesis committees. Thank you to my academic advisors, Profs. Ronald Parker and Michael Watts, without which I wouldn't have been able to plan my courses and stay on track to successfully graduate.

Our work wouldn't be possible without an excellent support staff. Thank you to Donna Gale and Dorothy Fleischer for everything you do to keep the offices in line. Thanks to Dave Foss, Sukru Cinar, and Bill Adams for maintaining the computer and network resources. And thanks to Al McGurl and Bill Gibbs for keeping the lights on, the locks opening, and the air flowing.

Most of the things you learn in graduate school come from the graduate students around you. For them, I am very grateful. The students I have known through Prof. Ippen's group have been some of the smartest, nicest, funniest people I have ever come across and I owe a lot to them. They are not just colleagues to me, they are all life-long friends.

Jason Sickler taught me everything I know about optics research; and continues to be a good friend as we collaborate on new life projects. Marcus Dahlem was a wonderful officemate (twice) and is a truly great friend to have. His boundless enthusiasm for life is contagious and I miss my daily dose of Marcus. My other multiyear office mate—Ali Motamedi—is a hard working guy who taught me the importance of hockey and always thinking big. Dave Chao defined patience and the slow and steady approach to work. His stark contrast to my personality made our conversations very interesting. Michelle Sander showed me just how much work could get done if you (over)extend yourself and I like to

think that our team efforts on some lasers greatly helped both of us to our Ph.D.s. The only student I've been able to help mentor in the lab is my current officemate, Katia Shtyrkova. Katia's love for life and nonchalant way of dealing with every possible problem that comes up is a valuable reminder to me that life is all about your attitude towards it. I wish her the best and know she will achieve great success in her career.

Through the past years, I have interacted with many people in the OQE group that deserve mention and recognition. Jeff Chen worked with Jason and me on fiber lasers and he is a fun guy to be around. Hyunil Byun was a very hard worker who achieved much in the lab; his discoveries led directly to many of my measurements. Jaime Viegas only visited for one year but that was too little. He brought an energy to every situation that could not be duplicated. There are many others who made my work dynamic and interesting over the years: Milos Popovic, Peter Rakich, Noah Chang, Andrew Benedick, Jonathan Birge, Jonathan Cox, Yu Gu, Duo Li, Michael Peng, and everyone in the optics and quantum electronics group during the past eight years.

Thank you to our research collaborates, Dr. Gale Petrich, Orit Shamir, and Sheila Nabanja from Prof. Kolodziejski's group.

To my many fellow graduate student friends I made at MIT, thank you so much for being there for fun adventures, for keeping me sane, and for buoying me up when I was down. I could write a page for each of you but the list will have to do: Dave Dunmeyer, Vanessa Wood, Nicole Dilello, Tim Heidel, Jennifer Roberts, Bill Richoux, Brandon Pierquet, Robert and Brooke Pilawa, Pedro Pinto, Joel Abrahamson, Joe Sullivan, and many more.

To my close friends here in the Boston area, thank you for being so awesome. I could not have survived this program without you: Jeff Simpson, Andrew Freeman, Cathy Hoelsher, Eric Johnson, Robert Sprick, Junjay Tan, and many others who have come through my life the past eight years. Thank you and here's to continuing adventures.

To my peeps from the American Jiu Jitsu Club, thank you for providing such an exciting and supportive environment to learn and improve on my martial arts, presentation, and instructional skills. And thank you all for being supportive friends.

To my family, my parents Richard and Carol Morse and my sister Kristin and her husband Ben; thank you from all my heart for your kindness and support and love that got me to MIT and through MIT. I will continue to take all that you have given me and try to use it wisely for a bright and successful future.

To my wonderful, supportive, caring, amazing, talented, forgiving girlfriend, Katia. My darling; getting this thesis finished and presented on time could not have happened without you—you were always a beacon of light when I was down, your happy outlooks countered my pessimism, and your sacrifices of time and emotional stability for me are deeply appreciated. Thank you.

-Jonathan Lee Morse, May 22, 2013

Table of Contents

List of Figures

List of Tables

Abbreviations

Alphabetical list of abbreviations used in this thesis.

- APM — Additive Pulse Mode-locking
- CW — Continuous Wave
- Er — Erbium
- FWHM — Full Width at Half Maximum
- GVD — Group Velocity Dispersion
- InGaAs — Indium Gallium Arsenide
- OSA — Optical Spectrum Analyzer
- P-APM — Polarization Additive Pulse Mode-locking
- PBS — Polarizing Beam Splitter
- PMT — Photomultiplier Tube
- RF — Radio Frequency
- SBR — Saturable Bragg Reflector
- SSA — Signal Source Analyzer
- SESAM — Semiconductor Saturable Absorber
- WDM — Wavelength Division Multiplexer

Chapter 1 Introduction

1.1 Mode-locked Fiber Lasers

Since the initial development of the laser over fifty years ago [1], [2], researchers have continued to push the technology to the physical limits of optical power, pulse energy, and pulse duration. Pulsed lasers were developed that initially took advantage of active [3] and passive [4], [5] Q-switching and eventually active [6] and passive [7], [8] mode-locking techniques to create extremely regularly spaced pulses trains at ever decreasing pulse widths [9], [10], [11]. The introduction of the erbium doped optical fiber [12], [13] brought these advances to the telecommunications wavelengths around 1550 nm. A variety of mode-locking mechanisms have been discovered and implemented in erbium doped fiber lasers that lead up to the systems described in this thesis.

One development to take advantage of creating erbium doped fiber lasers was the concept of the soliton laser [14]. This theory postulates a careful balance of the cavity dispersion and nonlinearity such that the pulse settles into a soliton wave and remains there while propagating through the laser medium [15]. The implications of this strong pulse shaping are, given enough energy, femtosecond duration pulse widths with extremely low pulse-to-pulse timing jitters.

Other outcomes are possible given the strong dispersion and nonlinearities available within a mode-locked fiber laser—such as stretched pulse lasers taking advantage of additive pulse mode-locking (APM) [16] and polarization additive pulse mode-locking [17], [18]. These techniques use the Kerr nonlinearities of the optical fiber to affect pulses differently depending on the instantaneous optical intensity. These lasers are also capable of generating short, femtosecond optical pulses but at relatively low repetition rates [19].

1.2 Motivating Applications

In recent years, the repetition rates of some erbium doped fiber lasers have been continuing to increase from 500 MHz [20], to 1 GHz [21], to 3 GHz [22] and the technological hurdles to maximize gain and minimize coupling losses are being overcome to stabilize and integrate these types of femtosecond laser sources into a system for a veriety of experimental uses.

Fiber lasers producing femtosecond pulses have also found use in many fields of basic research and are beginning to make an impact commercially. Specifically, ultrafast lasers operating near the telecommunications band (1550 nm wavelength) are important sources for high speed optical communications, frequency metrology [23], time resolved spectroscopy [24], optical arbitrary waveform generation [25], optical analog-to-digital conversion [26], frequency combs [27], [28], and other applications where an ultrafast time scale or a very stable frequency standard is needed.

In general, the above applications all demand short (100 femtoseconds or less), powerful pulses (tens of picojoules) at the fastest possible repetition rates (over 1 gigahertz) with close to zero pulse-to-pulse timing jitter. The goal of this work is to continue the development of optical sources at telecommunication wavelengths that meet these stringent requirements.

1.3 Thesis Organization

This thesis is arranged in the following manner to further explain important background information before presenting an evolution of erbium doped fiber lasers that increase in repetition rate while maintaining femtosecond regime pulses with tens of femtoseconds or less of timing jitter.

- **Chapter 2 – Background Principles**

  Mode-locking is defined and two mode-locking methods are explained. Advanced experimental techniques used to collect or analyze data in the subsequent experiments are broken down and explained.

- **Chapter 3 – High Repetition Rate, High Average Power, Femtosecond Erbium Fiber Sigma Lasers**

  A modification to the P-APM fiber laser is introduced and physically scaled to 300 MHz repetition rate.

- **Chapter 4 – 1 GHz Linear Cavity Laser – Free Space SBR**

  A 1 GHz repetition rate mode-locked fiber laser with a free space collimated beam section is detailed and used to conduct a comprehensive SBR performance study. Other cavity variations are explored to answer questions raised by the results of the first study.

- **Chapter 5 – 1 GHz Linear Cavity Laser – End Abutted SBR**

  Three distinct mode-locking states of a 1 GHz repetition rate mode-locked fiber laser with an end-abutted SBR are investigated and an understanding of the optimum operating conditions for a high repetition rate, low jitter, femtosecond fiber laser begins to emerge.

- **Chapter 6 – Conclusions and Future Work**

  The conclusions learned from three distinct generations of fiber laser designs are detailed and some promising directions for furthering this technology are discussed.

Bibliography - Chapter 1

[1] A. L. Schawlow and C. H. Townes, "Infrared and optical masers," *Physical Review*, vol. 112, no. 6, pp. 1940–1949, Dec. 1958.

[2] I. H. Maiman, "Stimulated optical radiation in ruby," *Nature*, vol. 187, pp. 493–494, Aug. 1960.

[3] F. J. McClung and R. W. Hellwarth, "Giant optical pulsations from ruby," *Journal of Applied Physics*, vol. 33, no. 3, pp. 828–829, 1962.

[4] P. Kafalas, J. I. Masters, and E. M. E. Murray, "Photosensitive liquid used as a nondestructive passive Q-switch in a ruby laser," *Journal of Applied Physics*, vol. 35, no. 8, pp. 2349–2350, Aug. 1964.

[5] G. Bret and F. Gires, "Giant-pulse laser and light amplifier using variable transmission coefficient glasses as light switches," *Applied Physics Letters*, vol. 4, no. 10, pp. 175–176, 1964.

[6] R. L. Fork, L. E. Hargrove, and M. A. Pollack, "Locking of He-Ne laser modes induced by synchronous intracavity modulation," *Applied Physics Letters*, vol. 5, no. 1, pp. 4–5, Jul. 1964.

[7] H. W. Mocker and R. J. Collins, "Mode competition and self-locking effects in a Q-switched ruby laser," *Applied Physics Letters*, vol. 7, no. 10, pp. 270–273, Nov. 1965.

[8] A. J. De Maria, D. A. Stetser, and H. Heynau, "Self mode-locking of lasers with saturable absorbers," *Applied Physics Letters*, vol. 8, no. 7, pp. 174–176, Apr. 1966.

[9] A. Dienes, E. P. Ippen, and C. V. Shank, "A mode-locked cw dye laser," *Applied Physics Letters*, vol. 19, no. 8, pp. 258–60, Oct. 1971.

[10] C. V. Shank, E. P. Ippen, and A. Dienes, "Passive mode locking of the CW dye laser," in *1972 international quantum electronics conference, digest of technical papers. (abstracts only), 8-11 May 1972*, 1972, vol. QE-8, p. 525.

[11] C. V. Shank and E. P. Ippen, "Sub-picosecond kilowatt pulses from a mode-locked c.w. dye laser," *Applied Physics Letters*, vol. 24, no. 8, pp. 373–5, Apr. 1974.

[12] R. J. Mears, L. Reekie, S. B. Poole, and D. N. Payne, "Low-threshold tunable CW and Q-switched fibre laser operating at 1.55 m," *Electronics Letters*, vol. 22, no. 3, pp. 159–60, Jan. 1986.

[13] A. Astakhov, M. Butusov, S. Galkin, N. Ermakova, and Y. Fedorov, "Fiber Laser with 1.54 Mu-M Radiation Wavelength," *Opt. Spektrosk.*, vol. 62, no. 1, pp. 230–232, Jan. 1987.

[14] L. F. Mollenauer and R. H. Stolen, "The soliton laser," *Optics Letters*, vol. 9, no. 1, pp. 13–15, Jan. 1984.

[15] H. A. Haus, "Theory of Mode Locking With A Fast Saturable Absorber.," *Journal of Applied Physics*, vol. 46, no. 7, pp. 3049–3058, 1975.

[16] H. A. Haus, E. P. Ippen, and K. Tamura, "Additive-pulse modelocking in fiber lasers," *IEEE Journal of Quantum Electronics*, vol. 30, no. 1, pp. 200–8, 1994.

[17] H. A. Haus, K. Tamura, L. E. Nelson, and E. P. Ippen, "Stretched-pulse additive pulse mode-locking in fiber ring lasers: theory and experiment," *IEEE Journal of Quantum Electronics*, vol. 31, no. 3, pp. 591–8, 1995.

[18] K. Tamura, H. A. Haus, and E. P. Ippen, "Self-Starting Additive Pulse Mode-Locked Erbium Fiber Ring Laser," *Electronics Letters*, vol. 28, no. 24, pp. 2226–2228, 1992.

[19] K. Tamura, E. P. Ippen, H. A. Haus, and L. E. Nelson, "77-Fs Pulse Generation from a Stretched-Pulse Mode-Locked All-Fiber Ring Laser," *Opt Lett Opt Lett*, vol. 18, no. 13, pp. 1080–1082, 1993.

[20] H. Byun, D. Pudo, J. Chen, E. P. Ippen, and F. X. Kartner, "High-repetition-rate, 491 MHz, femtosecond fiber laser with low timing jitter," *Opt. Lett.*, vol. 33, no. 19, pp. 2221–2223, 2008.

[21] H. Byun, M. Y. Sander, A. Motamedi, H. Shen, G. S. Petrich, L. A. Kolodziejski, E. P. Ippen, and F. X. Kartner, "Compact, stable 1 GHz femtosecond Er-doped fiber lasers," *Applied Optics*, vol. 49, no. 29, pp. 5577–5582, 2010.

[22] J. Chen, J. Sickler, E. Ippen, and F. Kaertner, "Fundamentally Mode-locked 3 GHz Femtosecond Erbium Fiber Laser," in *Ultrafast Phenomena XVI, Proceedings of the 16th International Conference, Palazzo dei Congressi Stresa, Italy, June 9--13, 2008*, 2008, pp. 727–729.

[23] S. Cundiff, J. Ye, and J. Hall, "Time meets frequency: Phase stabilization of ultrafast pulses and optical frequency metrology with modelocked lasers," in in *Leos 2001: 14th Annual Meeting of the Ieee Lasers & Electro-Optics Society, Vols 1 and 2, Proceedings*, New York: Ieee, 2001, pp. 903–903.

[24] T. Q. Ye, C. J. Arnold, D. I. Pattison, C. L. Anderton, D. Dukic, R. N. Perutz, R. E. Hester, and J. N. Moore, "Development of an ultrafast laser apparatus for time-

resolved UV-visible and infrared spectroscopy," *Applied Spectroscopy*, vol. 50, no. 5, pp. 597–607, 1996.

[25] E. Ippen, A. Benedick, J. Birge, H. Byun, L. J. Chen, G. Chang, D. Chao, J. Morse, A. Motamedi, M. Sander, and others, "Optical arbitrary waveform generation," in *Lasers and Electro-Optics (CLEO) and Quantum Electronics and Laser Science Conference (QELS), 2010 Conference on*, 2010, pp. 1–2.

[26] X. B. Hou, A. Daryoush, and W. Rosen, "Design of an ultra high-speed all-optical analog-to-digital converter," *Proceedings of the Ieee 2004 Radar Conference*, pp. 520–523, 2004.

[27] G. Overton, "Frequency combs - Optical arbitrary-waveform-generation technique shapes more than 100 spectral lines," *Laser Focus World*, vol. 43, p. 31–+, 2007.

[28] D. Chao, M. Y. Sander, G. Chang, J. L. Morse, J. A. Cox, G. S. Petrich, L. A. Kolodziejski, F. X. Kärtner, and E. P. Ippen, "Self-referenced Erbium fiber laser frequency comb at a GHz repetition rate," in *2012 Optical Fiber Communication Conference and Exposition and the National Fiber Optic Engineers Conference, OFC/NFOEC 2012, March 4, 2012 - March 8, 2012*, 2012.

Chapter 2 Background Principles

2.1 Introduction

This chapter includes definitions and explanations of theory and measurement techniques helpful to understand the results presented in Chapters 3, 4, and 5. Mode-locking mechanisms used in this thesis work are introduced. Next, the measurement techniques to acquire data on pulse widths and timing jitter are detailed. Once the pulse widths are measured, those numbers are compared with the expected output including the influence of fiber propagation between the laser and the measurement apparatus as determined by a split step time domain pulse propagation simulation. That technique and assumptions used in the output modeling are also explained here in Chapter 2. Finally, the concept of a vector soliton and the resulting modulation it places on the RF spectrum is demonstrated along with the recommended methods of eliminating it.

2.2 Mode-Locking

Chapter 1 mentioned a few applications for mode-locked lasers, but what exactly is a mode-locked laser? This section provides a high level overview of the topic and leaves further explanation to the copious available references on the topic [1], [2], [3], [4]. The purpose of this section is to introduce the reader to the specific mode-locking techniques applied to the lasers constructed and characterized in this thesis.

2.2.1 Laser Cavity Modes

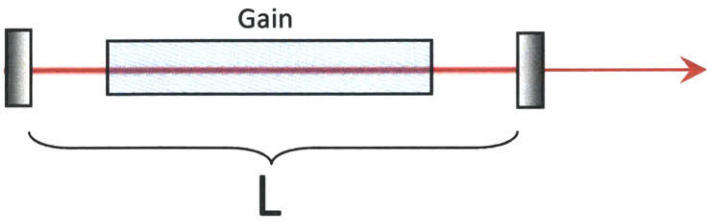

Figure 2-1 Basic laser cavity block model.

Assume a simple block model for a laser cavity: an optical gain medium placed between two parallel mirrors--like the diagram in Figure 2-1. Now consider what electromagnetic theory states about fields that may exist in the cavity. The primary constraint is that the electric field return to the same value in a round-trip so modes that may oscillate must have a frequency as defined in Equation 2-1.

$$f_m = \frac{m * c}{2 * L} \qquad \textbf{Equation 2-1}$$

Which means that the frequency of any allowed cavity mode is the number of optical cycles (m) times the speed of light (c) divided by one cavity round trip (2 times the optical length L because it is a linear cavity). Two of infinitely many possible modes are sketched in Figure 2-2.

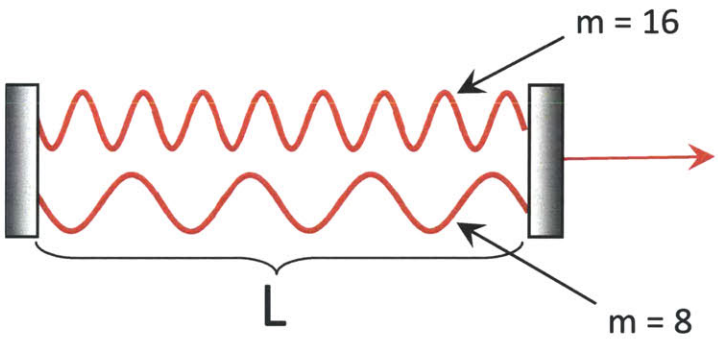

Figure 2-2 Diagram of two possible cavity modes. (Original figure courtesy of Jason Sickler)

The feedback constraints that keep an infinite number of modes from acquiring energy and rising out of the continuum are the frequency bandwidths of the mirrors and the gain medium. These two factors contribute high loss to frequencies outside the pass-bands and thus only a finite number of modes are preferred and will compete to absorb all of the energy the gain medium provides. These conditions describe the frequencies of the electric fields but say nothing about the phase.

For the simple block diagram of Figure 2-1, there is no element in the cavity to control the phase of the excited modes. If by some method the phases of the sinusoidal oscillations of each mode were synchronized correctly in time the superposition of those modes would form pulses. According to Fourier theory, the more sinusoidal frequencies available to sum together, the shorter the pulses will become. Finally, with the correct synchronization (i.e. mode-locking) the pulse will travel back and forth in the cavity.

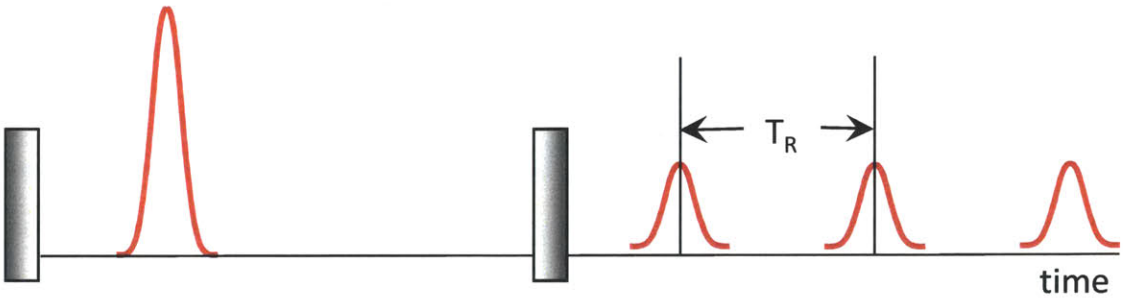

Figure 2-3 Sketch of a single intracavity pulse and the output pulse train (not to scale).

Figure 2-3 illustrates the output of a linear laser cavity with one intracavity pulse. At each reflection from the partially transmitting end mirror a fraction of the energy exits the cavity in the form of an output pulse. The periodicity of the output pulse train is determined by the group velocity of the pulse in the cavity and the length of the cavity and defines the repetition rate ($1/T_R$) of the laser.

2.2.2 Mode-Locking Mechanisms

The previous section described an overview of the formation of pulses from a simple two mirror laser cavity. The key element was control over the phase of each lasing cavity mode. However, it did not explain how those phases were synchronized. This section mentions several methods of aligning the phase of the lasing cavity modes—also known as mode-locking.

2.2.2.1 *Active Modelocking*

One straightforward way to force the phases of all the cavity modes together is to periodically introduce high loss in the cavity through some physical means like an optical chopper or an electro optic modulator. This is known as active mode-locking and the technique is widely used to generate pulses [5], [6], [7], [8], [9], [10]. However, active modelocking has limitations that typically restrict the shortest pulses to the picosecond regime.

It has the additional drawback of requiring bulky and complicated feedback electronics to synchronize the pulse modulation with the cavity repetition rate to generate a consistent pulse train. These locking electronics have good timing jitter performance at lower frequencies but beyond about 1 MHz they begin to introduce more noise to the pulse timing than a free running ultrafast optical oscillator. Therefore in the pursuit of high repetition rate, low jitter, femtosecond laser sources active modelocking is not a viable approach.

2.2.2.2 *Passive Modelocking via Saturable Absorption*

The idea behind mode-locking is using a temporal "gate" to add more loss to low intensity fields between pulses than to the higher intensity pulses themselves. The method we are interested in uses the optical pulse itself as the trigger of that "gate," and is able to produce pulses below 10 fs in duration [11]. The term given to this "self-gating" is passive mode-locking [12] and it is enabled by optical saturation of an absorption process within the cavity. This "saturable absorber" may be a real absorbing element or a result of optical interactions within a transparent nonlinear medium. Two variations of saturable absorbers are utilized in the lasers of this thesis and briefly described below.

2.2.2.2.1 Semiconductor Saturable Absorber

One example of a so-called "real" saturable absorber is a semiconductor material engineered to have quantum well absorption around the central wavelength the laser's gain medium. If deposited on a reflecting mirror this combination is known as a semiconductor

saturable absorber mirror (SESAM) [13]. If the mirror is formed of alternating high and low index of refraction layers of approximately ¼ wavelength thickness, it is known as a saturable Bragg reflector (SBR). As an example of an SBR structure, Figure 2-4 shows a schematic of the MIT VA86 SBR mirror stack and absorber with a protective pump reflecting coating deposited.

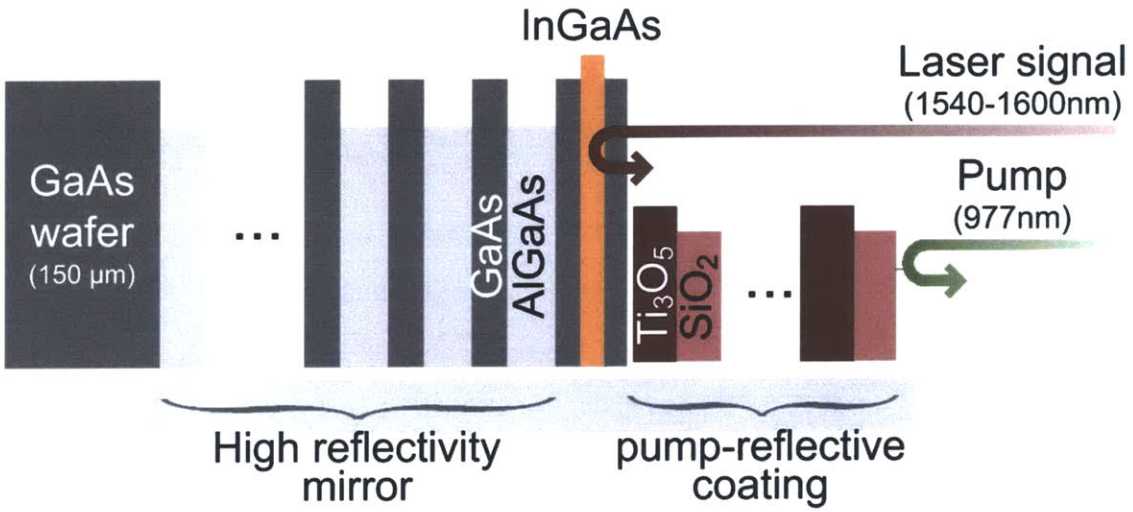

Figure 2-4 Side view schematic of the MIT VA86 SBR with pump reflection coating applied. (Figure courtesy of Michelle Sander)

SBR's have become a staple technology in the ultrafast laser field [13], [14], [15], [16], [17], [18], [19], [20], [21] and there are large parts of Ph.D. theses [22], [23] dedicated to their design and fabrication. Though an entire chapter on the SBR's used in the lasers of this thesis could be written, it is unnecessary and redundant to the explanations available in Hanfei Shen's [23], Hyunil Byun's [24], and Michelle Sander's [25] theses. The mirror specifications, designs, and fabrications for the MIT VA series are found in detail there. They are brought up in this chapter because SBR's play a critical part in the operation of the fiber lasers of this thesis and their origin and function needs to be addressed before the lasers can be introduced and explained.

The single quantum well SBR, such as the VA86 in Figure 2-4, functions as an intensity dependent optical window. When light with intensity below the saturation fluence

of the indium gallium arsenide (InGaAs) layer is incident, it is mostly absorbed. However, as the intensity increases (as for a forming pulse) then the InGaAs layer will optically "bleach" and allow the light to pass through where it will reflect off the mirror stack and stay in the cavity for further amplification by the gain medium.

As long as the InGaAs recovery time (nominally between 2 ps and 12 ps) is shorter than the time it takes the pulse to make one round trip (approximately 1 ns for a 1 GHz fiber cavity) the mirror is able to act as a repetitive intensity dependent loss mechanism which acts to keep the lasing cavity modes in phase. The SBR's characteristics such as linear loss and modulation depth play a significant role in maintaining pulsed operation and those effects are studied in detail in Chapters 3 and 4.

2.2.2.2.2 Polarization Additive Pulse Modelocking

One example of a so-called "artificial" saturable absorbing mechanism is polarization additive pulse mode-locking (P-APM) [26], [27], [28], [29], [30], [31]. This is a variation on additive pulse mode-locking (APM) where the nonlinearity affects the polarization of the pulse in an intensity dependent manner. The definitive description of this process is given in reference [32], but because the lasers in Chapter 3 utilize this technique it is summarized below.

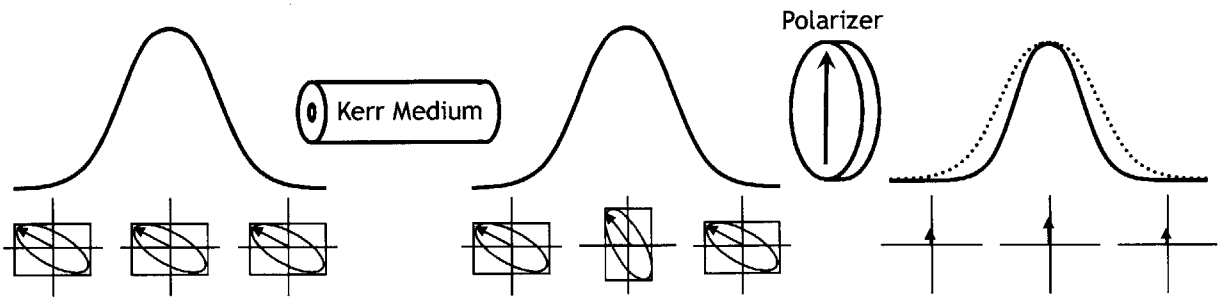

Figure 2-5 Temporal polarization evolution of the pulse when passing through a Kerr medium and a linear polarizer. The pulse peak is left unattenuated but the wings are reduced in amplitude—shortening the pulse. (Figure courtesy of Jason Sickler)

As illustrated by Figure 2-5, an optical pulse propagates through a Kerr medium, in this case an optical fiber. The state of the polarization of the pulse changes along the time

axis depending on its instantaneous power. If the pulse is intense enough, the nonlinear interactions with the glass will cause the polarization of the peak of the pulse to slightly rotate from the original polarization still propagating in the wings. Aligning a linear polarizer in the cavity after the fiber that aligns optimally with the polarization in the peak of the pulse will act as an amplitude filter on the wings and effectively shorten the pulse. The lost energy is regained in the next trip through the amplifying gain fiber.

This type of saturable absorption is instantaneous and has no relaxation time. However, its effects are small and require hundreds or thousands of round trips in the fiber to reach a steady state pulse width where the P-AMP effects are balancing the cavity's losses, gain, self-phase modulation, and dispersion effects. These effects are reduced when the fiber length is shortened, and the laser may be unable to self-start in such a state. One way to address this is to integrate another kind of saturable absorption that would seed the P-AMP pulse formation. The idea of combining a SBR into a P-APM mode-locked fiber laser is the topic of Chapter 3.

2.3 Measurement Techniques

For many of the laboratory measurement results presented in this thesis the procedure for collecting the data is straightforward. In the case of an output power reading, an optical spectrum recording, or a RF spectrum trace the signal light is directed into a detector or a fiber input port on the instrument and the data is recorded. Data processing occurs in software (adjustments like centering, normalization, and noise filtering) and the plotted results are available as figures in the thesis.

For some measurements, however, the information sought is not straightforward to obtain and an advanced instrument or procedure is necessary. This section details the theory and explains the procedure for the intensity autocorrelation, the phase-noise to timing-jitter conversion, the soliton theory pulse width model, and the split step time domain numerical simulation techniques.

2.3.1 Autocorrelation

To measure the time domain width of an optical pulse, physical principles require you to have a reference that is shorter than that pulse. What if that pulse is shorter than any available electrical reference source? One option is to use the pulse itself as a reference to determine how short it is. A technique to do just that was first developed in 1967 [33] and is known by the term "background free intensity autocorrelation". This thesis refers to it as autocorrelation, for brevity. Autocorrelation has become a standard pulse width measurement technique and detailed descriptions may be found in the standard textbooks on nonlinear and ultrafast optics [34], [1], so I will only briefly touch on it here. Figure 2-6 is a schematic of the measurement borrowed from Professor Kärtner's 2008 Ultrafast Optics class notes [2] that illustrates the process well enough for the purposes of this explanation.

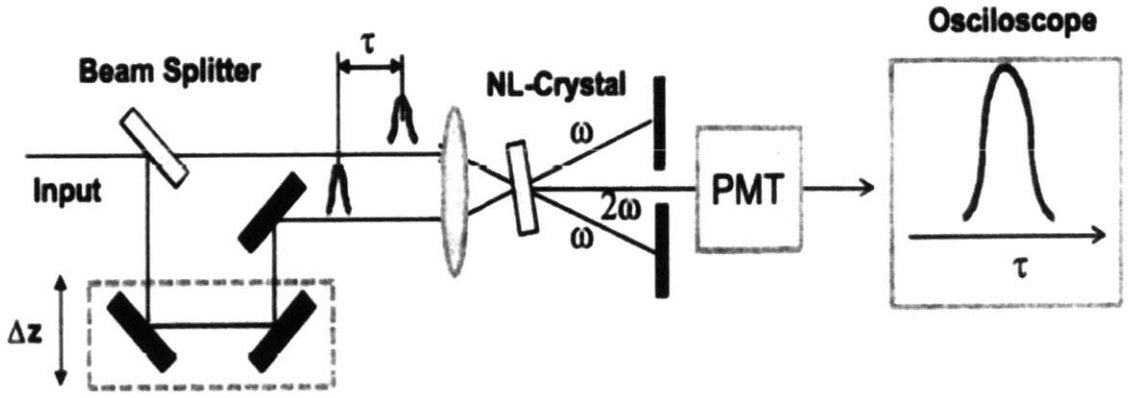

Figure 2-6 Basic schematic of an autocorrelation measurement. (adapted from Figure 9.1 in [2])

The concept behind the measurement is not complex—take the optical pulse you want to measure and split it into two copies. Design one beam path to be fixed and the other to be variable in length. Cross the beam paths of these two pulses together in a nonlinear medium where second harmonic frequency generation will occur. Position a detector sensitive to this higher frequency in the path so that only the light resulting from the momentum conserving nonlinear interaction of the two beams will propagate. Thus, the two input pulses and any second harmonic light they individually self-generate will be blocked

by the iris and only light generated by their interaction will be recorded. As the variable beam path is altered in length, the electrical signal output by the detector (photomultiplier tube (PMT) in this case) will rise and fall proportional to the overlap of the pulses in the nonlinear medium.

The measurements reported in this thesis use this technique to record autocorrelation traces with a small addition. To reduce the noise floor of the measurement, an optical chopper synchronized to a lock-in amplifier was used for the PMT signal measurement. The chopper was placed in the path of the variable path length beam which was of lower intensity than the other beam. This enabled autocorrelations to be taken down to 35 dB below the peak.

Once the output of the PMT is recorded and plotted a pulse-shaped image displays on the screen. This autocorrelation pulse is not the same width as the original input pulse to the beam splitter however. It must be deconvolved to account for the fact that this is an optical pulse convolved with itself. Mathematically that is a solved problem for both Gaussian and sech pulse shapes with the formulas below.

2.3.1.1 Gaussian pulse shape

For a Gaussian pulse, if the input pulse is assumed to be Equation 2-2, the autocorrelation is the Gaussian of Equation 2-3.

$$I(t) = exp\left[-\left(\frac{2\sqrt{\ln 2} * t}{\Delta\tau_p^{FWHM}}\right)^2\right] \qquad \textbf{Equation 2-2}$$

$$A^2(\tau) = exp\left[-\left(\frac{2\sqrt{\ln 2} * \tau}{\Delta\tau_A^{FWHM}}\right)^2\right] \qquad \textbf{Equation 2-3}$$

$$\Delta\tau_p^{FWHM} = \frac{\Delta\tau_A^{FWHM}}{1.41} \qquad \textbf{Equation 2-4}$$

Equation 2-4 is the relationship between the full width at half maximum pulse width for a Gaussian pulse shape. Practically, this means that the pulse width of the autocorrelation pulse (which is measured) is divided by the factor of 1.41 to obtain the width of the original input pulse.

2.3.1.2 Sech pulse shape

The same operation can be done for a sech pulse; if the input pulse is assumed to be Equation 2-5, the autocorrelation of that pulse is shown in Equation 2-6.

$$I(t) = sech^2\left[\frac{1.7627 * t}{\Delta\tau_p^{FWHM}}\right] \qquad \textbf{Equation 2-5}$$

$$A^2(\tau) = \frac{3}{sinh^2\left[\frac{2.7196 * \tau}{\Delta\tau_A^{FWHM}}\right]}\left[\frac{2.7196 * \tau}{\Delta\tau_A^{FWHM}} * coth\left(\frac{2.7196 * \tau}{\Delta\tau_A^{FWHM}}\right) - 1\right] \qquad \textbf{Equation 2-6}$$

$$\Delta\tau_p^{FWHM} = \frac{\Delta\tau_A^{FWHM}}{1.54} \qquad \textbf{Equation 2-7}$$

Equation 2-7 is the relationship between the full width at half maximum pulse width for a sech pulse shape. Practically, this means that the pulse width of the autocorrelation pulse (which is measured) is divided by the factor of 1.54 to obtain the width of the original input pulse.

2.3.2 Phase Noise and Timing Jitter

An important characteristic of femtosecond lasers is their capability of supporting very low pulse-to-pulse timing drift—also known as timing jitter. Therefore, it is useful to have a measurement method for characterizing the timing jitter of a laser oscillator. One method to calculate jitter is to directly measure the phase noise of the laser output signal. This is done by mixing the electrical signal from a biased photodetector with a very stable electronic oscillator. Jitter is obtained by integrating that phase noise from the highest

frequency of interest down to the frequency below which you could remove any noise through detection and correction techniques.

For the timing jitter measurement the technique is to isolate one of the harmonics in the RF domain, amplify and filter it, then feed that signal into a Signal Source Analyzer[1] to obtain the phase noise, $S\varphi$ over a wide range of frequencies ($f_{max} - f_{min}$). Figure 2-7 diagrams the measurement procedure in the lab.

Figure 2-7 Schematic of phase noise measurement. The tuning of the RF filter can be changed to any desired frequency by choosing the proper filter.

In an example measurement from the 1560 nm state of the linear cavity end abutted laser (Chapter 5), the fundamental harmonic – 1.0367 GHz – from the detected RF signal was isolated by a tunable bandpass filter[2] tuned to 1.04 GHz (analog dial) and passed through a RF amplifier[3] before being passed to the signal source analyzer. The SSA does several steps but basically mixes the incoming signal with a very low noise local electrical oscillator and records the output through a range of frequencies. This can then be displayed as a plot of phase noise as a function of frequency. Figure 2-8 is a captured screen shot of the SSA after saving the data trace.

---

[1] Agilent, Model: E5052A

[2] Telonic Industries Inc., Tunable bandpass filter Model TTF 1550-5-5EE

[3] Mini Circuits, Model 2KL-2 RF amplifier

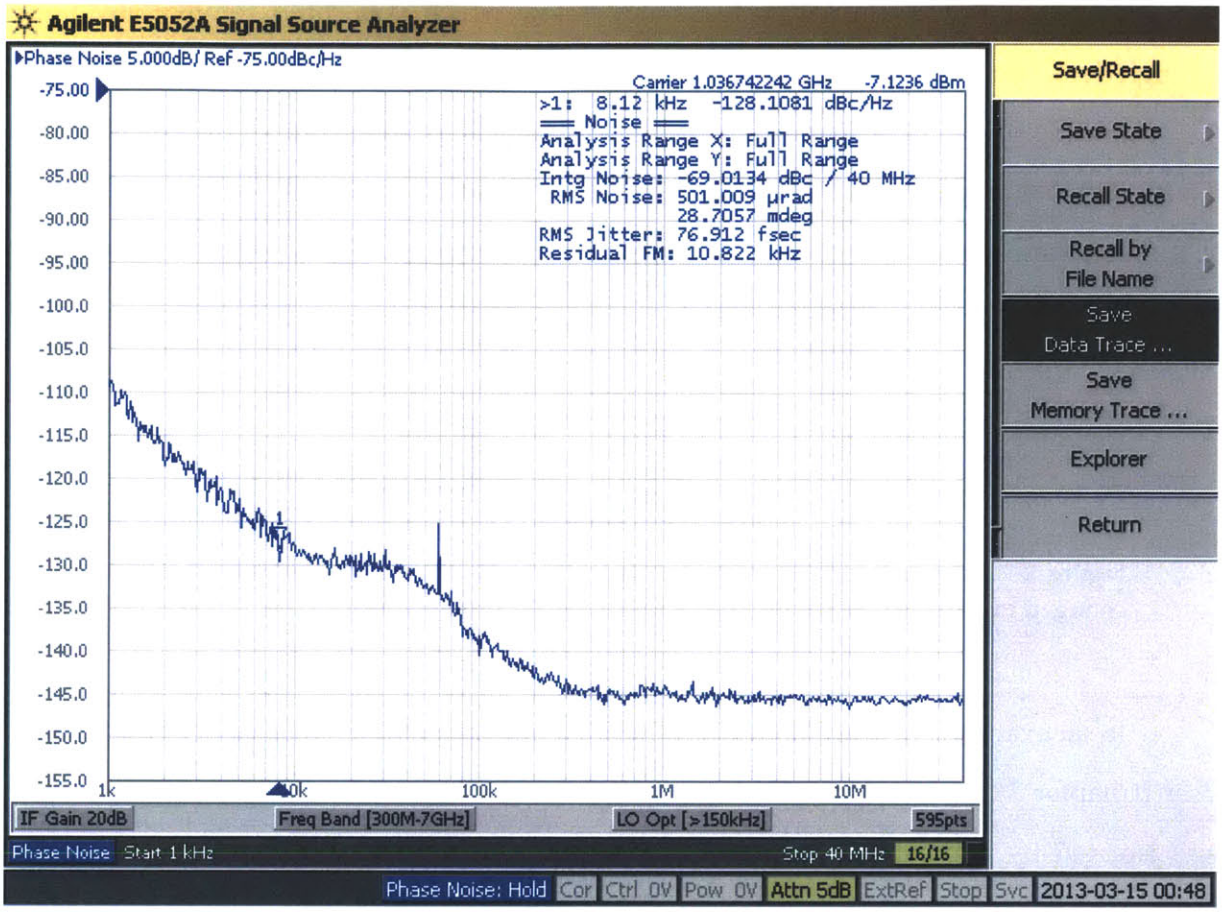

Figure 2-8 Sample screenshot of the Agilent E5052A Signal Source Analyzer.

This phase noise can be integrated and scaled according to Equation 2-8 [2].

$$\Delta t = \frac{1}{2\pi * f_R}\sqrt{2\int_{f_{min}}^{f_{max}} S_\varphi \, df} \qquad \textbf{Equation 2-8}$$

The timing jitter, Δt, is obtained by integrating the phase noise from f_{min} to f_{max} and factoring in the laser repetition rate, f_R. For the data shown in Figure 2-8, f_{min} was chosen to be 1 KHz because noise sources below that frequency can be corrected for though local reference sources, feedback electronics, and piezoelectric cavity mirrors for example. f_{max} was chosen to be the point where the downward trending line meets the noises floor of the measurement. For the example data, that frequency was chosen to be 1 MHz. Once the

calculations of Equation 2-8 are carried out and plotted together with the phase noise we obtain Figure 2-9.

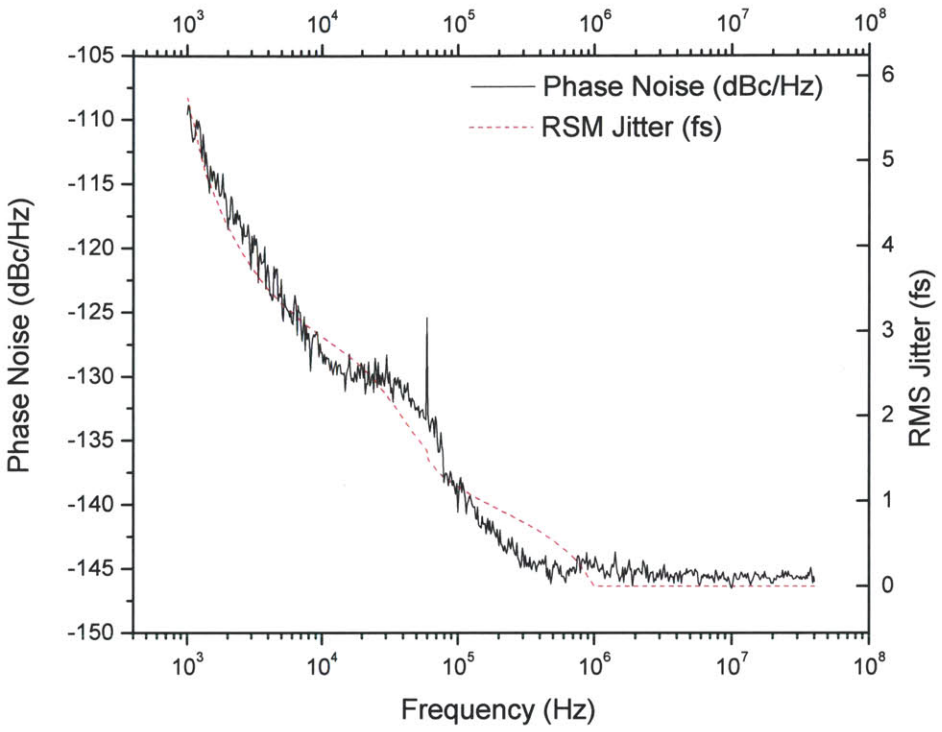

Figure 2-9 Phase noise and integrated timing jitter for the sample dataset.

The final number to report is the value of the jitter at the f_{min} frequency--5.75 fs in this example. This procedure was carried out in the same manner for all timing jitter measurements reported in the following chapters.

2.3.3 Soliton Theory Pulse Width Model

In the Haus master equation [35] (based upon the nonlinear Schrodinger equation) the pulses propagating in an optical cavity undergo influences from gain, loss, dispersion, self-phase modulation, and self-amplitude modulation. Recalling that the hyperbolic secant pulse shape is a valid analytical solution to the master equation, the following constraint upon that solution is imposed.

$$\tau = \frac{2 * |\beta''|}{\delta_{Tot} * E_P}$$ **Equation 2-9**

Equation 2-9 is a variation on the soliton area theorem which roughly states that the width of the pulse (τ) is proportional to the total dispersion (β'') and inversely proportional to the nonlinearity (δ) and the total energy (E_P) contained within the pulse. Others have explained this equation and its derivation in depth ([36], [37]) so it is presented here to explain where the "soliton theory" pulse width estimations in Chapter 5 originate.

The literature writes this equation in a few different variations depending upon the conditions being tested. It was challenging to determine what proper form of the relationship to use so that the units of the equation all came out correct. Presented here are the values used for simulating soliton pulse widths that result from one round trip through the cavity of the 1 GHz linear cavity end-abutted erbium fiber laser presented in Chapter 5.

As this is an ultrafast laser, the final pulse width, τ, has the units of femtoseconds (fs). The dispersion is represented by β'', which in this equation represents the total dispersion in the cavity (units of fs^2). This is the sum of the fiber group velocity dispersion and the dispersion introduced by the saturable mirror. Hynil and Michelle have measured and confirmed that the MIT pump reflection coated VA86 SBR has a GVD of -1300 fs^2 [38] around the 1550 nm wavelength. The manufacturer data sheets state the dispersion of the Er80 – (8/125) erbium doped gain fiber to be ~-20 fs^2/mm, and the dispersion of SMF is stated at -20.7 fs^2/mm. Accounting for the 92 mm of gain fiber, the 7 mm of SMF and the fact that this is a linear cavity and the pulses pass through each fiber twice in one round trip, the total dispersion value comes out at -5270 fs^2.

The next term in the equation is the nonlinearity. It is not straightforward to properly define this term. Various sources use differing symbols and different units but call it the same thing. What was decided upon for this analysis is the following: the nonlinearity (δ) divided by the effective area leads to the self-phase modulation per unit length (δ_L) which when multiplied by the fiber length becomes the total self-phase modulation (δ_{Tot}) to input to Equation 2-9.

Because the nonlinearity depends upon the center wavelength (λ_0), the δ_{Tot} term will be wavelength dependent in the final formula. To begin we assume that the nonlinear index (n_2) of silica glass fiber is $3*10^{-20}$ m^2/W and the wave vector (K_0) equals $2*\pi/\lambda_0$. Since $\delta = K_0*n_2$ we arrive at Equation 2-10 for the nonlinearity in the fiber.

$$\delta = \frac{6\pi * 10^{-11}}{\lambda_0}\left(\frac{m}{W}\right) \qquad \textbf{Equation 2-10}$$

Dividing the nonlinearity by the effective mode field diameter in each fiber (70.9 μm^2 for Er80 and 84.9 μm^2 for SMF) and multiplying by two times the length of each fiber (92 mm and 7 mm) yields the formula in Equation 2-9 for the total self-phase modulation present in one round trip of this fiber laser cavity.

$$\delta_{Tot} = \frac{0.520}{\lambda_0}\left(\frac{1}{W}\right) \qquad \textbf{Equation 2-11}$$

The final term is the pulse energy, something obtained from knowing the laser output power (P_0), the output coupler factor (10%), and the repetition rate (f_{rep}) by the relationship in Equation 2-12.

$$E_P = \frac{P_0 * 10}{f_{rep}} \qquad \textbf{Equation 2-12}$$

Combining Equation 2-10, Equation 2-11, and Equation 2-12 into Equation 2-9 and properly accounting for the units and orders of magnitude yields a formula for the soliton pulse width given the central wavelength (in nanometers), the output power (in milliwatts), and repetition rate (in gigahertz) as the only necessary inputs.

$$\tau = \frac{2.027}{\frac{P_0}{f_{rep} * \lambda_0}}(fs) \qquad \textbf{Equation 2-13}$$

The nonlinear index of the fiber is not the same, however, for different polarizations. The above number is an average often used but the more accurate number for the case of linear polarization in the fiber is $3.2*10^{-20}$ m^2/W [39]. If the polarization is elliptical or circular the value of the nonlinear index can be reduced by as much as $1/3^{rd}$ of this upper limit. Therefore Equation 2-13 is modified to allow flexibility in the values of n_2 as well to attempt to calculate the most accurate possible pulse width predictions for any given set of laser state output powers.

$$\tau = \frac{6.081}{\frac{P_0 * n_2}{f_{rep} * \lambda_0}} (fs) \qquad \textbf{Equation 2-14}$$

Finally we arrive at Equation 2-14, the formula used to generate the data for the soliton theory pulse width plots in Chapter 5.

2.3.4 Split Step Time Domain Numerical Simulation

Modeling an optical pulse traveling down a medium like an optical fiber is a straightforward simulation that can be done via a mathematical technique known as split-step time-domain modeling. This technique is powerful but standard enough to be taught in the normal nonlinear and ultrafast optics textbooks [1], [34] and graduate courses [2]. The model can be written for effects as simple as linear dispersion or as complex as nonlinear effects like self-phase modulation and Raman shifts. The purpose for explaining it in this section is not to break down how the simulation is done, the references above do that; but to detail what inputs were used and what assumptions were made to take the measured laser characteristics and attempt to model the ideal transform limited pulse propagation down the fiber used in the laboratory experiment in Chapter 5.

2.3.4.1 *Pulse Inputs*

The split step simulation MATLAB code used came from a working sample of code graciously shared by Katia Shtyrkova. This script is written to take the following pulse inputs:

- Initial Pulse Width (fs)
- Average Power (mW)
- Repetition Rate (GHz)
- Center Wavelength (nm)

Once the input pulse characteristics are entered, the choice of a sech or Gaussian pulse envelope is selected as both pulse shape options are available in the code.

2.3.4.2 *Fiber Specifications*

The electric field vector for a simulated pulse in the selected shape is passed through three different lengths of fiber with appropriate dispersions and mode field diameters. Figure 2-10 illustrates the geometry and configuration of the fiber lengths the pulses passed through prior to any measurements being taken.

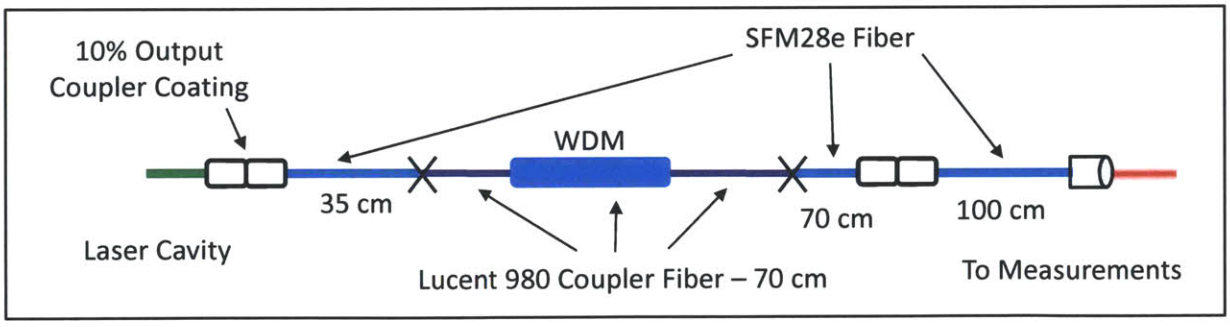

Figure 2-10 Schematic of fiber coupled linear cavity erbium fiber laser output fiber sections.

As seen in Figure 2-10, the pulses exit the laser cavity at the output coupler and pass through 275 cm of fiber before being measured or characterized in any way. The first 35 cm and the final 170 cm is Corning SMF28e single mode fiber with its wavelength dependent dispersion following Equation 2-15.

$$D(\lambda) = \frac{S_0}{4}\left[\lambda - \frac{\lambda_0^4}{\lambda^3}\right] \left(\frac{ps}{nm\ km}\right)$$ **Equation 2-15**

The dispersion is a function of the wavelength (λ), the zero dispersion wavelength (λ_0), and the zero dispersion slope (S_0). For this fiber, the specification sheet states that the zero dispersion slope is 0.086 (ps/(nm^2*km)) and the zero dispersion wavelength is located at 1313 nm. The mode field diameter is 10.4 μm^2, the nonlinearity is $3*10^{-16}$ (cm^2/W), and the linear loss coefficient is $0.2*10^{-5}$ (dB/cm).

For the WDM packaging and connecting fiber pigtails, a different fiber[4] was used that has very low dispersion around the 1550 nm wavelength. The wavelength dependent dispersion for this fiber is not calculated but comes from a linear fit of experimental data taken by the manufacturer, OFS. Special thanks to Dr. John Fini of OFS for providing the experimental data plot.

$$D(\lambda) = 0.04032258 * \lambda - 63.75 \left(\frac{ps}{nm\ km}\right)$$ **Equation 2-16**

The dispersion values obtained by the linear fit of Equation 2-16 are only valid for λ values from 1550 nm to 1580 nm but that window is sufficient for these simulations.

To complete the fiber specification section of the simulation code, the mode field diameter of the Lucent 980 Coupler fiber is given to be 7.5 μm^2 for 1550 nm wavelength light, the nonlinearity is $3*10^{-16}$ (cm^2/W), and the linear loss coefficient is $0.2*10^{-5}$ (dB/cm).

2.3.4.3 Simulations

To obtain reasonable results from the simulation requires careful choices and multiple iterations of the number of simulation steps, the time and frequency domain vector sizes, and the choice of the estimated losses at the fiber splice points. The calculated electric field vector with the chosen pulse shape envelope is stepped through first 35 cm of SMF fiber, then 70 cm of Lucent 980 Coupler fiber, then 170 cm of SMF fiber and the effects of

[4] OFS, Model: "Lucent 980 Coupler" or BF05635-02, CL 980 16 Photonic Fiber

linear group velocity dispersion and nonlinear self-phase modulation are calculated at each step. The final output field is squared and the real pulse envelope plotted with the input and output FWHM pulse widths displayed to determine how the pulse width evolved through the fiber propagation.

2.4 Vector Solitons

One undesirable characteristic that began to emerge from the linear cavity fiber lasers of Chapter 4 and Chapter 5 was the tendency for modulation sidebands to be detected around the otherwise clean lines of the RF spectral data. Depending upon the state or fiber configuration or coupling of the laser, the sidebands would appear in varying number and varying distances (in frequency) from the main line. A good example of this behavior is visible in Figure 2-11(a).

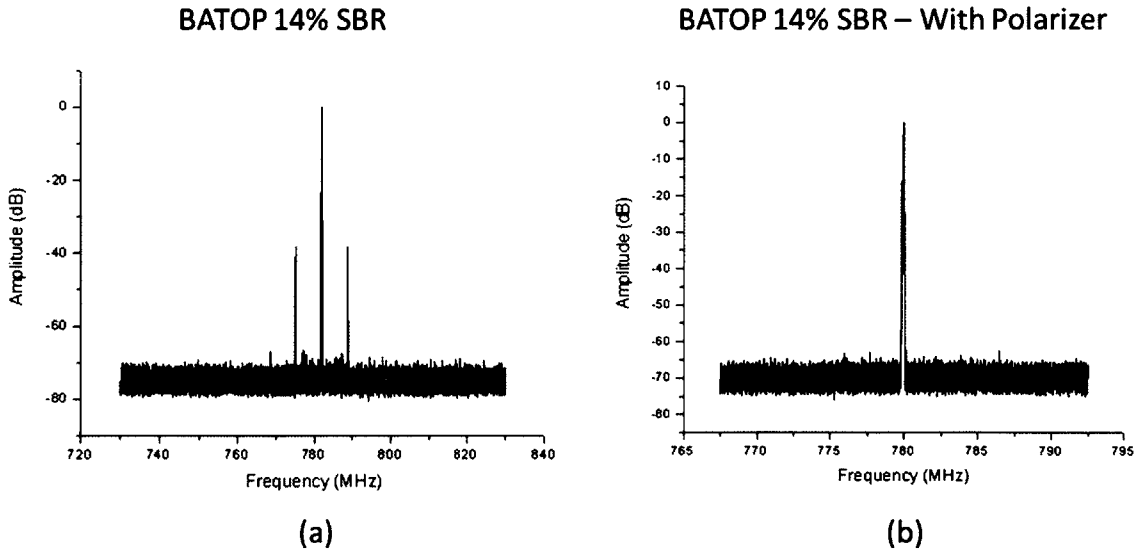

Figure 2-11 Example data from Chapter 4, notice the sidebands in figure (a) and their absence in figure (b).

When this behavior was first noticed the cause of it was unknown. It became a problem because it was showing up in the spectrum of every high repetition rate linear cavity laser we would build. Sometimes the side bands could be suppressed but unless their

cause was determined we could not know for certain how to eliminate them. In addition, these sidebands correlated to highly increased timing jitter measurements and that meant they had to be eliminated to achieve our objective of low jitter laser sources.

Fortunately, tests performed by Hyunil Byun and Michelle Sander helped to narrow down the cause to a phenomenon known as vector solitons [40]. This is a consequence of using non-polarization maintaining fiber in the cavity. In a standard single mode fiber, there are two equally valid polarization eigenmodes and light will generally propagate in both of them simultaneously. If the fiber was perfectly symmetrical and unstressed, these modes would co-propagate and the overall polarization would not change in the fiber. However, real fibers are all slightly birefringent due to manufacturing stresses and the result is two polarization states propagating at slightly different rates through the fiber. As they travel, the ellipticity of the overall optical mode in the fiber evolves at a period much longer than the round trip time of the cavity. This polarization evolution produces a small amplitude modulation on the pulse train that manifests as frequency sidebands in the RF spectral measurements.

This effect is understood [41] and can be controlled [42]. Independently controlling the two polarization states within a laser cavity is usually straightforward—a polarization controller is put in the cavity. In a free space laser this would be a PBS or a linear polarizer. In a long fiber laser polarization control paddles or fiber compression polarization controllers could be used. In these very short fiber lasers with either zero or very little free space available for an optic, controlling the fiber polarization becomes more of a challenge. The one option available is the simple action of bending and twisting the fiber [43] until the period of the slowly evolving polarization is matched to the round trip length of the cavity. This is called forming polarization-locked vector solitons (PLVS's) and is the technique used to minimize and eliminate the polarization sidebands detected on the output measurements of the high repetition rate linear cavity fiber lasers.

2.5 Conclusions

This chapter detailed definitions and explanations of theory and measurement techniques helpful to understand the results presented in Chapters 3, 4, and 5. There was a brief review of mode-locking and how it can occur within a laser cavity. Many mode-locking techniques exist and descriptions of the two mechanism used by the systems in this thesis—SBR mode-locking and P-APM—were presented.

The next sections dealt with laboratory measurement techniques. The background-free intensity autocorrelation, used to measure pulse width, is detailed along with the necessary pulse shape deconvolution factors. Next, timing jitter calculations from phase noise measurements are explained with example data from a system described in Chapter 5.

Finally, the inputs and assumptions behind the split-step time-domain pulse propagation simulation used to predict the output pulses from the coupling fibers were listed, and the concept of vector soliton behavior within a laser cavity was introduced.

As the explanations of the different lasers are presented throughout the subsequent chapters, the reader is encouraged to return to this Chapter to address any confusion that may arise as to how certain measurements or calculations were made and what assumptions went into them.

Bibliography - Chapter 2

[1] A. Weiner, *Ultrafast Optics*. John Wiley & Sons, 2011.

[2] F. X. Kaertner, *6.638 Ultrafast Optics - Fall 2008 Class Textbook*. 2008.

[3] B. E. A. Saleh and M. C. Teich, *Fundamentals of Photonics*. Wiley, 2007.

[4] A. E. Siegman, *Lasers*. University Science Books, 1986.

[5] D. C. Hanna, A. Kazer, M. W. Phillips, D. P. Shepherd, and P. J. Suni, "Active Mode-Locking of an Yb - Er Fiber Laser," *Electron. Lett.*, vol. 25, no. 2, pp. 95–96, 1989.

[6] M. Hofer, M. E. Fermann, F. Haberl, and J. E. Townsend, "Active-Mode Locking of a Neodymium-Doped Fiber Laser Using Intracavity Pulse-Compression," *Opt. Lett.*, vol. 15, no. 24, pp. 1467–1469, 1990.

[7] D. J. Jones, H. A. Haus, and E. P. Ippen, "Subpicosecond solitons in an actively mode-locked fiber laser," *Opt. Lett.*, vol. 21, no. 22, pp. 1818–1820, 1996.

[8] D. Foursa, P. Emplit, R. Leners, and L. Meuleman, "18GHz from a sigma-cavity Er-fibre laser with dispersion management and rational harmonic active mode-locking," *Electron. Lett.*, vol. 33, no. 6, pp. 486–488, 1997.

[9] S. Longhi, S. Taccheo, and P. Laporta, "High-repetition-rate picosecond pulse generation at 1.5 mu m by intracavity laser frequency modulation," *Opt. Lett.*, vol. 22, no. 21, pp. 1642–1644, 1997.

[10] K. Sato, A. Hirano, and H. Ishii, "Chirp-compensated 40-GHz mode-locked lasers integrated with electroabsorption modulators and chirped gratings," *Ieee J. Sel. Top. Quantum Electron.*, vol. 5, no. 3, pp. 590–595, 1999.

[11] I. D. Jung, F. X. Kaertner, N. Matuschek, D. H. Sutter, F. Morier-Genoud, Z. Shi, V. Scheuer, M. Tilsch, T. Tschudi, and U. Keller, "Semiconductor saturable absorber mirrors supporting sub-10-fs pulses," *Appl. Phys. B Lasers Opt.*, vol. B65, no. 2, pp. 137–50, 1997.

[12] E. P. Ippen, "Principles of Passive-Mode Locking," *Appl Phys B-Lasers O Appl Phys B-Lasers O*, vol. 58, no. 3, pp. 159–170, 1994.

[13] U. Keller, K. J. Weingarten, F. X. Kartner, D. Kopf, B. Braun, I. D. Jung, R. Fluck, C. Honninger, N. Matuschek, and J. A. derAu, "Semiconductor saturable absorber mirrors (SESAM's) for femtosecond to nanosecond pulse generation in solid-state lasers," *Ieee J. Sel. Top. Quantum Electron.*, vol. 2, no. 3, pp. 435–453, 1996.

[14] M. N. Islam, E. R. Sunderman, I. Barjoseph, N. Sauer, and T. Y. Chang, "Multiple Quantum Well Passive-Mode Locking of a Nacl Color Center Laser," *Appl. Phys. Lett.*, vol. 54, no. 13, pp. 1203–1205, 1989.

[15] B. G. Kim, E. Garmire, S. G. Hummel, and P. D. Dapkus, "Nonlinear Bragg Reflector Based on Saturable Absorption," *Appl. Phys. Lett.*, vol. 54, no. 12, pp. 1095–1097, 1989.

[16] D. Kopf, G. Zhang, R. Fluck, M. Moser, and U. Keller, "All-in-one dispersion-compensating saturable absorber mirror for compact femtosecond laser sources," *Opt. Lett.*, vol. 21, no. 7, pp. 486–488, 1996.

[17] S. Nabanja, M. Y. Sander, J. Morse, K. Shtyrkova, G. S. Petrich, L. A. Kolodziejski, F. X. Kartner, and E. P. Ippen, "Widely tunable large area SBRs for ultra-short pulse generation," in *2012 Conference on Lasers and Electro-Optics, CLEO 2012, May 6, 2012 - May 11, 2012*, 2012.

[18] A. A. Erchak, D. J. Ripin, J. T. Gopinath, H. M. Shen, F. X. Kaertner, G. S. Petrich, L. A. Kolodziejski, and E. P. Ippen, "Large scale oxidation of AlAs layers for broadband saturable Bragg reflectors," in *Technical Digest. Summaries of papers presented at the Conference on Lasers and Electro-Optics. Conference Edition, 19-24 May 2002*, Long Beach, CA, USA, 2002, vol. vol.1, p. 225 vol.1.

[19] D. J. Ripin, J. T. Gopinath, H. M. Shen, A. A. Erchak, G. S. Petrich, L. A. Kolodziejski, F. X. Kartner, and E. P. Ippen, "Oxidized GaAs/AlAs mirror with a quantum-well saturable absorber for ultrashort-pulse Cr/sup 4+/:YAG laser," *Opt. Commun.*, vol. 214, no. 1–6, pp. 285–9, 2002.

[20] S. N. Tandon, J. T. Gopinath, T. R. Schibli, G. S. Petrich, L. A. Kolodziejski, F. X. Kaertner, and E. P. Ippen, "Saturable Absorbers with Large Area Broadband Bragg Reflectors for Femtosecond Pulse Generation," in *Conference on Laser and Electro-Optics*, Baltimore, MD, 2003.

[21] S. N. Tandon, J. T. Gopinath, H. M. Shen, G. S. Petrich, L. A. Kolodziejski, F. X. Kaertner, and E. P. Ippen, "Broadband saturable Bragg reflectors from the infrared to visible using oxidized AlAs," in *Conference on Laser and Electro-Optics*, San Francisco, CA, 2004.

[22] S. Tandon, "Engineering light using large area photonic crystal devices," 2005.

[23] H. M. Shen, "Novel broadband light sources and pulse generation techniques at 1.5 [mu]m," Massachusetts Institute of Technology, 2009.

[24] H. Byun, "Integrated high-repetition-rate femtosecond lasers at 1.55 [mu]m," Massachusetts Institute of Technology, 2010.

[25] M. Y. Sander, "High repetition rate fiber and integrated waveguide femtosecond lasers," Massachusetts Institute of Technology, 2012.

[26] K. Tamura, C. R. Doerr, L. E. Nelson, H. A. Haus, and E. P. Ippen, "Technique for obtaining high-energy ultrashort pulses from an additive-pulse mode-locked erbium-doped fiber ring laser," *Opt. Lett.*, vol. 19, no. 1, pp. 46–8, 1994.

[27] H. A. Haus, E. P. Ippen, and K. Tamura, "Additive-pulse modelocking in fiber lasers," *Ieee J. Quantum Electron.*, vol. 30, no. 1, pp. 200–8, 1994.

[28] H. A. Haus, K. Tamura, L. E. Nelson, and E. P. Ippen, "Stretched-pulse additive pulse mode-locking in fiber ring lasers: theory and experiment," *Ieee J. Quantum Electron.*, vol. 31, no. 3, pp. 591–8, 1995.

[29] K. Tamura, H. A. Haus, and E. P. Ippen, "Self-Starting Additive Pulse Mode-Locked Erbium Fiber Ring Laser," *Electron. Lett.*, vol. 28, no. 24, pp. 2226–2228, 1992.

[30] K. Tamura, J. Jacobson, E. P. Ippen, H. A. Haus, and J. G. Fujimoto, "Unidirectional Ring Resonators for Self-Starting Passively Mode-Locked Lasers," *Opt. Lett.*, vol. 18, no. 3, pp. 220–222, 1993.

[31] K. Tamura, E. P. Ippen, and H. A. Haus, "Pulse Dynamics in Stretched-Pulse Fiber Lasers," *Appl. Phys. Lett.*, vol. 67, no. 2, pp. 158–160, 1995.

[32] K. Tamura, E. P. Ippen, H. A. Haus, and L. E. Nelson, "77-Fs Pulse Generation from a Stretched-Pulse Mode-Locked All-Fiber Ring Laser," *Opt Lett Opt Lett*, vol. 18, no. 13, pp. 1080–1082, 1993.

[33] J. A. Armstrong, "Measurement of picosecond laser pulse widths," *Appl. Phys. Lett.*, vol. 10, no. 1, pp. 16–18, Jan. 1967.

[34] R. W. Boyd, *Nonlinear optics*. Boston: Academic Press, 1992.

[35] H. A. Haus, "Theory of Forced Mode-Locking," *Ieee J Quantum Elect Ieee J Quantum Elect*, vol. QE11, no. 7, pp. 323–330, 1975.

[36] J. W. Sickler, "High repetition rate mode-locked erbium-doped fiber lasers with complete electric field control," Massachusetts Institute of Technology, 2008.

[37] J. Chen, "High repetition rate fiber lasers," Massachusetts Institute of Technology, 2009.

[38] H. Byun, M. Y. Sander, A. Motamedi, H. Shen, G. S. Petrich, L. A. Kolodziejski, E. P. Ippen, and F. X. Kartner, "Compact, stable 1 GHz femtosecond Er-doped fiber lasers," *Appl. Opt.*, vol. 49, no. 29, pp. 5577–5582, 2010.

[39] G. P. Agrawal, *Nonlinear fiber optics*, vol. 3rd. San Diego: Academic Press, 2001.

[40] D. N. Christodoulides and R. I. Joseph, "Vector solitons in birefringent nonlinear dispersive media," *Opt. Lett.*, vol. 13, no. 1, pp. 53–55, Jan. 1988.

[41] S. Cundiff, B. Collings, and W. Knox, "Polarization locking in an isotropic, modelocked soliton Er/Yb fiber laser," *Opt. Express*, vol. 1, no. 1, pp. 12–21, Jul. 1997.

[42] N. N. Akhmediev, J. M. Soto-Crespo, S. T. Cundiff, B. C. Collings, and W. H. Knox, "Phase locking and periodic evolution of solitons in passively mode-locked fiber lasers with a semiconductor saturable absorber," *Opt. Lett.*, vol. 23, no. 11, pp. 852–854, Jun. 1998.

[43] A. M. Smith, "Birefringence induced by bends and twists in single-mode optical fiber," *Appl. Opt.*, vol. 19, no. 15, pp. 2606–2611, Aug. 1980.

Chapter 3 High Repetition Rate, High Average Power, Femtosecond Erbium Fiber Sigma Lasers

3.1 Introduction

What makes ultrafast lasers uniquely useful is the duration of the time domain pulse. Pulses on the order of 100 femtoseconds (fs) in duration or less are now common. By Fourier duality, an ultra-short event in time corresponds to an unusually large range of frequency components. The previous chapter detailed some of the practical applications of these systems.

Femtosecond lasers constructed out of optical fiber components are particularly interesting because of their compact size, ruggedness, and insensitivity to mechanical misalignment. There are several methods that can be employed to construct a femtosecond fiber laser but the primary differentiator is the direction the light is traveling through the fiber. Recall, that to create an optical laser cavity the light has to have a path that returns the pulse to the same physical place each round trip. If the light travels down a fiber, reflects from a mirror or some other device, and then back through the same piece of fiber, such a photonic device is usually described as a linear cavity fiber laser. However, if the light is able to travel in a continuous loop without crossing back on itself, the system is a type of ring cavity laser. This chapter describes two versions of a ring cavity laser—specifically sigma ring lasers. [1]

Sigma cavity fiber lasers are versatile because the light travels through both fiber and free space optical components. This conveys the advantages of fiber amplification to the flexibility of free space waveplates, mirrors, or other components. The designation sigma is used because, from an overhead view, the laser cavity looks like the lower case Greek letter "σ." What differentiates a sigma cavity from a traditional unidirectional ring laser is the

"arm" off of it enabled via a polarizing beam cube or a circulator. Usually a plane mirror on a translation stage is placed at the end of the arm to enable dynamic cavity length adjustments.

To obtain ultra-short pulses in what would otherwise be a continuous wave (CW) fiber laser, both polarization additive-pulse mode-locking (P-APM) [2] and/or saturable Bragg reflector (SBR) mode-locking [3], [4] can be used. These schemes have been applied successfully to soliton [5], [6], and stretched-pulse [7] fiber lasers. Our first sigma laser (taking advantage of both mode-locking mechanisms) was constructed using mostly standard optical components [8], [9] and operated at a repetition rate of 234 MHz. This design was compressed into a physically smaller system that scales the repetition rate beyond 300 MHz using many custom built components [10]. This was the first time to the author's knowledge that a fundamentally mode-locked erbium fiber sigma laser had exceeded 300 MHz while maintaining high output power of 60 mW.

The 234 MHz and 300 MHz lasers are similar so it follows that their output characteristics be reported side-by-side rather than one full description followed by a second mostly identical one. Thus the following sections reflect that logic. First, the laser designs are described and illustrated. Then their standard output measurements are plotted and compared. Finally conclusions are drawn about the system limits and possible future developments.

3.2 Laser Designs

3.2.1 Initial Sigma Laser Design

The laser, illustrated in Figure 3-1 and photographed in Figure 3-2, is pumped by two, 750 mW, 980 nm diodes[5] that are polarization multiplexed via fiber coupler[6]. This assembly is capable of an output of up to 1.2 watts of single mode 980 nm light. No pump isolator was necessary because the ring design prevents any significant power feedback to the pump diodes.

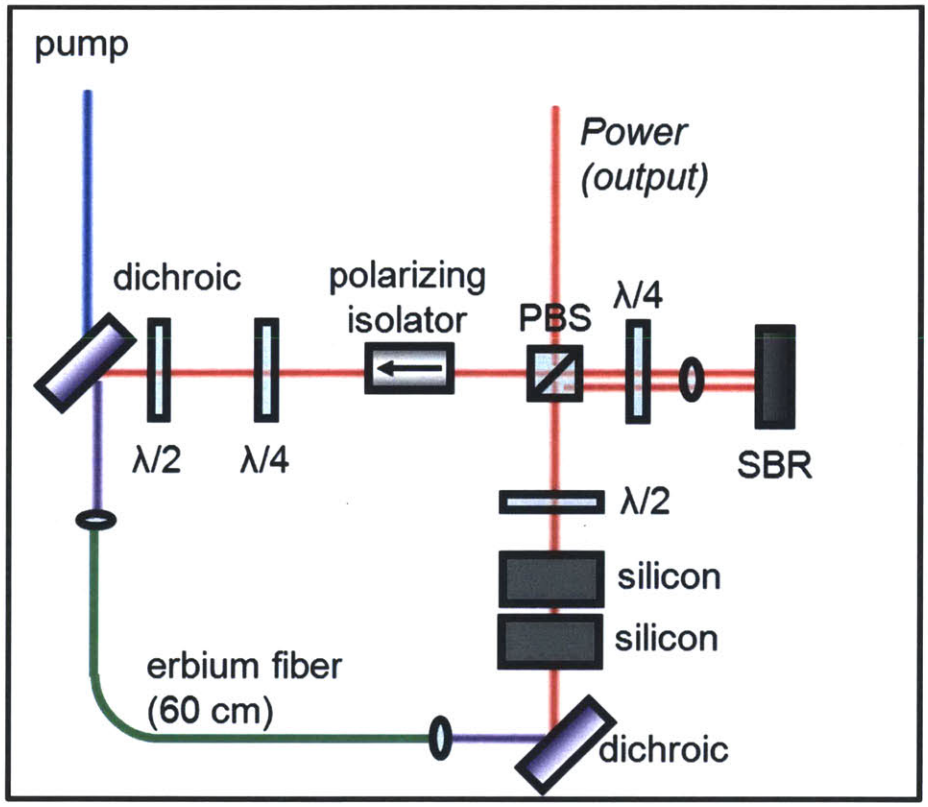

Figure 3-1 Initial design schematic for sigma fiber laser.

[5] Bookham, Inc., Model: LC96UF74-20R

[6] SIFAM Fibre Optics (via Optimark Fiber Optics), Model: FFP-5M3280G10

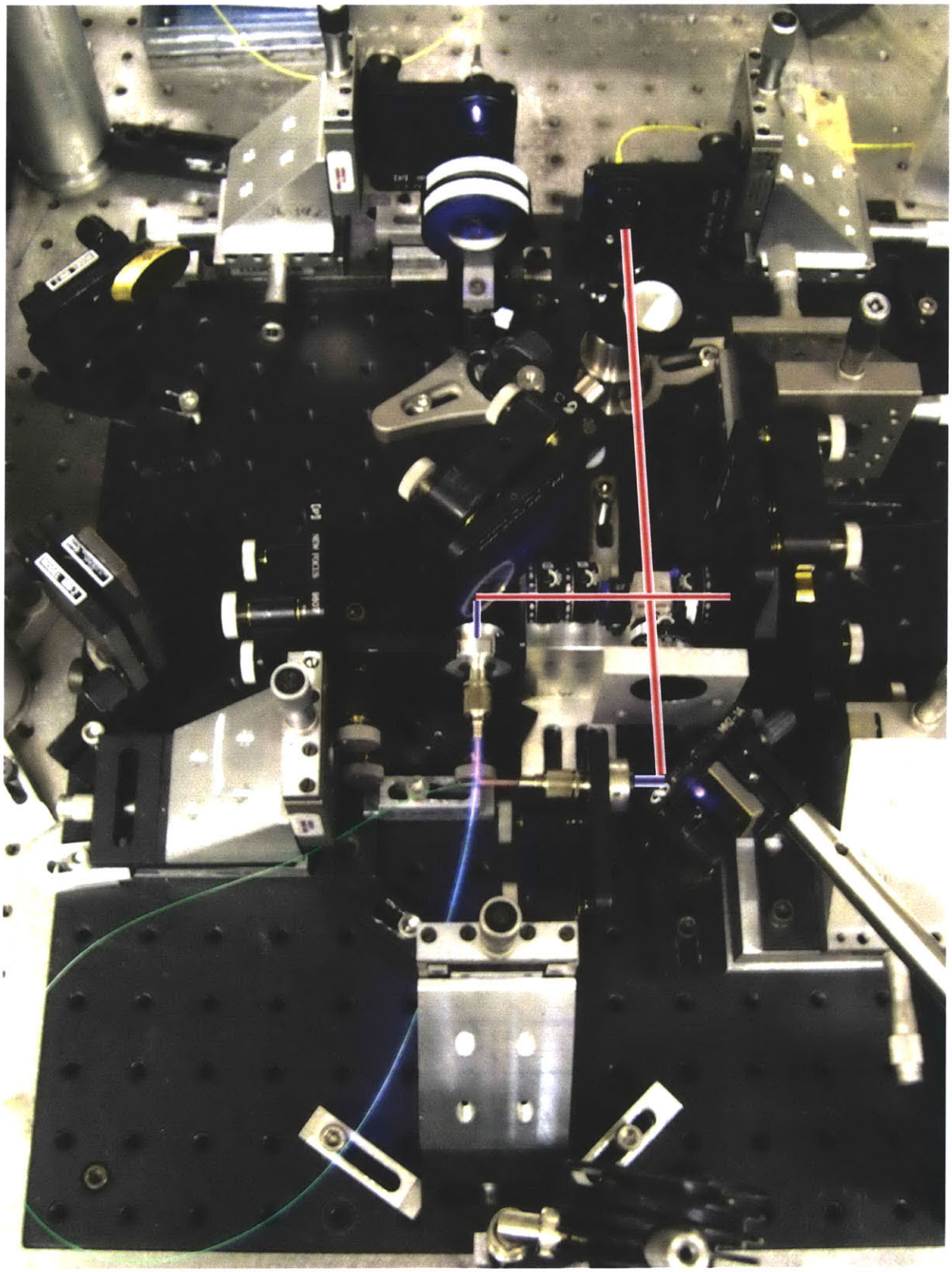

Figure 3-2 Photograph of the complete 234 MHz fiber laser in operation. The blue colors are scattered pump light picked up by the camera's sensor and the purple and red lines represent the free space beam path.

The pump light is coupled into the laser cavity via free space optics[7] to avoid the need for WDM fiber couplers that would extend the overall cavity length. Specifically, the gain fiber is optically pumped through a short-wave-pass 980 nm/1550 nm dichroic mirror.[8] This mirror maintains the 1550 nm signal in the cavity while passing the pump light through to the fiber. The erbium-doped fiber that is used is a high absorption specialty fiber.[9] This fiber was epoxied and wet polished into standard FC/APC connectors and screwed into a fixed collimation package[10] for mounting. The second short-wave-pass dichroic mirror allows unabsorbed pump light to exit the cavity, and the anti-reflection-coated silicon windows[11] ensure that no pump light will interfere with SBR operation as silicon absorbs strongly below 1 micron but transmits clearly at 1.55 microns. Once the erbium is pumped and signal pulses form, they must be carefully controlled in the cavity.

Pulse control is accomplished via a variety of interacting components. The first half-wave plate (HWP)[12] controls the input to the polarization beam splitter (PBS) by reorienting the primary axis of the polarization ellipse. The PBS[13] thus acts both as the cavity output coupler and the polarization-dependent loss mechanism. The horizontally-polarized (relative to the optical table) components of the beam are passed straight through the beam cube and thus constitute the laser output. The vertically-polarized (relative to the optical table) portion of the beam is reflected by the interface in the beam cube and enters the linear arm of the cavity; where it is focused on the SBR by an aspheric lens[14]. The linear path includes a quarter-wave plate (QWP) oriented so that the vertically-polarized beam returns to the PBS horizontally-polarized. After passing again through the PBS, a polarizing

---

[7] Thorlabs, Model: LA1708-B (1st) and LC1120-B (2nd)
[8] CVI Melles-Griot, Model: SWP-45-RU1550-TU775-PW-1025
[9] Liekki Corporation, Model: ER80-8/125
[10] Thorlabs, Model: F240APC-1550
[11] ISP Optics Corp., Si windows, size 12.7x5
[12] All waveplates are zero-order at 1550 nm
[13] Coated for 1550 nm, Unknown origin
[14] Thorlabs, Model: C220-TM, f = 11 mm

isolator[15] ensures unidirectional operation. Finally, a HWP and QWP pair enable full control over the polarization state that is launched into the gain fiber.

3.2.1.1 Saturable Bragg Reflectors (SBRs)

One purpose of this laser was to test the performance characteristics of several commercial semiconductor saturable absorbing mirrors (SESAMS)—usually referred to as saturable Bragg reflectors (SBR's) in this thesis. Table 3-1 lists the part numbers and some design characteristics of four BATOP commercial SBRs we tested in this laser.

Table 3-1 BATOP SBR characteristics that were tested in this laser.

Model Number	Linear Loss	Modulation Depth	Saturation Fluence	Recovery Time
SAM-1550-09-25.4s	9%	6%	50 $\mu J/cm^2$	2 *ps*
SAM-1550-20-25.4s	20%	12%	50 $\mu J/cm^2$	12 *ps*
SAM-1550-23-25.4s	23%	14%	25 $\mu J/cm^2$	2 *ps*
SAM-1550-35-25.4s	35%	21%	50 $\mu J/cm^2$	2 *ps*

All four of these mirrors were tested in the cavity and all resulted in mode-locking. See the 234 MHz results section for discussion and plots.

3.2.2 Reduced Size Sigma Laser Design

The first generation laser demonstrated that stretched-pulse mode-locking could be achieved with a saturable absorber mirror and P-APM effects in the gain fiber. This second laser was built with the purpose to test how high the repetition rate could be pushed while maintaining the ability to generate ultra-short pulses.

Figure 3-3 illustrates the full layout of the reduced cavity length 300 MHz sigma fiber laser.

[15] Isowave, Model: I-16-JM-3.5-4, Single Stage Round

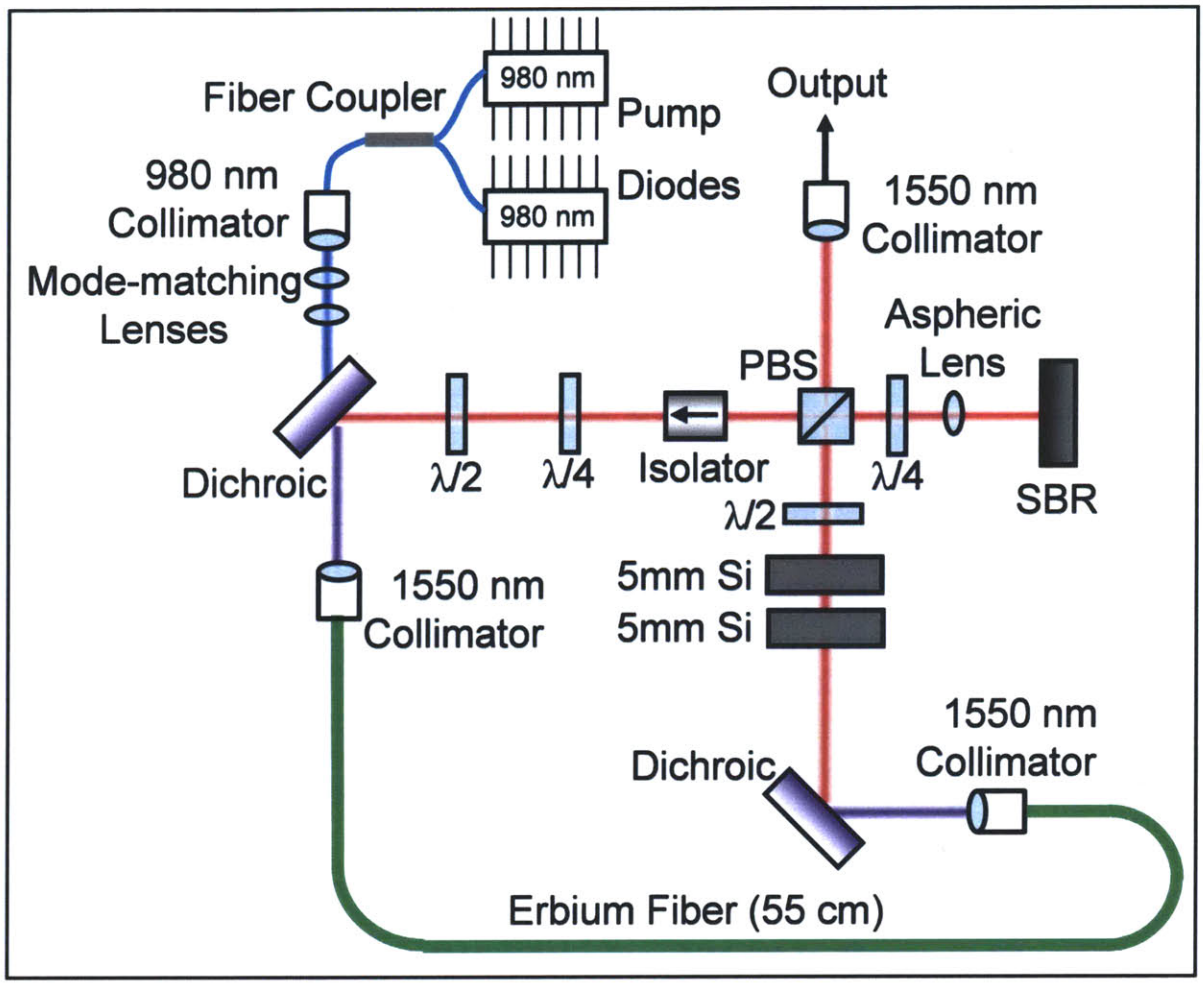

Figure 3-3 Compact sigma cavity mode-locked fiber laser design.

This compact laser was designed for the smallest possible free space cavity. This allowed us to keep a longer length of gain fiber, which enabled higher intra-cavity gain leading to high output powers. The short cavity was achieved by a combination of ordering the smallest components available and custom mounting. Every optic in the beam path is held by a mount that we designed and machined ourselves. Each mirror, waveplate, etc. is approximately one millimeter from its neighboring components. By these extensive efforts we were able to reduce the free space cavity beam path to just 16 cm. That length includes the double pass in the linear section of the sigma arm. Figure 3-4 is a photograph of the laser layout.

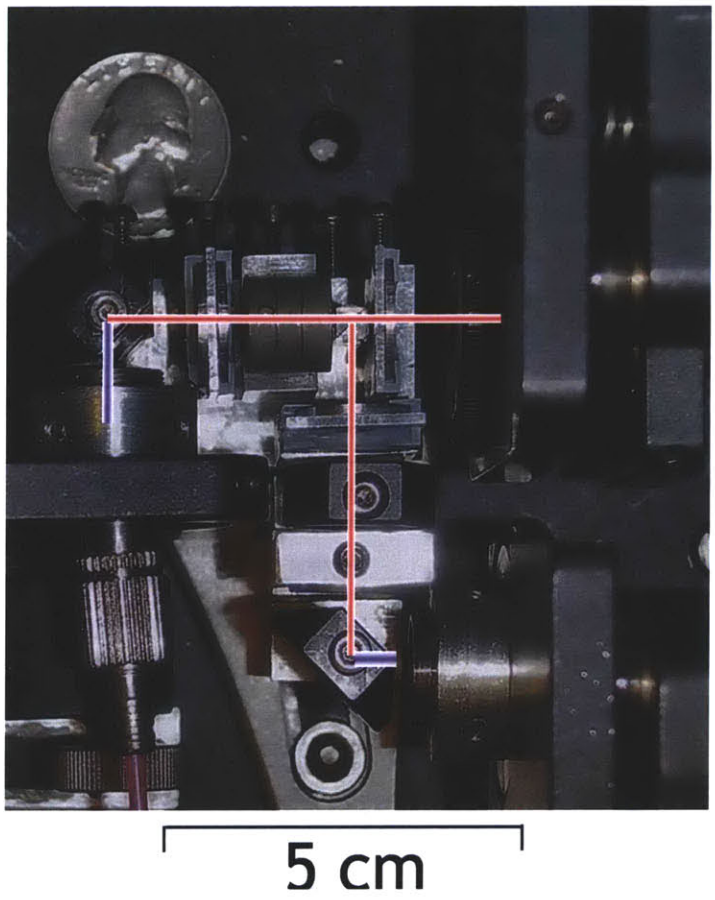

Figure 3-4 Photograph of 300 MHz cavity. Almost all component mounting parts were custom manufactured to decrease the cavity length. Quarter placed for size comparison.

There are minor differences between the original system and this updated one. First, 5 cm was removed from the length of the erbium gain fiber. This reduced the optical path length by ~7.5 cm due to the index of refraction of the glass fiber being greater than one. Shortening the fiber also reduces the number of pump photons that can be absorbed before the fiber is "bleached" so a careful balance between the cavity losses and gain must be maintained to ensure proper operation.

In addition, almost every optic in the free space section was replaced for space reasons. The dichroic mirrors have the same optical coating on the same substrate material as the previous system; we simply ordered them sized to fit a ½" mount instead of the previous 1" diameter mount. As you can see in the system photograph (Figure 3-4) the mounts for the mirrors were milled at 45 degree angles to gain precious millimeters of path

length. The waveplates and the beam cube are also new for this laser. Small, thin quarter and half waveplates[16] were ordered and thin aluminum discs with insets were custom made to hold them. Dual sided Teflon® disk holders were designed and fabricated in house to hold these small parts in the laser cavity and still allow for in-situ rotation (through the use of a custom aluminum and rubber band tool created for the task). The 10 mm beam cube was replaced with an extra small polarizing beam cube[17] that acts as the central anchor of the laser and the point through which all of the critical beam alignment had to occur. Fortunately, the 3 mm cube was sufficiently larger than the 1.5 mm beam diameter to allow for some alignment adjustments. All other components are the same as used in the 234 MHz laser system.

All four BATOP SBRs were implemented in the laser, but the one that yielded the shortest pulses is SAM-1550-09-25.4s. Recall from Table 3-1 that this is the lowest linear loss SBR at 9% and only 6% modulation depth. All data and results from the 300 MHz laser use this SBR.

In typical stretched-pulse erbium fiber ring lasers [7] the normal group-velocity dispersion (GVD) gain fiber is balanced by anomalous GVD single-mode fiber. The net cavity GVD is small, but the alternating sign of the GVD causes the pulse width to stretch and compress dramatically as it traverses the cavity. Alternatively, as can be seen in Figure 3-5, this design balances the gain fiber's anomalous GVD with the large normal GVD of silicon windows.

The large dispersion of the silicon enables stretched-pulse operation at this higher repetition rate because it replaces the long piece of normal dispersion single-mode fiber with a (relatively) thin window of silicon. This means the laser can accommodate a longer gain fiber length and maintain high output powers.

---

[16] Thorlabs, Models: WPQ501 and WPQ502

[17] Thorlabs, Model: PBS3

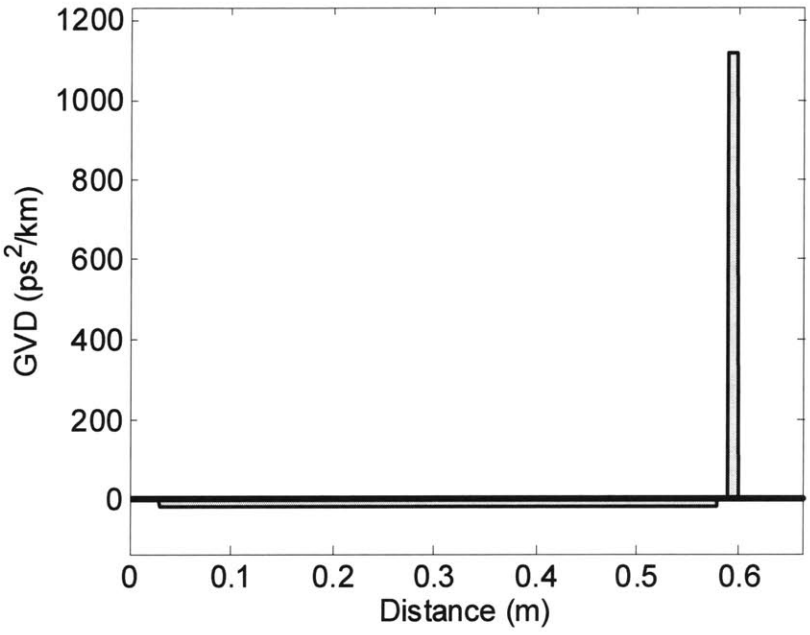

Figure 3-5 Dispersion profile of the 300 MHz laser cavity.

3.3 Results and Discussion

3.3.1 234 MHz Laser

The laser is self-starting and stably mode-locks with all four test SBRs. Because the laser does not mode-lock when the SBR is replaced by a broadband high reflectivity silver mirror, we can conclude that the SBR's pulse shaping effects enable self-starting. However, when the polarization launched into the gain fiber is in a linear state, mode-locking could not be achieved while using the SBRs, which indicates that polarization additive-pulse mode-locking (P-APM) is occurring and necessary for pulsed operation.

3.3.1.1 Optical Spectra

The left side of Figure 3-6 plots the transform-limited pulse duration as derived from the optical spectrum as a function of the output pulse energy. All optical spectra were measured and recorded on an optical spectrum analyzer (OSA)[18] by collecting the laser

[18] Hewlett Packard Inc., Model: 70004A

output beam into a single mode fiber with an aspheric lens and then screwing the fiber into the OSA fiber coupled input port. From this data, it appears that the modulation depth of the SBR does not affect pulse shaping because the results (with the exception of the highest modulation depth SBR) lie along the same contour. This indicates that pulse shaping is dominated by P-APM. Also, the 12% modulation depth SBR absorber has a 12 ps recovery time, whereas the other SBRs have a 2 ps recovery time. The fact that these differences do not affect the pulse characteristics further supports the assumption that P-APM is shaping the final pulse.

The right side of Figure 3-6 plots the maximum bandwidth optical spectra obtained with each SBR. The absence of resonant sidebands (a wider scan window was checked) and the measured normal chirp on the output pulses are clear indications that the laser is operating in the stretched-pulse regime. The net GVD is -630 fs^2, excluding any phase response of the SBR, so sub-100 fs pulses with moderate pulse energies should be expected, and are measured through autocorrelation.

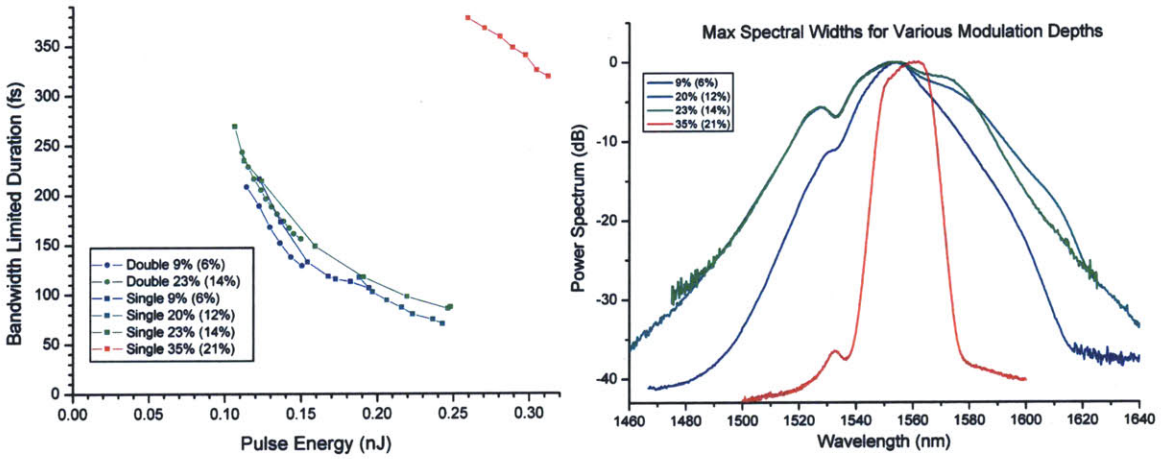

Figure 3-6 (Left) Bandwidth-limited pulse duration as a function of pulse energy. Single and Double refer to the number of intracavity pulses, and the values refer to the linear loss and modulation depth of the SBR tested. (Right) The broadest optical spectra using various SBRs. The values refer to the linear loss and modulation depth of the SBR tested.

One will also notice in the spectra of Figure 3-6 that the SBR with 21% modulation depth provides a distinctly different operating state. The rectangular spectrum and higher

pulse energies are consistent with a stretched-pulse laser with net normal GVD [11]. This makes sense as the normal GVD contribution comes from the phase response of the SBR, which is dominated by the absorption resonance, and hence, increases with the strength of that resonance. Given that the location of the SBR band edge is at 1550 nm, the normal GVD contribution should be on the long wavelength side of the band edge. The location of the spectrum, relatively to the band edge, is consistent with these expectations.

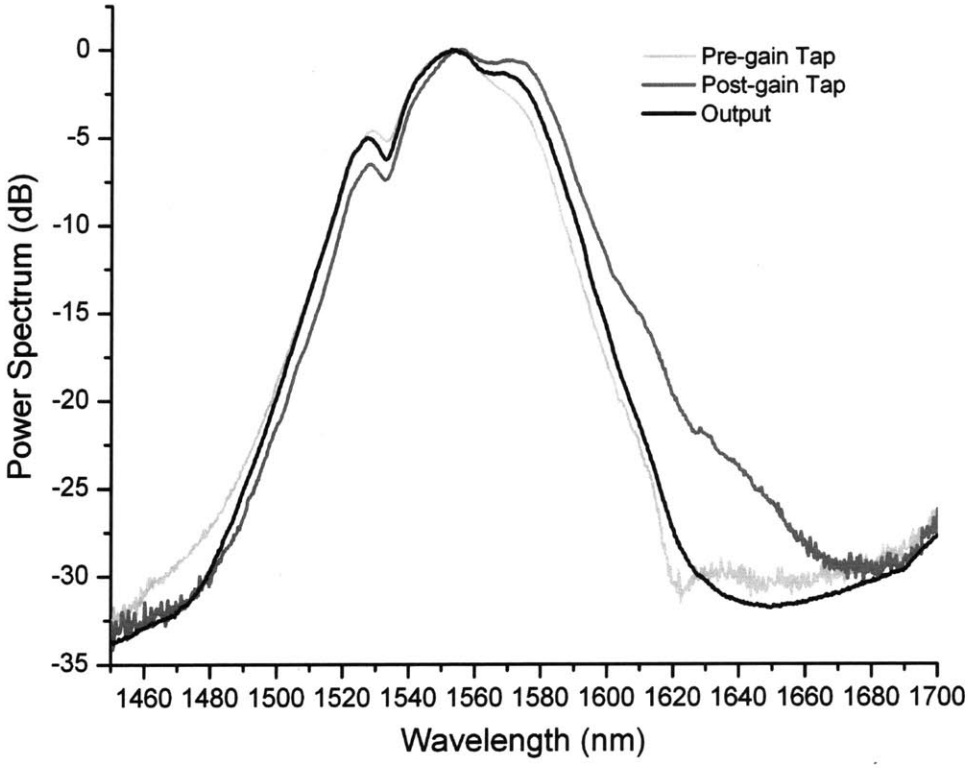

Figure 3-7 Optical spectra for the best state obtained with the 14% modulation depth SBR. The "Tap" traces refer to the spectral shape at different locations inside the laser cavity while the "Output" trace is a trace of the output beam.

Figure 3-7 helps to provide a more complete characterization of the laser operation using the 14% modulation depth SBR. In Figure 3-7 the optical spectrum of the output port and (dichroic) tap ports before and after the gain fiber are shown. To obtain the "tap" port data, a glass slide was placed in the cavity beam path at that location at a small angle. The slide results in ~4% of the beam power being reflected out of the cavity where it was

collected and measured. Calculating the Fourier transform of the output optical spectrum yields an 86 fs transform-limited pulse width.

3.3.1.2 Autocorrelations

The free space output beam is also sent into a custom, in-house intensity autocorrelator. This system was built following the principles found in reference [12], Chapter 9. A nonlinear crystal and photomultiplier tube are utilized to generate and detect the second harmonic nonlinear interaction of the pulse with a time shifted copy of itself. The autocorrelation trace plotted in Figure 3-8 (left) is curve fitted and decorrelated to indicate a Gaussian-shaped pulse with a duration of 100 fs. This pulse was measured after passing through -16,250 fs^2 of GVD outside of the cavity.

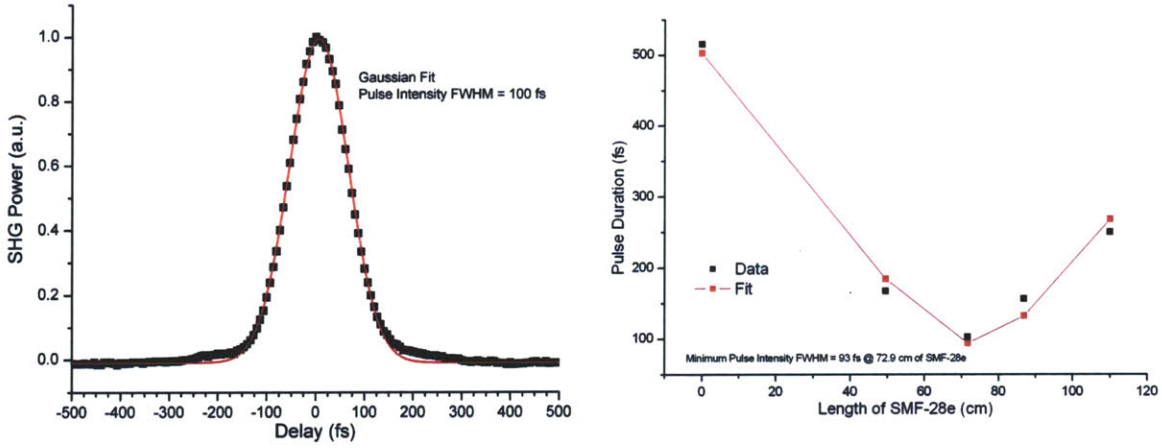

Figure 3-8 Autocorrelation measurement data (black squares) and a Gaussian curve fit corresponding to 100 fs pulses (left). Finding the minimum pulse duration by increasing GVD compensation (right).

The pulse was guided through free space mirrors into a length of single mode silica fiber[19]. The fiber is anomalously dispersive at the 1550 nm wavelength (β_2 = -20.6 fs^2/mm) so it is possible to linearly recompress a normally chirped pulse by passing it through the appropriate length of fiber.

[19] Corning, Inc., Model: SMF-28e

Several pulse width measurements were taken by varying the fiber lengths to the autocorrelator. Figure 3-8 (right) plots the data and curve fit data of the pulse duration as a function of external chirp compensation and points to an optimally compressed pulse of 93 fs using ~-18,000 fs^2 of GVD. The real data point of 100 fs is close to that and within experimental and measurement error.

3.3.1.3 RF Spectra

Figure 3-9 is a trace of the RF spectrum of the laser output. The output light is detected on a DC-biased photo detector[20] and the resulting electrical signal is recorded by a RF spectrum analyzer[21]. The generally flat spectral envelope combined with the smooth optical spectrum of the left side of Figure 3-9 verifies single-pulse operation. The photo detector does not have a perfectly flat frequency response and that is cause for the slight amplitude shaping evident in the plot.

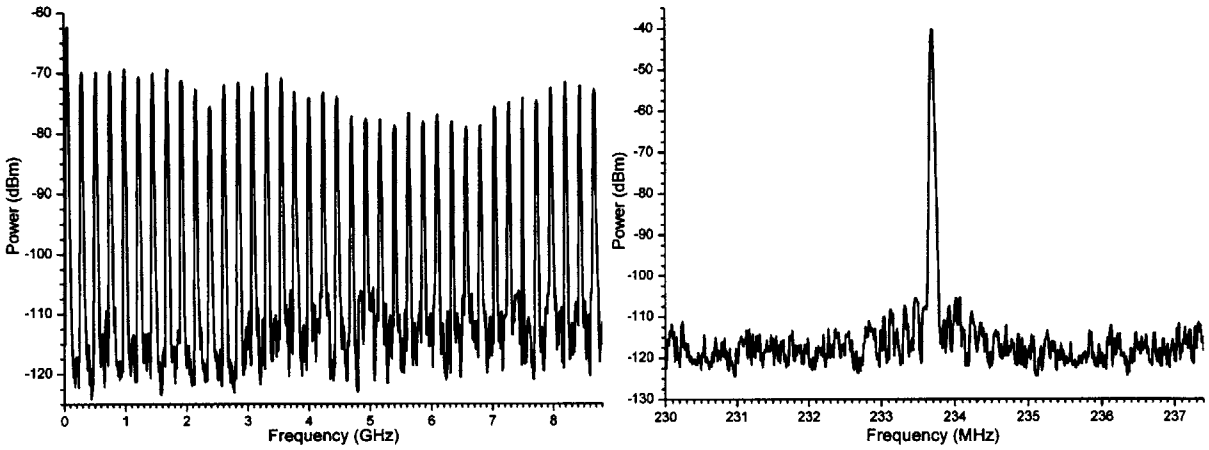

Figure 3-9 Full span RF spectra showing a smooth spectral envelope (left), indicating single-pulse operation and fundamental RF line (right) showing the fundamental frequency.

The right side of Figure 3-9 is an enhanced view of the fundamental frequency of the cavity. The main peak is clean and any noise is suppressed over 50 dB so we can say with

[20] Discovery Semiconductor, Model: DSC-40S, Serial: 402307

[21] Avantest, Model: R3565

confidence that the laser is operating in a single pulse mode-locking state with a repetition rate of just below 234 MHz.

3.3.1.4 Jitter

Recall that an important characteristic of femtosecond lasers is their low pulse-to-pulse timing drift—also known as timing jitter. Chapter 2 explained how jitter was calculated from phase noise data. In this measurement, the 9th harmonic – 2.1 GHz – from the detected RF signal was isolated by a tunable bandpass filter[22] tuned to 2.1 GHz and passed through a RF amplifier[23] before being passed to the signal source analyzer (SSA) [24]. The SSA performs several steps and displays a plot of phase noise as a function of frequency.

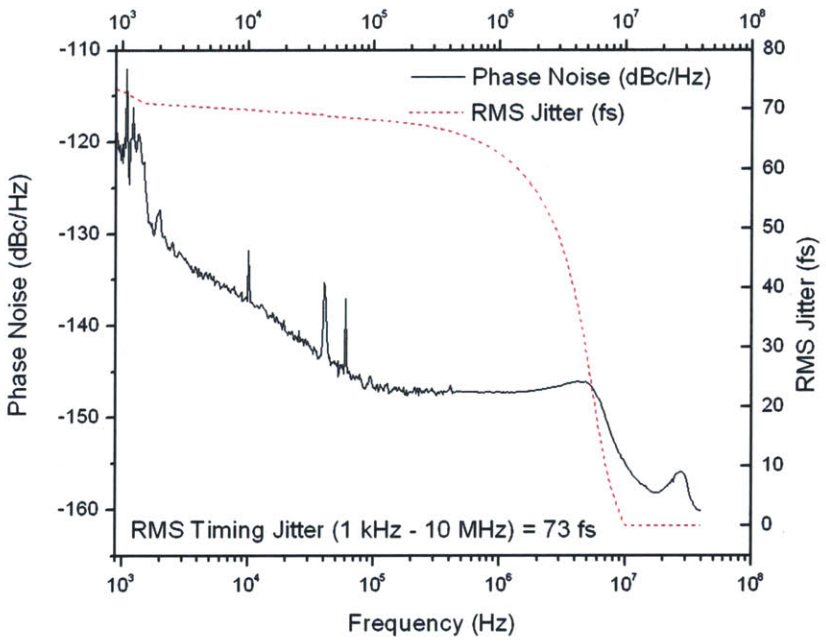

Figure 3-10 Phase noise and RMS timing jitter as integrated from 1 kHz to 10 MHz.

Figure 3-10 plots the phase noise in black and the RMS timing jitter in red. The phase noise was integrated from 10 MHz down to 1 kHz. Integrating this range is a reasonable

[22] Telonic Industries Inc., Tunable bandpass filter Model TTF 1550-5-5EE
[23] Unknown which amplifier was used for this data
[24] Agilent, Model: E5052A

assumption because most noise sources below 1 kHz are removable through electronic feedback techniques and are also likely caused by electronic noise in the filtering and amplifying process to begin with. Noise above 10 MHz is generally below the noise floor of the detection process. Thus, integrating in the range described resulted in sub 100 fs timing jitter measurements for this laser. The plot in Figure 3-10 for example shows a timing jitter measurement of 73 fs.

3.3.1.5 Output Power and Pulse Energy

As configured above, the laser operates at a repetition rate of 234 MHz. The measured average output power is 57.6 mW corresponding to an output pulse energy of 246 pJ. The power measurement is obtained by connecting the collimated fiber output and directing the light into the detector head of an optical power meter[25]. The measured pulse duration full-width half-maximum is 100 fs, and that is reasonably close to the theoretical optical spectrum Fourier transfer limit of 89 fs. Increased efforts to perfectly match the dispersion compensation to what is exiting the laser could have possibly pushed the measured pulse width down to 90 fs but that was deemed an unnecessary undertaking as the data we have is sufficient to verify our claims.

3.3.2 300 MHz Laser

The purpose of this laser is to find the highest possible repetition rate while maintaining single pulse mode-locking operation. This section reports on the performance of the cavity when it is scaled to 300 MHz. Figure 3-11 is a plot of the laser output power and operating states of the 300 MHz configuration as the pump power is varied from zero mW to the maximum 1.2 W. The lasing threshold is approximately 100 mW of pump after which the output power climbs linearly with a continuous wave output. Around 400 mW of pump the intracavity power is high enough to be affected by nonlinear effects of the SBR and fiber and the laser begins to single pulse mode-lock. This state is stable and holds until around 900 mW of pump. At that point there is an excess of energy in the cavity for the

[25] Hewlett Packard Inc., Model: 8152A

single pulse condition and some higher order cavity modes begin to lase as well. This results in a multiple pulsing condition where the frequency comb is no longer stable or flat and the output pulse train is no longer uniform in intensity or timing.

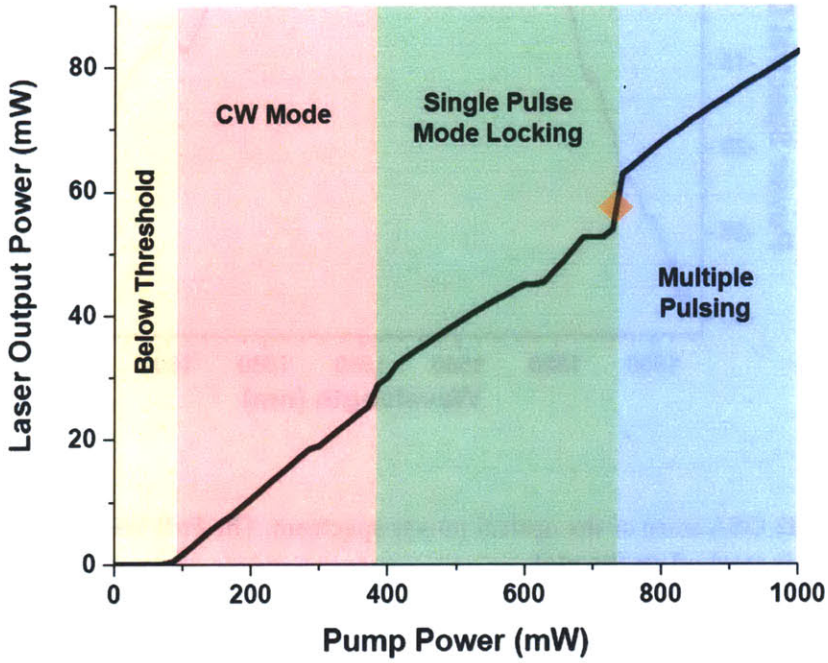

Figure 3-11 Laser operating states and output power for increasing pump power

All of the data presented from this point forward were collected with the laser operating at 61.1 mW—the maximum output power and minimum pulse width obtained while still single pulse mode-locked. This point is marked with an orange diamond in Figure 3-11. The output pulse optical spectrum, RF spectra, autocorrelations, and power measurements of this laser proceed in the same manner and on the same instruments as for the previous system.

3.3.2.1 Optical Spectra

Figure 3-12 is the measured optical power spectrum, which a Fourier transform indicates would support a time domain pulse as short as 84 fs.

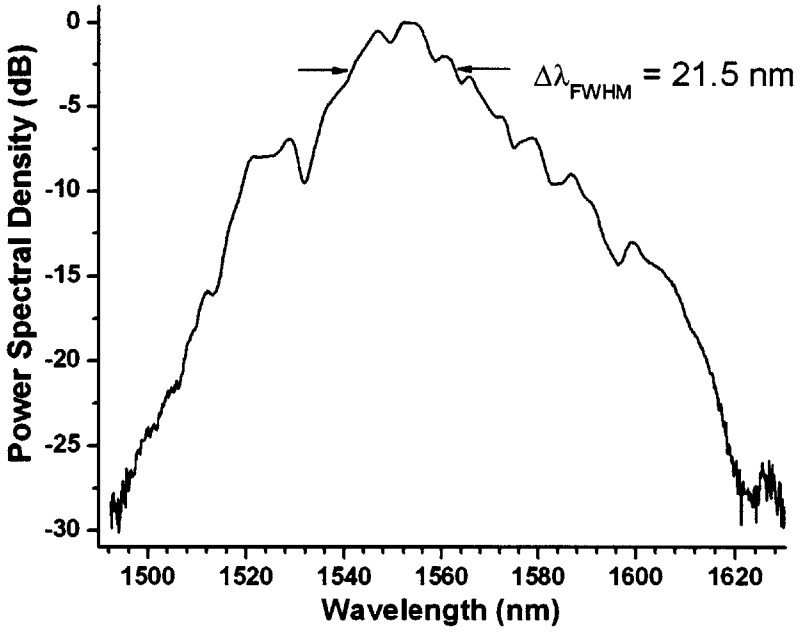

Figure 3-12 OSA trace of the optical power spectrum. The Full Width at Half Maximum (FWHM) is marked on the plot.

Looking at a wider wavelength window indicated no significant power outside this peak. The spectral shape, the absence of resonant sidebands, and the significant normal chirp of the output pulses reinforce that the laser is operating in the stretched-pulse regime. [7]

3.3.2.2 Simulation

Jeff Chen, one of the collaborators and co-authors performed a brief simulation of the pulse width for the 300 MHz laser as it would travel through the dispersive and non-linear effects of the cavity.

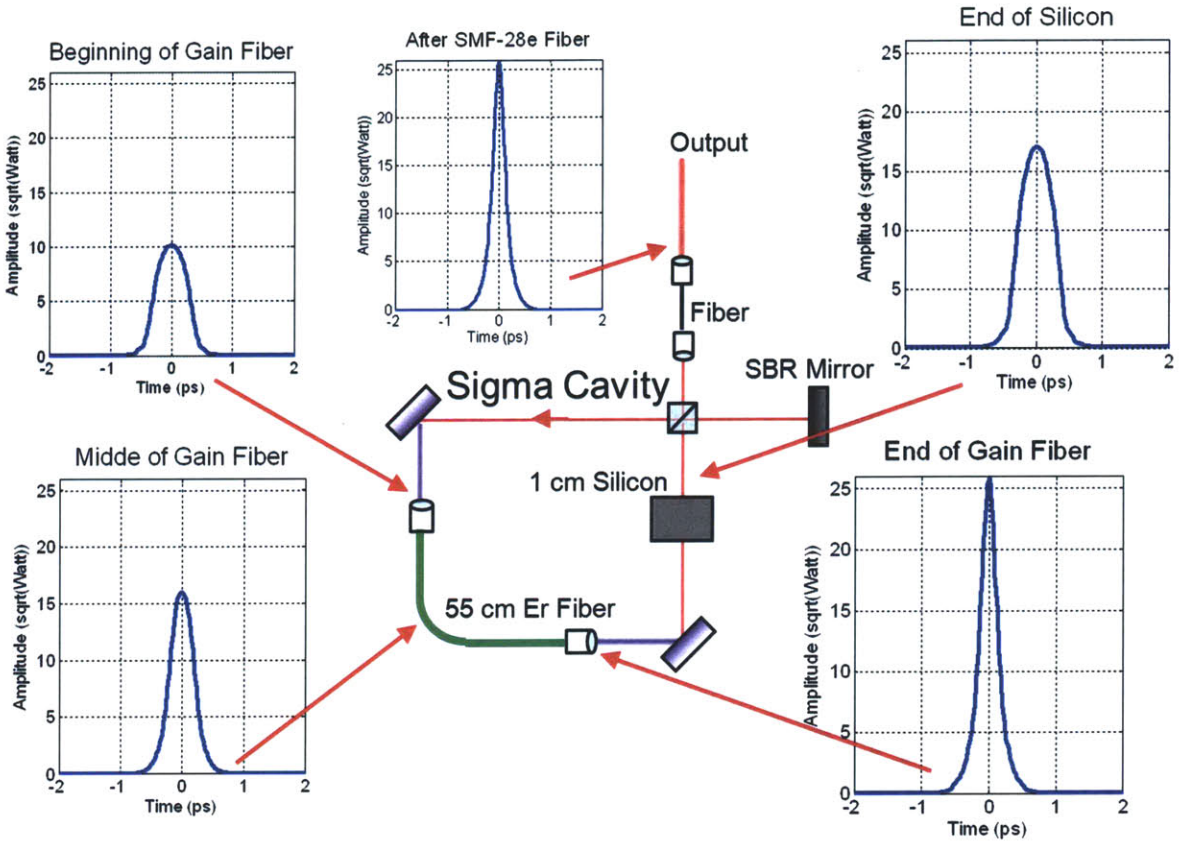

Figure 3-13 Time domain pulse width simulation as energy travels around the cavity.

This simulation is mostly for illustrative purposes as the characteristics of the fiber, SBR, and other elements were not modeled perfectly. The model predicts that the pulse will enter the gain fiber with some amplitude and experience amplification and pulse shortening by the end of the fiber. The highly normally dispersive silicon will broaden the pulse prior to the beam cube but the length of anomalously dispersive fiber in the output will recompress the pulse for measurements. Figure 3-7 from the previous 234 MHz system provided evidence of this in fact being the case because the optical spectrum was broadened as it evolved through the gain fiber. Recall that a broader spectrum correlates to a shorter pulse width in time.

Subsequent measurements of the pulse widths will demonstrate that the pulses are indeed exiting the cavity in a normally chirped state and require recompression to achieve the shortest pulse width measurements.

3.3.2.3 Autocorrelations

Figure 3-14 (left) provides an autocorrelation and Gaussian fit of the shortest observed pulse, which corresponds to a 108 fs pulse. This was obtained using -11,240 fs^2 of GVD to compensate the output pulse chirp. The pulse was again guided through free space mirrors into a length of single mode silica fiber[26]. The fiber is anomalously dispersive at the 1550 nm wavelength (β_2 = -20.6 fs^2/mm) so it is possible to linearly recompress a normally chirped pulse by simply passing it through a length of optical fiber.

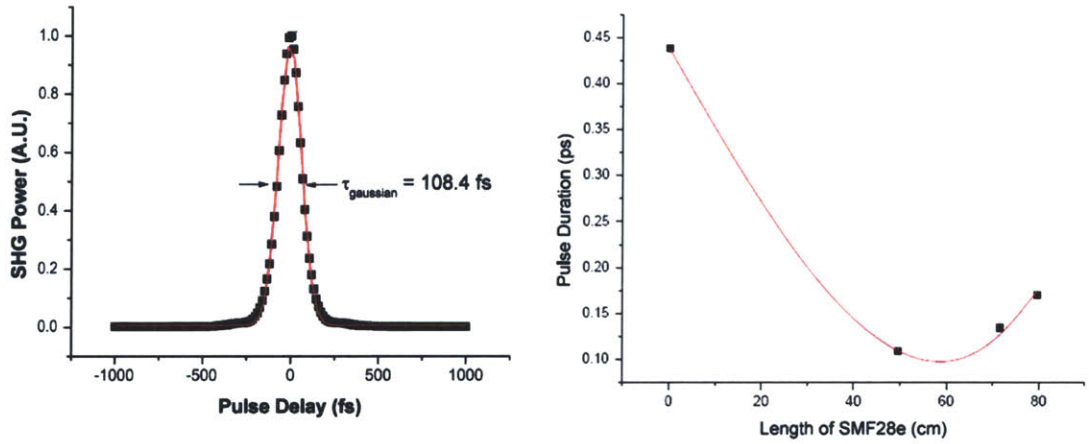

Figure 3-14. (Left) Autocorrelation data with Gaussian pulse shape fit. (Right) Decreasing pulse duration with increasing GVD compensation.

Various lengths of connectorized fibers were available and Figure 3-14 plots some of those pulse width results. The pulse duration data points were obtained from curve fitting autocorrelation traces. The pulse duration versus compensating GVD measurements indicate that perfect dispersion compensation might yield pulses as short as 86 fs. As with the larger system, the extra work necessary to achieve that exact measurement was not necessary to demonstrate the function of the laser.

[26] Corning, Inc., Model: SMF-28e

3.3.2.4 *RF Spectra*

Figure 3-15 shows the RF spectra of the laser output. On the left, the flat spectral envelope, combined with the smooth optical spectrum verifies single-pulse operation. On the right is a tight trace of the 301 MHz fundamental mode beat, which displays greater than 40 dB of noise suppression and provides further evidence of a single-pulsing mode-locked state.

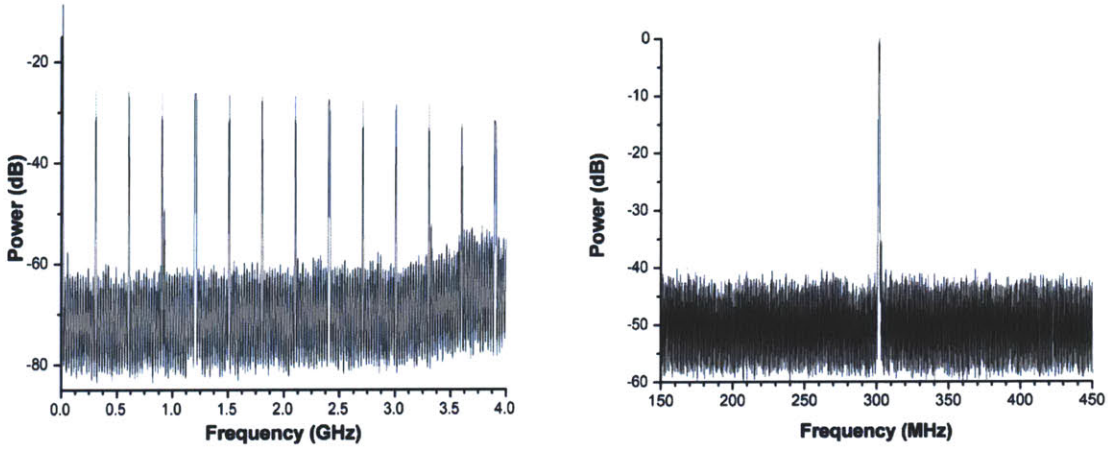

Figure 3-15. Detected RF frequency from DC to 4 GHz demonstrating flat envelope. Detected fundamental RF line. (left) The direct measurement of the repetition rate. (right)

3.3.2.5 *Output Power and Pulse Energy*

By taking the 61.1 mW of measured output power and dividing by the 301 MHz repetition rate, a pulse energy of 203 pJ is demonstrated. This is about 85% the pulse energy of the longer 234 MHz system but that is reasonable due to the shorter length of erbium gain fiber in this cavity and the higher repetition rate.

3.3.2.6 *Jitter*

Using the same measurement technique and instruments as the previous system, the pulse-to-pulse RMS timing jitter of this system is 33 fs if you integrate the phase noise from 1 kHz to 10 MHz. Since laser noise below 1 kHz can be compensated for with feedback

electronics and piezo actuators, the jitter accumulated from those frequencies can be omitted from the reported jitter. Figure 3-16 plots the relevant regions of the phase noise and integrated timing jitter.

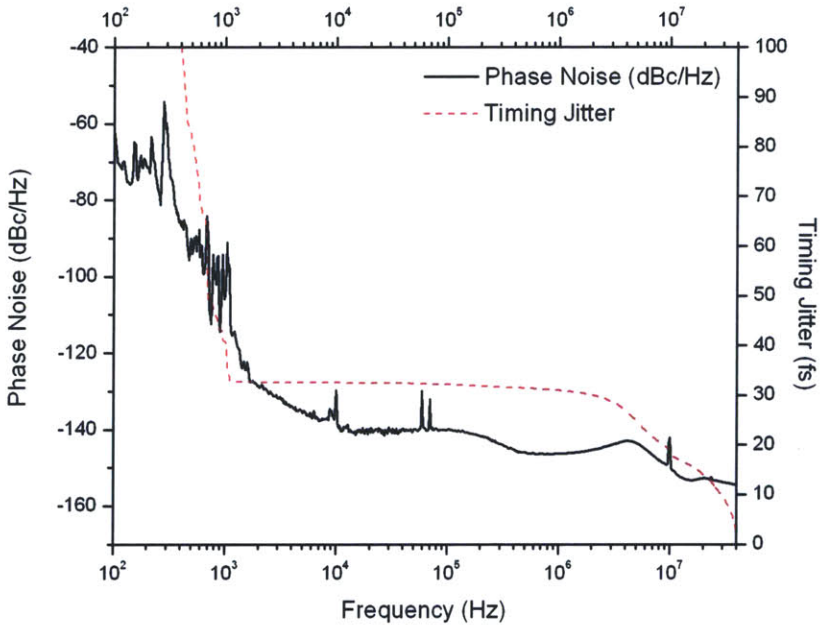

Figure 3-16 The phase noise and integrated RMS timing jitter of the 300 MHz laser.

3.4 Conclusions

In conclusion, this chapter has described the design, construction, and test results of two similar fundamentally mode-locked erbium fiber sigma cavity lasers operating at repetition rates of 234 MHz and 301 MHz, respectively.

The idea of using a sigma cavity enabled longer fiber lengths and a free-space optical section allowing for the in-cavity placement of a semiconductor saturable absorbing mirror. This mirror's properties shortened the pulses being formed out of the continuum enough that the P-APM effects in the gain fiber were able to dominate and shorten the pulse further.

The actual assembly and tuning of the lasers was fairly involved but did not require inventing any new alignment or measurement techniques. Many custom parts did have to be sourced or manufactured to properly hold everything in place but those were solvable challenges.

As for performance, both systems could be pumped and settled into single pulse mode-locking states. Output powers were in the tens of milliwatts and pulse energies were around a couple of hundreds of picojoules which make these laser systems potentially useful as the source light for a variety of laboratory experiments.

Bibliography - Chapter 3

[1] D. Foursa, P. Emplit, R. Leners, and L. Meuleman, "18GHz from a sigma-cavity Er-fibre laser with dispersion management and rational harmonic active mode-locking," *Electronics Letters*, vol. 33, no. 6, pp. 486–488, 1997.

[2] H. A. Haus, E. P. Ippen, and K. Tamura, "Additive-pulse modelocking in fiber lasers," *IEEE Journal of Quantum Electronics*, vol. 30, no. 1, pp. 200–8, 1994.

[3] H. Haus, "Theory of Mode Locking With A Slow Saturable Absorber," *IEEE Journal of Quantum Electronics*, vol. QE-11, no. 9, pp. 736–746, 1975.

[4] G. Spuhler, R. Paschotta, M. Kullberg, M. Graf, M. Moser, E. Mix, G. Huber, C. Harder, and U. Keller, "A passively Q-switched Yb : YAG microchip laser," *Appl. Phys. B-Lasers Opt.*, vol. 72, no. 3, pp. 285–287, Feb. 2001.

[5] J. Chen, J. W. Sickler, E. P. Ippen, and F. X. Kartner, "High repetition rate, low jitter, low intensity noise, fundamentally mode-locked 167 fs soliton Er-fiber laser," *Optics Letters*, vol. 32, no. 11, pp. 1566–1568, 2007.

[6] T. Wilken, T. W. Hansch, R. Holzwarth, P. Adel, and M. Mei, "Low phase noise 250 MHz repetition rate fiber fs laser for frequency comb applications," in *CLEO '07. 2007 Conference on Lasers and Electro-Optics, 5-11 May 2007*, Piscataway, NJ, USA, 2007, pp. 572–3.

[7] K. Tamura, E. P. Ippen, H. A. Haus, and L. E. Nelson, "77-Fs Pulse Generation from a Stretched-Pulse Mode-Locked All-Fiber Ring Laser," *Opt Lett Opt Lett*, vol. 18, no. 13, pp. 1080–1082, 1993.

[8] H. Byun, J. Sickler, J. Morse, J. Chen, D. Pudo, E. P. Ippen, and F. X. Kärtner, "Femtosecond passively mode-locked fiber lasers using saturable Bragg reflectors," in *Ultrafast Phenomena XVI*, vol. 92, P. Corkum, S. Silvestri, K. A. Nelson, E. Riedle, and R. W. Schoenlein, Eds. Berlin, Heidelberg: Springer Berlin Heidelberg, 2009, pp. 768–770.

[9] J. W. Sickler, "High repetition rate mode-locked erbium-doped fiber lasers with complete electric field control," 2008.

[10] J. L. Morse, J. W. Sickler, J. Chen, F. X. Kartner, and E. P. Ippen, "High repetition rate, high average power, femtosecond erbium fiber ring laser," in *2009 Conference on Lasers and Electro-Optics and 2009 Conference on Quantum Electronics and Laser Science Conference, CLEO/QELS 2009, June 2, 2009 - June 4, 2009*, Baltimore, MD, United states, 2009.

[11] K. R. Tamura, "Additive Pulse Mode-Locked Erbium-Doped Fiber Lasers," Massachusetts Institute of Technology, Electrical Engineering and Computer Science, Cambridge, MA, 1994.

[12] F. X. Kaertner, *6.638 Ultrafast Optics - Fall 2008 Class Textbook*. 2008.

Chapter 4 1 GHz Linear Cavity Laser – Free Space SBR

4.1 Introduction

New theoretical research in our group had concluded that existing technologies (such as single mode pump diodes) and components (highly doped fibers, SBR's, etc.) could be combined to attain fundamentally mode-locked multi GHz repetition rate fiber lasers [1]. Based upon the success of other high repetition rate linear fiber lasers in our research group [2], Dave Chao and I initially believed we could construct a 1 GHz fiber laser that would function as a seed oscillator for his frequency comb experiment. That effort was successful and is detailed here in section 4.2, but ultimately it was not the source he used for the 1550 nm fiber frequency comb [3].

Hyunil Byun's linear cavity fiber laser [4] demonstrated that a relatively short length (few tens of millimeters) of Liekki specialty Erbium doped gain fiber (Er-80 – 8/125) could have enough gain to overcome losses and achieve lasing when placed between two mirrors. Moreover, if one of those mirrors was a saturable absorber, pulsed operation was possible. We tried to experimentally determine if similar performance was possible when instead of being end abutted, the SBR was instead free space coupled to the fiber through the uses of lenses.

Metrics used to determine performance of these systems include: the optical spectrum's shape and 3 dB point bandwidth, the RF spectrum's flat harmonic envelope and smooth noise floor around the fundamental harmonic, and the laser's output power. Timing jitter measurements of these experiments were not systematically taken and therefore cannot be reported.

This chapter describes and explains six versions of this short erbium doped fiber, linear cavity, GHz repetition rate laser, free space SBR coupled laser.

- The first generation - free space pumping and output coupling
- The second generation - fiber coupled pumping for SBR experiments

- "L" cavity fiber coupled pump rejection and polarizer test cavity
- Highest possible repetition rate - 1.25 GHz cavity
- Experimental Oxidized SBR test system at 314 MHz
- Second generation - Reengineered with intra-cavity polarizer

Each of these systems will be diagramed, described, and their results analyzed in the following sections.

4.2 Generation One: Free Space Pump and Output

4.2.1 Linear Laser Cavity Design

The first generation linear cavity 1 GHz fiber laser's design is straightforward. The entire optical cavity consists of one piece of optical fiber, two mirrors, and two lenses. Figure 4-1 is a sketch of the initial design for this cavity.

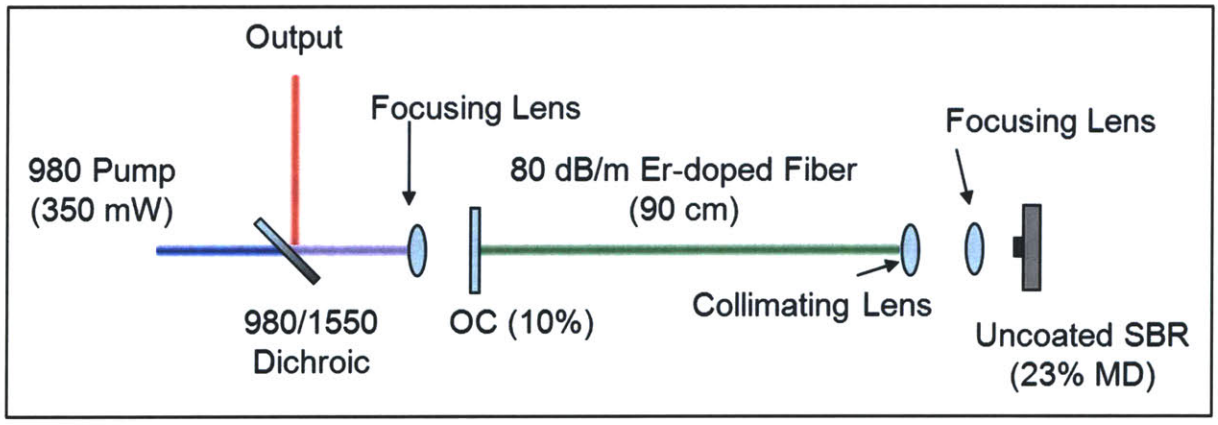

Figure 4-1 Initial test design schematic of a free space coupled linear cavity fiber laser.

There are many practical challenges associated with building this design into a laser. One challenge of a linear cavity is finding the optimal way to insert the pump light into the cavity and extract the signal light out of the pump light's beam path. Free space pumping through a dichroic mirror[27] had worked in the past [5] so we chose to use the same

[27] CVI Melles-Griot, Model: SWP-45-RU1550-TU775-PW-1025

implementation here. There were several other design logistics in figuring out how to turn the ideas of Figure 4-1 into an actual system.

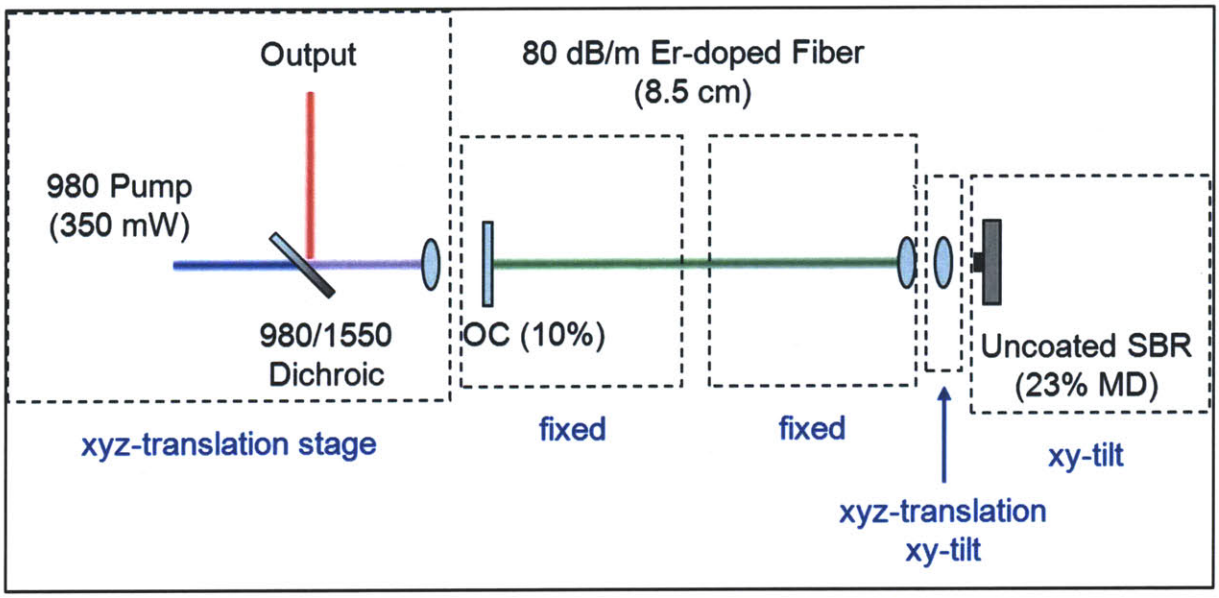

Figure 4-2 Practical stage mount layout of free space coupled linear cavity fiber laser.

As illustrated in Figure 4-2, two sensitive alignments were required to physically couple light into the fiber and then image the other end onto the SBR through two aspheric lenses. It took some trial and error; Figure 4-3 is a photograph of one of our early attempts at mounting the optics. It was known from previous work that mounting the pump collimator, dichroic mirror, and fiber coupling aspheric lens together on the table of a Nanomax™ stage[28] was the best way to align the light into and out of the fiber. This fiber end could be secured in a mount directly tied to the optical board, along with the output coupler and collimator package on the other side. Since the collimator defined the fixed beam path however, the SBR and the focusing lens needed careful mounting to both have the necessary degrees of freedom for adjustment; but also to mechanically fit in the small physical space allocated to those parts.

[28] Thorlabs, Model: MAX312D NanoMax300 with differential drives and piezo adjustment

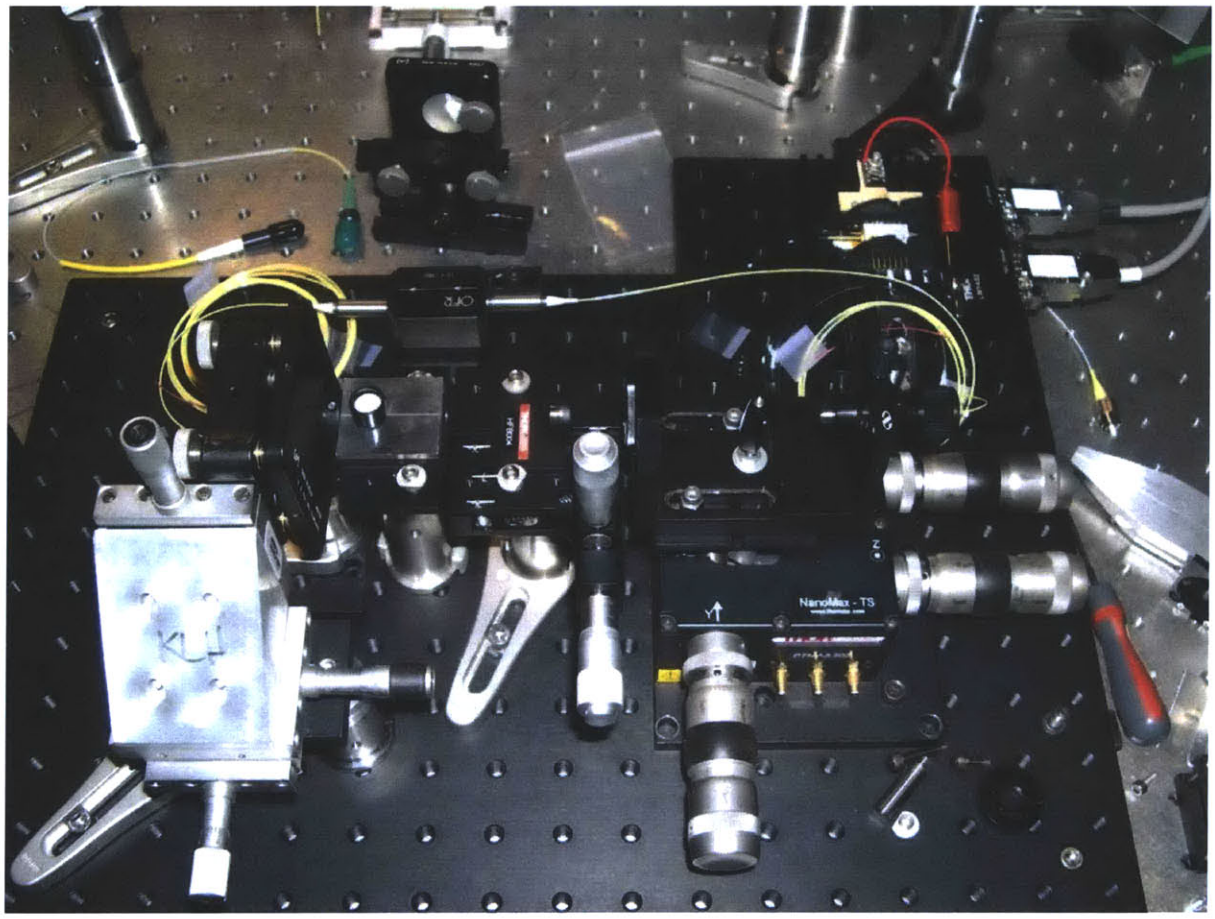

Figure 4-3 Photograph of early attempts to construct the 1 GHz laser design. The fiber is not yet installed, nor is the output coupler.

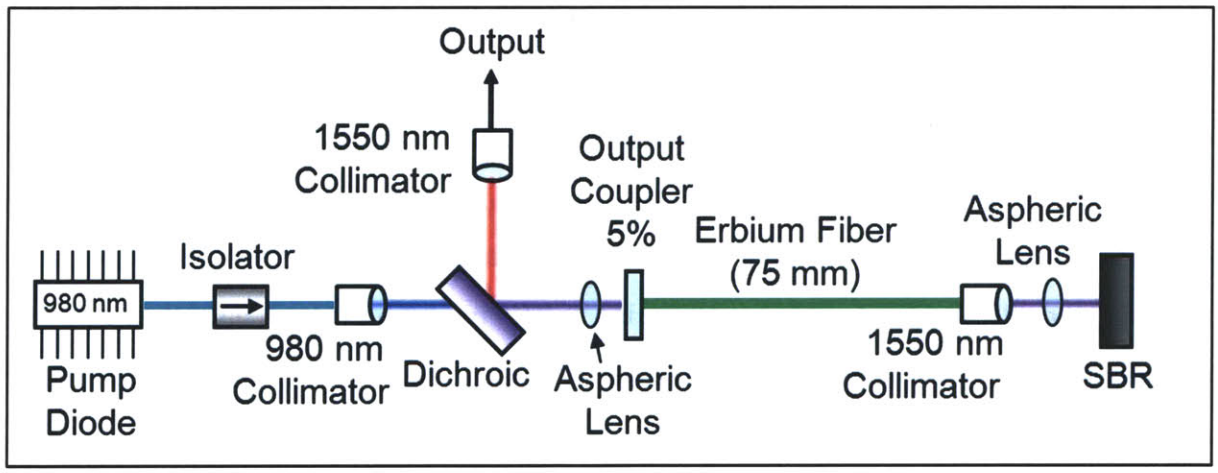

Figure 4-4 Schematic of 1 GHz fiber laser with free space output and SBR coupling.

After several iterations the design was settled upon and built into a working laser. Figure 4-4 is a more complete diagram of the final laser as set up in the laboratory.

This laser is pumped by a single 750 mW 980 nm pump diode[29]. This diode is fusion spliced to a fiber coupled isolator[30] which is subsequently fusion spliced to a 1.064 μm collimating lens package[31]. Including an isolator will reduce the amount of pump energy available by about 20% – 30 % but the benefit is no back reflected light can re-enter the diode and damage or destroy it.

The pump beam is now spatially collimated and passes through the dichroic mirror to the aspheric focusing lens[32]. This lens focuses the 1.5 mm beam (diameter) into a 10 μm spot at the 11 mm focal distance. Eleven millimeters is enough space to fit a thin silica window layered with a 95% reflective / 5% transmitting coating on one side[33]. This coating is referred to as the "output coupler" since it primarily acts as a cavity mirror but it allows a small percentage of the cavity energy to leak out with each reflection.

The end of the erbium doped fiber has been epoxied into an FC/PC connector and carefully polished to a flat surface. The flat surface can be mechanically placed square against the output coupler in an attempt to eliminate any gap in the mirror to fiber interface. Once the pump light has been focused into the fiber core, the erbium atoms begin to absorb and emit photons around the 1550 nm wavelength. This light is waveguided to the end of the 75 mm long fiber and here it is imaged onto a saturable absorbing mirror with two lenses.

The SBR-facing end of the fiber has been epoxied and polished into an angled, or FC/APC connector. This enables the fiber end to be directed screwed into a collimator package[34] that both serves to hold the fiber in place and collimate the beam via its integrated

---

[29] Bookham, Inc., Model: LC96UF74-20R
[30] Thorlabs, Model: IO-F-980
[31] OFR, Model: CFS-T-5-1064
[32] Thorlabs, Model: C220-TME-C
[33] CVI Melles-Griot, Model: PR1-1550-95-0512
[34] Thorlabs, Model: F240FC - 1550

aspheric lens. One more aspheric lens[35] is necessary to focus the 1550 nm collimated light down to a diffraction limited spot on the SBR. This lens pair also compresses the spot size from a 10 μm diameter in the fiber core to a 3.4 μm diameter spot on the SBR. This helps initiate mode-locking by providing a 7 times increase in optical fluence on the SBR with no increase in pulse energy.

Once the saturable absorber influences the pulses by attenuating the lower energy modes in the "wings"; the more intense central part of the pulse travels back down the fiber toward the output coupler. The fiber is short, the pulse energies low, and there is no polarizing element to enable P-APM to occur. However, the fiber still contributes to the pulse shaping. SBR enabled soliton mode-locking is the dominant mechanism in this and all subsequent short, linear laser cavities. Nonlinear effects, primarily self-phase modulation serve to balance the linear effect of anomalous dispersion as the soliton pulse propagates through the fiber.

At the output coupler, 5% of the pulse energy is transmitted through the mirror and out into free space. This light is collimated by the aspheric lens and reflected out of the pump light beam path by the dichroic mirror. At this point, there remains a small portion of the pump light in the reflected beam and the signal can be passed through an anti-reflection-coated silicon window to fully block all remaining 980 nm light that might interfere with the resulting measurements.

4.2.1.1 SBR Choice

The only SBR that worked to mode-lock this laser was the BATOP SAM-1550-35-25.4s. This SBR was high linear loss (35%) but also had a lower saturation fluence (20 μJ/cm^2) and short recovery time (2 ps). Its deep modulation depth of 21% however, is the reason this SBR was able to enable mode-locking behavior in this high loss cavity. Thus, all results obtained for this laser came with SBR in the cavity.

[35] Thorlabs, Model: C330TME-C

4.2.2 Linear Laser Results

Once the full component configuration was carefully aligned, the system was able to achieve a self-starting soliton mode-locked state. Because focusing a free space beam into the core of a single mode fiber is a sensitive procedure, alignment, stability, and repeatability were issues that needed to be addressed. In addition, focusing a beam down to a 3.4 μm spot on the surface of a mirror and getting it to reflect perfectly back upon its incident path also requires special alignment care and techniques. Initial results for the power output of the laser are plotted in Figure 4-5.

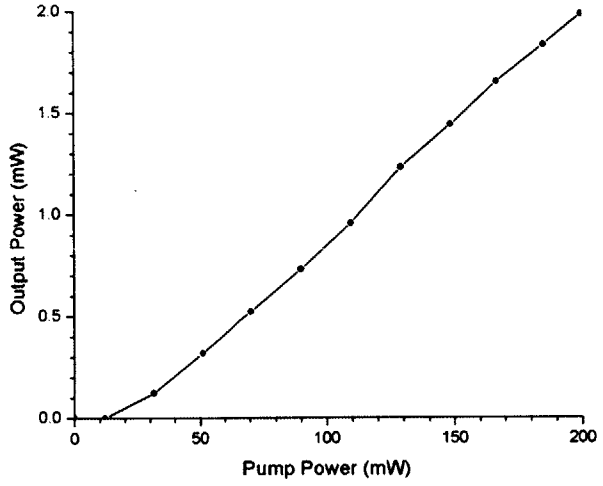

Figure 4-5 Laser operating efficiency. Note the laser threshold at ~10 mW of pump and the steady linear trend in the data.

Overall, the system operated at 1% efficiency and had a continuous-wave lasing threshold of 10 mW of pump power. The output power was low due to the large intra-cavity losses inherent in the design that images the fiber end on a mirror.

The state detailed in the rest of this section was taken at full pump power of the single diode—approximately 200 mW of pump power into the fiber after isolator and coupling losses.

4.2.2.1 *Optical Spectra*

The free space coupling and SBR interfaces meant this laser had large losses and as such it did not settle into a mode-locked state.

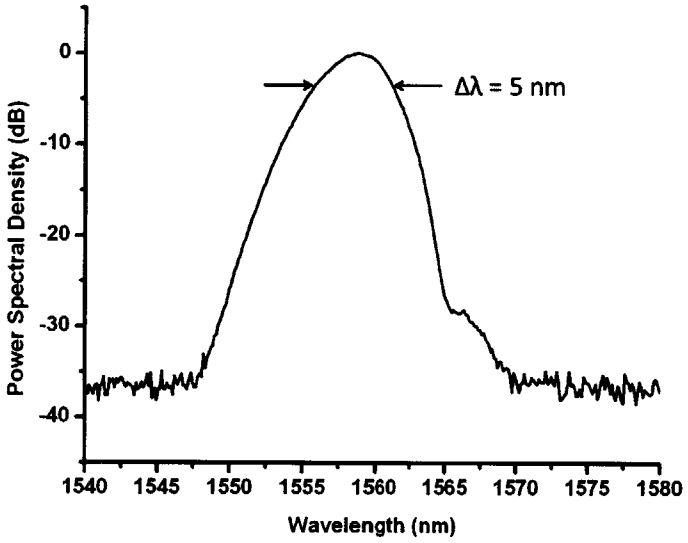

Figure 4-6 Optical spectrum of the best performing mode-locked state.

For example, the optical spectrum of Figure 4-6 is not symmetrical about the center wavelength of 1560 nm. This may be due to wavelength dependent filtering by the gain window or one of the components in the optical cavity. This state sustained a 3 dB bandwidth of 5 nm which corresponds to 510 fs transform limited pulse widths.

4.2.2.2 *RF Spectra*

Next the output beam was collected and detected by a photodetector for RF spectral analysis. The left plot of Figure 4-7 plots the clean and flat harmonic beat lines demonstrating that single pulse mode-locking is occurring.

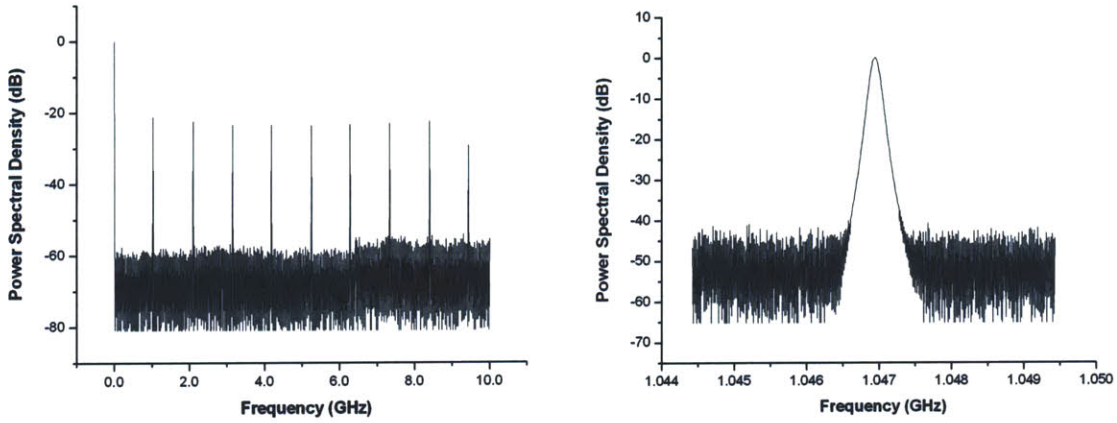

Figure 4-7 Full span RF spectra (right) and Fundamental RF line (right) for the best performing mode-locked state.

Enhancing the fundamental frequency on the right side of Figure 4-7 reveals a cavity repetition rate of 1.047 GHz. The line appears broadened in the figure because the data was saved on a RF spectral analyzer with an incorrect setting for the resolution bandwidth. Unfortunatley this is the only recorded data avalible for this laser in this state. Looking at the lines in the long range plot clearly shows sharp peaks with no sidebands or broadening and the fundamental line data would have as well had the resolution bandwidth been set narrower.

4.2.2.3 Output Power / Pulse Energy

In its optimal operating state the laser produced approximately 2 mW of 1560 nm output power. The laser is just above a 1 GHz repetition rate so that corresponds to 2 pJ pulse energies. The pulses were estimated to be ~500 fs in duration based upon the OSA trace data. This was an experimental system that we did not fully characterize before redesigning, thus autocorrelations or timing jitter measurements were not taken of this state.

4.2.3 Discussion

The objective was to take some of the ideas from previous high repetition lasers our group had built and see if a 1 GHz linear cavity fiber laser could be built. After design

tweaks and testing, a mode-locked state was obtained with an OSA measured spectral width of 5 nm and a repetition rate of 1.047 GHz. Two milliwatts of output power were possible from 200 mW of input power. This 1% efficiency is mostly due to the high coupling losses in the cavity and the high linear losses of the SBR that was needed to mode-lock the laser. The next generation design optimizes the input coupling losses leading to a test platform for different SBR mirrors.

4.3 Generation Two: Fiber Coupled Pump and Output

4.3.1 Laser System Design

The entire pumping and output coupling parts of the system changed for generation two of the GHz linear cavity free-space SBR-coupled fiber laser. This fiber coupling is a large improvement on the coupling losses the free space setup experienced. The initial ideas for this design were first documented by Jeff Chen in his Ph.D. thesis [6]. Figure 4-8 is the schematic of the entire system.

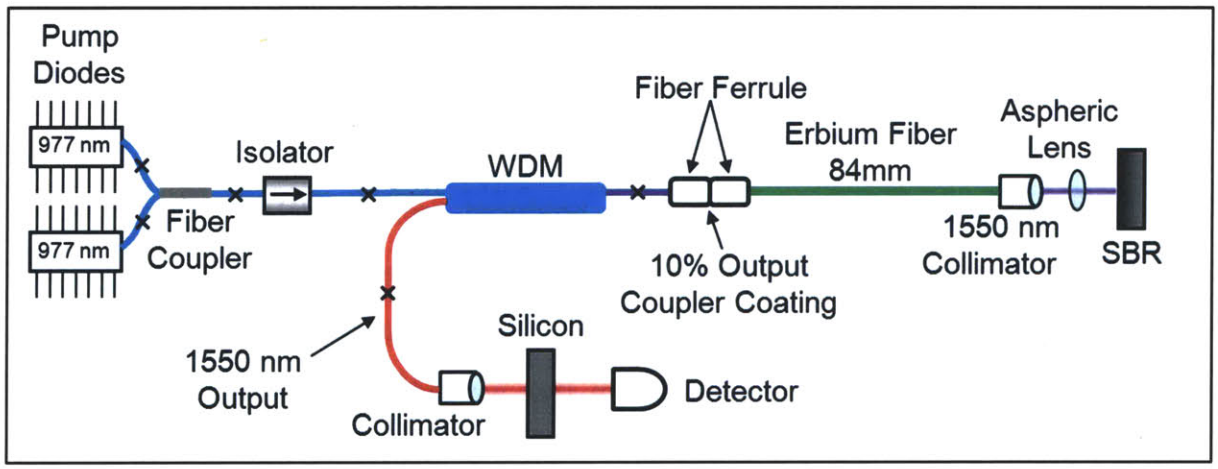

Figure 4-8 Schematic of the fiber coupled free space SBR 1 GHz linear cavity fiber laser.

4.3.1.1 The Pump

Since this laser was to be a test system for the performance of commercial and new in-house designed and fabricated saturable absorber mirrors, it needed more power than the first generation system had. Single mode pump diodes were still limited to approximately 600 mW of power, so we used two of them[36]. It is possible to take two single mode pump diodes and combine their power into the core of a single fiber as long as they couple into orthogonal polarization modes of the fiber. This is accomplished by fusion splicing the polarization maintaining fiber's fast axis to fast axis for one diode and fast axis to slow axis for the other one. These splices are made to the input pigtails of an all-fiber polarization combiner[37]. The output fiber of the device has both diodes' light traveling down the same single mode core in orthogonal polarizations.

Now that all 1.2 W of our pump light is in the polarization maintaining (PM) fiber, it can be spliced to a fiber-coupled isolator[38]. This isolator happens to use non-PM fiber but that is acceptable for our application of non-PM erbium fiber pumping. The isolator is a necessary part that prevents any pump or signal light from back reflecting into the pump diodes possibly damaging or destroying them. Unfortunately, the isolator also reduces the pump power available by about 20%. This combined with the slight losses at all of the fusion splice points means that the real, available 980 nm pump power is limited to approximately 800 mW. This level of pump power is usually sufficient for the testing purposes of this laser as there was typically still more available pump at powers where the mode-locking states would begin to break down.

4.3.1.1.1 Pump Diode Characterization

The 660 mW JDSU single mode 977 nm pump diodes used to pump the laser are designed to be stable and linear as long as the drive current is within a manufacturer specified range. For these diodes, that range was ~35 mA for the laser threshold up to 1200

---

[36] JDSU, Model: 30-7602-600

[37] SIFAM Fibre Optics (via Optimark Fiber Optics), Model: FFP-5M3280G10

[38] OFR, Model: IO-F-980

mA for the maximum stable operation. Since two diodes are being used to pump the laser cavity, the question was raised as to how linear the combination of these diodes really is. A test was done to ascertain this information.

First, a high reflecting, non-saturable absorbing 1550 nm mirror was placed at end of the cavity so there would be no Q-switching and no power artifacts from attempts at mode-locking in the output. Then, for the "serial" test the first diode was brought up to full power before the second diode was turned on and also brought up to full power. Figure 4-9(a) plots the laser's 1550 nm output power for this test. Next, for the "parallel" test both diodes were slowly stepped up in current together up to their maximum stable output power. Figure 4-9(b) plots the results of the parallel test.

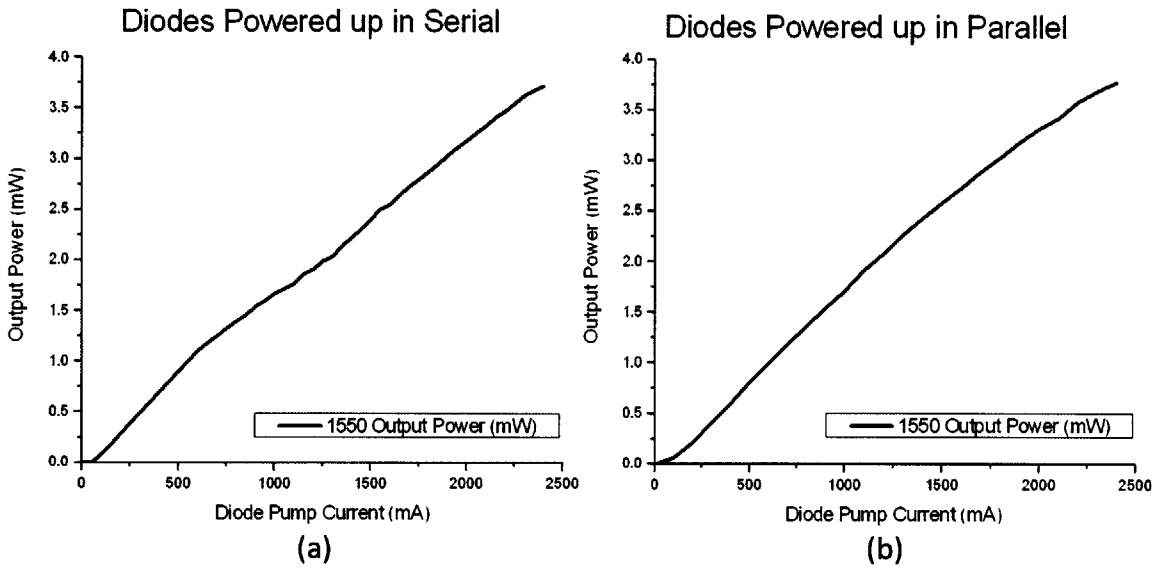

Figure 4-9 Dual pump diode operation experiment. The output power was measured out of the CW laser where a 1550 nm high reflecting mirror was in the position of the SBR.

Fortunately, both diodes performed linearly as designed and the results do not show much difference between the two pumping methods. Yes, there is a slight concavity to the output power for the first diode in the serial test and a very slight concavity to the entire curve in the parallel test but linear fits of each data set had R^2 values of over 0.99. The conclusion is that the pump diodes are linear and it does not matter if they are used in a serial or parallel manner.

4.3.1.2 *The Coupling*

The next important change that makes this fundamentally more of a "fiber" laser is the use of a wavelength division multiplexer (WDM) as the input/output coupler. This WDM is constructed to allow 980 nm light to stay in the same fiber and pass right through the device with essentially no loss. 1550 nm light, however, is evanescently coupled from the combined port fiber to the 1550 mode fiber, again with very little loss. Practically, this means that one fiber can bring both the pump light to and the output light away from the cavity's output coupler. In addition, the output light can be separated and measured without the free space optical losses of the previous system's dichroic mirror.

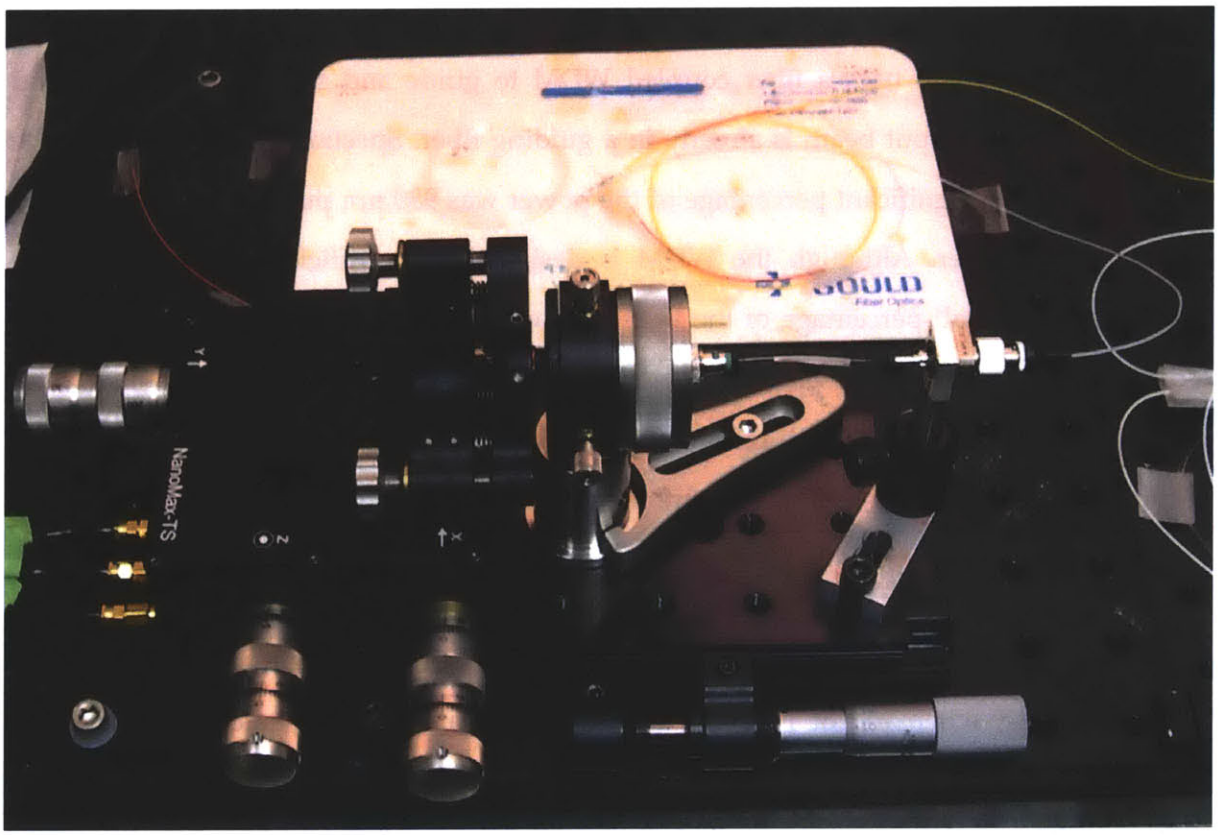

Figure 4-10 Photograph of fiber coupled free space SBR 1 GHz linear cavity fiber laser.

Figure 4-10 is a photograph of the setup that shows clearly the WDM and fiber coils that guide the pump and signal light. The small blue cylinder in the top center of the white

card is the WDM package and the white fiber leading to the suspended piece of gain fiber is the input/output fiber with the output coupler coating.

That fiber and coating is the second advance this system has over the free space coupling system. Instead of using a free space optic consisting of a silica glass window and a partially reflective coating to serve as a cavity end mirror and output coupler; we had the coating deposited directly on to the polished end of a standard FC/PC single mode fiber. The coating layers were designed to allow 10% of the light at the 1550 wavelength to be transmitted and the remainder of the power to be reflected. As a result, we have a fixed 10% output coupler with excellent mechanical alignment and repeatability for any future fiber coupled lasers which use this input/output scheme.

One final note about the new WDM design involves the output beam. Since this generation-two design uses a fiber coupled WDM to guide and separate the pump and signal beams, the output beam is already in a guiding fiber. Spectral measurements of the output revealed a significant percentage of the power was 980 nm pump light that coupled into the signal fiber. Although the WDM is designed to be efficient at separating the wavelengths, a small percentage of the light does cross couple and in this case that really did matter as our signal was on the order of 1% of our pump power. Figure 4-8 illustrates how this was addressed—an anti-reflection coated silicon window was simply placed in the output beam path prior to further measurements being taken.

4.3.1.3 The Cavity

The fiber and SBR end of the schematic in Figure 4-8 appear identical to the fiber and SBR end of the schematic of Figure 4-4. But the actual opto-mechanical setup is very different. These differences were implemented to simplify alignment, enhance the ability to exchange SBR's, and decrease the cavity losses as much as possible.

The same fiber (Liekki Er-80 – 8/125) is used with similar connectorization—the ceramic core of an FC/PC connector on the input end and a complete FC/APC connector on the SBR end to eliminate back reflections. Instead of holding the flat polished fiber connector against an output coupling optic we only have to slide the FC/PC core into a standard

ceramic fiber mating connector until it makes contact with the input/output fiber screwed into the other side. Figure 4-10 shows the two fibers mated in the connector.

One advantage this design has over the end abutted SBR cavity is the short section of collimated light between the two focusing lenses. This space allows the flexibility to fine tune the repetition rate to anything within the physical limits of the lenses physically touching or the beam diverging so much that it doesn't focus onto the SBR properly. The generation one design did not have the ability to take advantage of this degree of freedom without misaligning the focal length of the SBR lens. This design integrates a linear translation ring[39] into the mount that holds the screw in collimation package. The 4 mm travel range corresponds to a repetition rate tuning bandwidth of 27.5 MHz.

The translation ring is attached to the frame of the aspheric focusing lens mount[40]. This mounting system was chosen because it eliminates some of the alignment variations seen in the generation one design. The collimating lens and the focusing lens are held parallel to each other within the constraints of the machined tolerances. The LM1XY mount is designed to center a lens normal to a collimated beam and it does it well with the proper thread adaptor rings.

4.3.1.4 The Saturable Bragg Reflector

One further challenge was to enable a simple exchange of SBR mirrors without disturbing the other critically aligned components. The LM1XY mount also serves to anchor the end of the fiber and the lenses to the long range translation stage bolted to the optical breadboard. As seen in Figure 4-10, the other end of the fiber is also bolted to this stage. Therefore, the stage allows the entire laser to be moved several centimeters away from the SBR without losing any other alignments or risking damage to the delicate fiber. The nature of this design also means that this stage adjustment screw also provides for course adjustment of the focal plane of the aspheric lens.

---

[39] Thorlabs, Model: SM1ZM non-rotating zoom housing

[40] Thorlabs, Model: LM1XY translating lens mount

For fine SBR position adjustments, a precision tip/tilt mount[41] is mounted to a high resolution 3-axis stage[42]. This stage is also connected to the optional piezo controller unit[43] that enables sub-micron position movements via piezoelectric actuators in the stage. The tight spot of the 3.1 mm focal length lens necessitated having this fine level of control, especially in the axial, or "Z" direction of motion.

At the mirror mounting end of the cavity, the SBR samples are mounted to 1" or ½" diameter copper blocks with either silver epoxy or double sided tape. These blocks hold the mirror and help dissipate the thermal load on the chip (when attached with silver paste). The 1" mounting blocks are directly mounted in the Ultima and a ½" to 1" adaptor ring is needed if the block is small. An involved alignment procedure was developed to ensure the mirror surface was properly normal to the incident beam and it was found that this was the most critical step in lowering the coupling losses within the laser cavity.

4.3.1.5 SBR's Tested

The purpose of the first generation laser was to see if a 1 GHz cavity was even possible with this type of fiber and configuration. The purpose of the second generation cavity was to learn how different SBR's affected the cavity dynamics and ultimately give us information to design the optimal SBR's for our lasers. Table 4-1 is a full summary of the specifications of the SBR's tested.

---

[41] Newport, Model: U100-A2K Ultima clear edge mirror mount

[42] Thorlabs, Model: MAX312D NanoMax300 with differential drives and piezo adjustment

[43] Thorlabs, Model: MDT693A Open-Loop piezo controller

Table 4-1 Saturable absorbers tested and their performance characteristics.

SBR Identifier	Linear Loss	Modulation Depth	Saturation Fluence	Recovery Time
SAM-1550-09-25.4s	9%	6%	50 $\mu J/cm^2$	2 *ps*
SAM-1550-20-25.4s	20%	12%	50 $\mu J/cm^2$	12 *ps*
SAM-1550-23-25.4s	23%	14%	25 $\mu J/cm^2$	2 *ps*
SAM-1550-35-25.4s	35%	21%	50 $\mu J/cm^2$	2 *ps*
VA86	1.1%	3.9%	11 $\mu J/cm^2$	9 *ps*
VA86 PRC	1.1%	12%	3.7 $\mu J/cm^2$	9 *ps*
VA147	8%	7.5%	4.7 $\mu J/cm^2$	10.5 *ps*
VA148	6.2%	4%	5.4 $\mu J/cm^2$	10.5 *ps*

4.3.2 Second Generation Linear Laser Results

The generation-two free-space SBR 1 GHz linear cavity erbium fiber laser system performed, in general, better than the generation-one system. Its purpose was to test different SBR's. Results from the eight different mirrors are detailed in this section.

4.3.2.1 BATOP 21% Modulation Depth

It is reasonable to assume that the same mirror that worked in the first generation laser would also enable mode-locking in the lower loss improved version. So the BATOP SAM-1550-35-25.4 mirror was aligned in the cavity and the pump power slowly brought up. It did yield a mode-locking state and representative examples of the results are discussed in the following sections.

4.3.2.1.1 Optical Spectrum

A range of optical spectra were recorded, Figure 4-11 plots the optimal laser state, as achieved with 214 mW of pump power. This spectrum is more symmetric than the generation-one spectrum (recall Figure 4-6) but it still retains slight attenuation in the longer wavelengths.

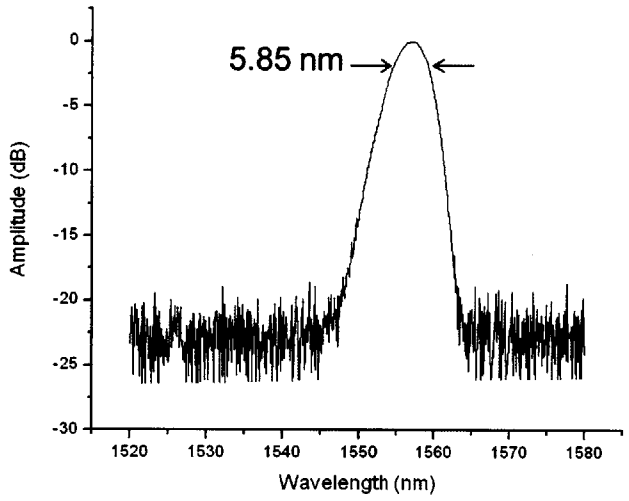

Figure 4-11 Optical Spectrum for 1 GHz laser with BATOP 21% modulation depth SBR.

The 5.85 nm 3 dB bandwidth centered at a wavelength of 1557 nm corresponds to a transform limited pulse duration of 436 fs. No autocorrelation traces were taken of this state.

4.3.2.1.2 RF Spectra

The multi-harmonic "long-range" detected RF spectrum for this state is plotted on the left side of Figure 4-12. There is a low frequency spike that can be attributed to noise in the detection system. Overall, the envelope of the fundamental and subsequent harmonic frequencies is flat indicating single-pulse mode-locking operation.

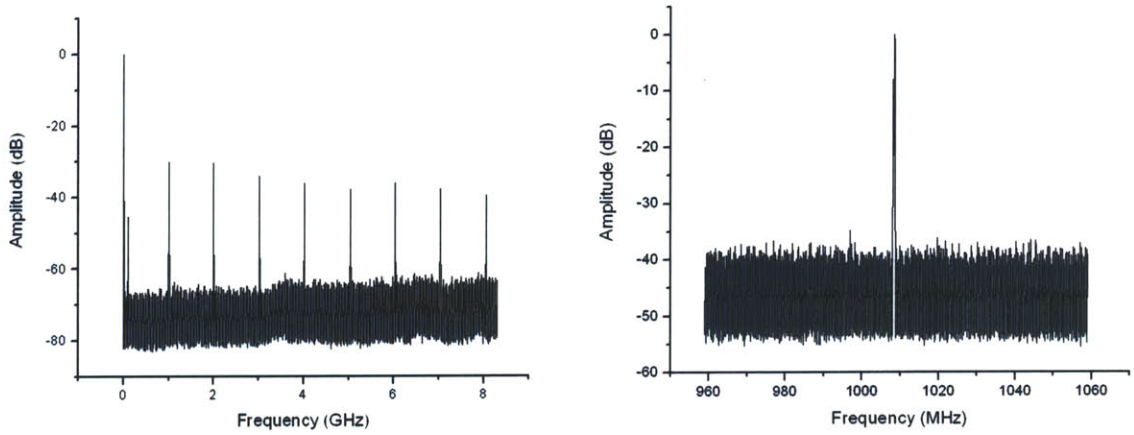

Figure 4-12 Long range RF spectrum (left) and fundamental RF line (right) for 1 GHz laser with BATOP 21% modulation depth SBR.

Enhancing the plot of the fundamental frequency we arrive at the right side of Figure 4-12. Here we see measured evidence that the laser repetition rate is a clean 1.009 GHz.

4.3.2.1.3 Output Power / Pulse Energy

The generation-two linear cavity, free-space SBR-coupled, erbium fiber laser mode-locked with the 21% SBR BATOP SAM-1550-35-25.4. For a pump power of 214 mW this laser output 1.06 mW of 1550 nm light. This corresponds to a pulse energy of 1.05 pJ and an efficiency of 0.5%.

4.3.2.1.4 SBR Burning

For this high loss SBR the upper limit on output power and performance appeared to be SBR failure in the cavity. As the pump was increased beyond 214 mW the output power plummeted and the laser fell out of mode-locking. Upon microscope inspection of the mirror however, no visible damage was found and the previous mode-locking states could be regained by moving to a new focal spot on the mirror. This became a trend that held through the entire SBR study.

4.3.2.2 BATOP 14% Modulation Depth

Following the successful 21% modulation depth BATOP SBR test, the BATOP SAM-1550-23-25.4 mirror was placed and carefully aligned in the cavity. This mirror, as specified in Table 4-1, has less linear loss and a lower modulation depth. The assumption going into the test was that the output powers would be higher because of the reduced cavity losses. The question was: would the modulation depth be enough to enable mode-locking. It turned out it was, and the results of the broadest spectral bandwidth state are detailed in the following sub-sections.

4.3.2.2.1 Optical Spectrum

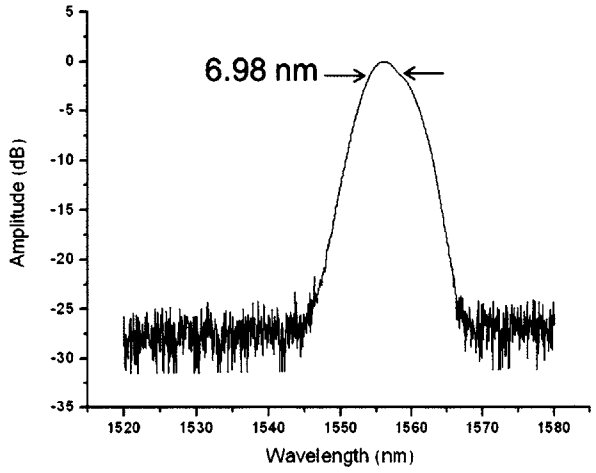

Figure 4-13 Optical Spectrum for 1 GHz laser with BATOP 14% modulation depth SBR.

Once the laser achieved mode-locking, the optimal laser state was located and recorded. For this SBR that was achieved with 400 mW of pump power. The shape seen in Figure 4-13 is somewhat narrow in the wings relative to a sech spectrum and asymmetry near the peak but overall it is a spectrum indicative of a mode-locking state.

The 6.98 nm 3 dB bandwidth centered at a wavelength of 1556 nm corresponds to a transform limited pulse duration of 365 fs. No autocorrelation traces were taken of this state.

4.3.2.2.2 RF Spectra

The multi-harmonic "long-range" detected RF spectrum for this state is plotted on the left side of Figure 4-14. Overall, the envelope of the fundamental and subsequent harmonic frequencies is flat indicating single-pulse mode-locking operation. The low frequency noise sidebands are still present and some of them are attributed to vector soliton behavior and others to the detection setup.

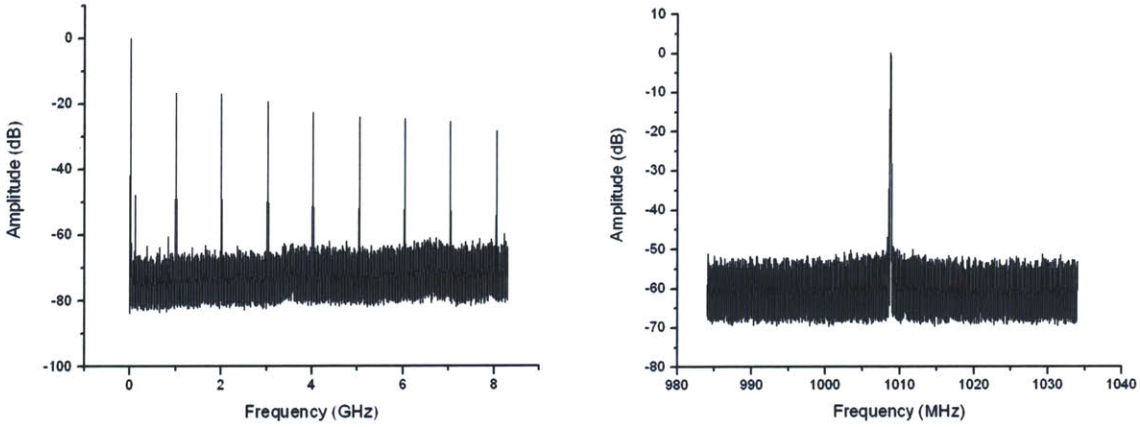

Figure 4-14 Long range RF spectrum (left) and fundamental RF line (right) for 1 GHz laser with BATOP 14% modulation depth SBR.

Fortunately, the vector solitons could be minimized through cavity manipulation and the trace of the fundamental frequency (1.009 GHz) is plotted on the right of Figure 4-14.

4.3.2.2.3 Output Power / Pulse Energy

The generation-two linear cavity, free-space SBR-coupled, erbium fiber laser also mode-locked with SBR BATOP SAM-1550-23-25.4. Given a pump power of 400 mW this laser output 2.80 mW of 1550 nm light for a pulse energy of 2.78 pJ and an efficiency of 0.7%.

4.3.2.3 BATOP 12% Modulation Depth

Following the successful 14% modulation depth BATOP SBR test, the 12% BATOP SAM-1550-20-25.4 mirror was then placed and carefully aligned in the cavity. This mirror, as specified in Table 4-1, has yet again less linear loss and a slightly lower modulation depth. However, the important difference between this SBR and the 14% SBR is both the saturation fluence and the recovery time. The 12% SBR needs twice the fluence to saturate and initiate pulse shaping effects. Also, the recovery time is much longer for this mirror so its effects at filtering continuum modes will be reduced compared to the other BATOP mirrors. We did not know if these effects would inhibit mode-locking but the experiment revealed that they did not. The results of the broadest spectral bandwidth state are detailed in the following sub-sections.

4.3.2.3.1 Optical Spectrum

Once the laser achieved mode-locking, the optimal laser state was located and recorded. For this SBR that was achieved with 336 mW of pump power. The spectrum plotted in Figure 4-15 is centered at 1557 nm and has the same narrow shape as the other BATOP mirrors. There is less asymmetry near the peak and overall it is a spectrum indicative of a solid mode-locking state.

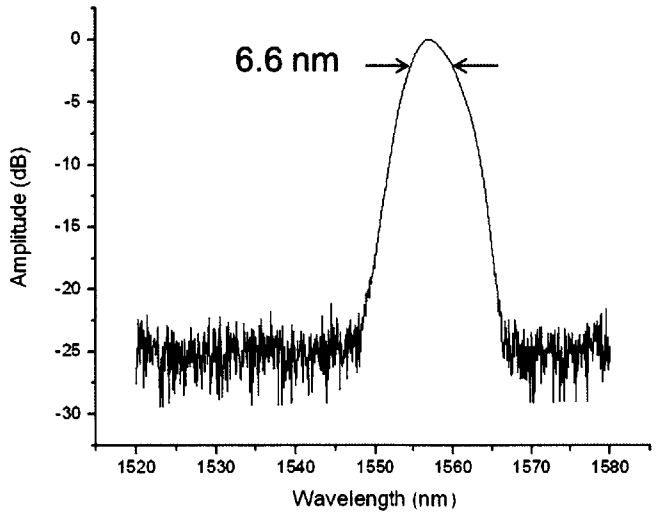

Figure 4-15 Optical Spectrum for 1 GHz laser with BATOP 12% modulation depth SBR.

The 6.60 nm 3 dB bandwidth centered at a wavelength of 1557 nm corresponds to a transform limited pulse duration of 386 fs. No autocorrelation traces were taken of this state.

4.3.2.3.2 RF Spectra

The multi-harmonic "long-range" detected RF spectrum for this state is plotted on the left side of Figure 4-16. Overall, the envelope of the fundamental and subsequent harmonic frequencies is flat indicating single-pulse mode-locking operation.

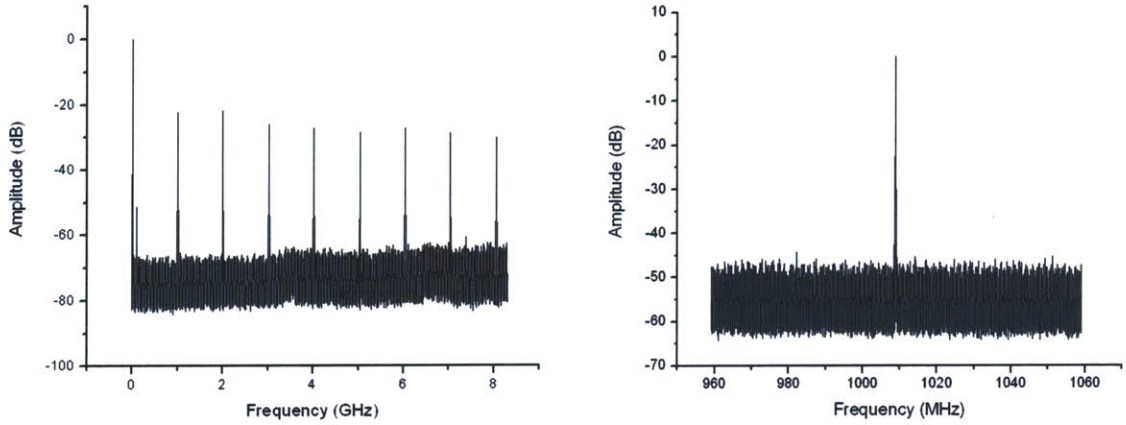

Figure 4-16 Long range RF spectrum (left) and Fundamental RF line (right) for 1 GHz laser with BATOP 12% modulation depth SBR.

As the laser length has not changed between tests, the repetition rate remains a solid 1.009 GHz and the right hand plot of Figure 4-16 confirms that nicely. Also, the 50 dB suppression of any sidebands confirm that any vector soliton effects have been eliminated for this state as well.

4.3.2.3.3 Output Power / Pulse Energy

The generation-two linear cavity, free-space SBR-coupled, erbium fiber laser also mode-locked with 12% SBR BATOP SAM-1550-20-25.4. Given a pump power of 336 mW this laser output 1.75 mW of 1550 nm light for a pulse energy of 1.73 pJ and an efficiency of 0.5%.

4.3.2.4 BATOP 6% Modulation Depth

The final BATOP SBR tested had only 6% modulation depth. Following the successful 12% modulation depth BATOP SBR test, the BATOP SAM-1550-09-25.4 mirror was then placed and carefully aligned in the cavity. This mirror, as specified in Table 4-1, has yet again less linear loss and a lower modulation depth. It has the same higher saturation fluence as the 12% mirror but less loss and the faster, 2 ps recovery time. It was hoped that reducing the loss of the mirror would increase the intra-cavity power and enable stronger soliton effects for shorter pulses but unfortunately that was not the case. Results of the broadest spectral bandwidth state are detailed in the following sub-sections.

4.3.2.4.1 Optical Spectrum

Once the laser achieved mode-locking, the optimal laser state was located and recorded. It took the maximum pump power of 740 mW to obtain this state. The spectrum plotted in Figure 4-17 is centered at 1556 nm and is much narrower than the state the other BATOP mirrors produced. At least it is still a clean spectrum indicative of a mode-locking state.

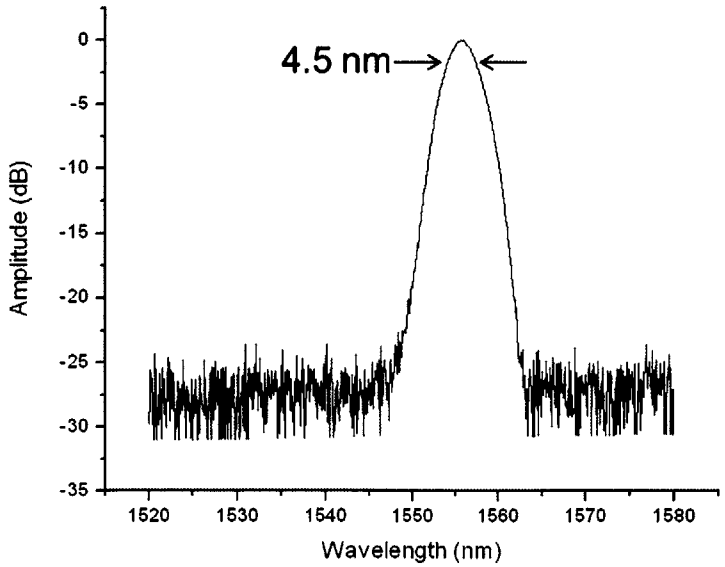

Figure 4-17 Optical Spectrum for 1 GHz laser with BATOP 6% modulation depth SBR.

The 4.50 nm 3 dB bandwidth centered at a wavelength of 1556 nm corresponds to a transform limited pulse duration of 565 fs. No autocorrelation traces were taken of this state.

4.3.2.4.2 RF Spectrum

The multi-harmonic "long-range" detected RF spectrum for this state is plotted in Figure 4-18. Overall, the envelope of the fundamental and subsequent harmonic frequencies is flat indicating single-pulse mode-locking operation. Unfortunately, the data for a zoom in view of the fundamental frequency was not available for this state but the repetition rate was still 1.009 GHz and there are no strong beat lines around the fundamental in Figure 4-18 so we can conclude this was a stable mode-locking state.

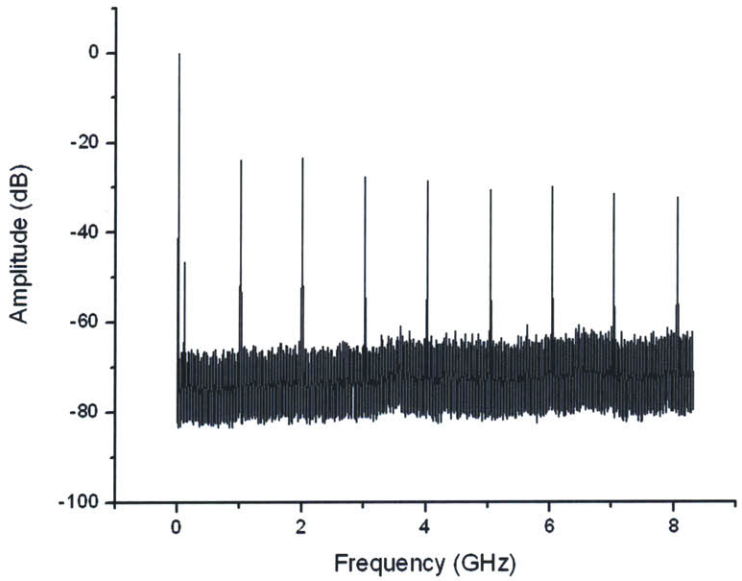

Figure 4-18 Long range RF spectrum for 1 GHz laser with BATOP 6% modulation depth SBR.

4.3.2.4.3 Output Power / Pulse Energy

The generation-two linear cavity, free-space SBR-coupled, erbium fiber laser also mode-locked with 6% SBR BATOP SAM-1550-09-25.4. Given a pump power of 740 mW this

laser output 2.08 mW of 1550 nm light for a pulse energy of 2.06 pJ and an efficiency of just 0.3%.

4.3.2.5 MIT VA86

Now that a characterization of the commercial SBR's was complete, this laser could be used to test the in-house SBR's fabricated by our collaborators at MIT. The first mirror to test is designated VA86. This mirror's design was described in detail in Chapter 2 and its results are presented in the following sub-sections. These results were challenging to obtain and almost impossible to repeat because the mirror surface would burn very easily as the power was increased. However, these figures do demonstrate what is possible if the mirror survives through the initial Q-switching phase of the pulse forming process.

4.3.2.5.1 Optical Spectrum

This is the first spectrum out of this soliton laser that actually had the $sech^2$ pulse shape predicted by soliton theory [7]. The bandwidth is comparable to the BATOP results but there is a more gradual roll-off of the spectral shape (see Figure 4-19) for this mirror possibly indicating a broader bandwidth reflectivity to the mirror.

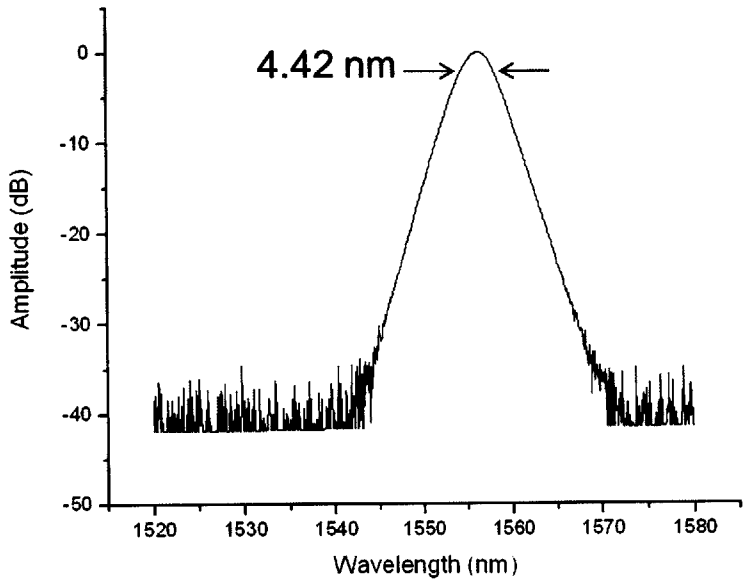

Figure 4-19 Optical Spectrum for 1 GHz laser with MIT VA86 SBR.

The 4.42 nm 3 dB bandwidth centered at a wavelength of 1556 nm corresponds to a transform limited pulse duration of 576 fs. No autocorrelation traces were taken of this state.

4.3.2.5.2 RF Spectra

The long range RF spectrum is plotted on the left of Figure 4-20. Notable features of this plot include the flat spectral envelope, and the strong sidebands on the fundamental and first harmonic. These sidebands are indicative of vector soliton behavior and can be reduced through inducing birefringence in the fiber or introducing another means of polarization preference within the cavity.

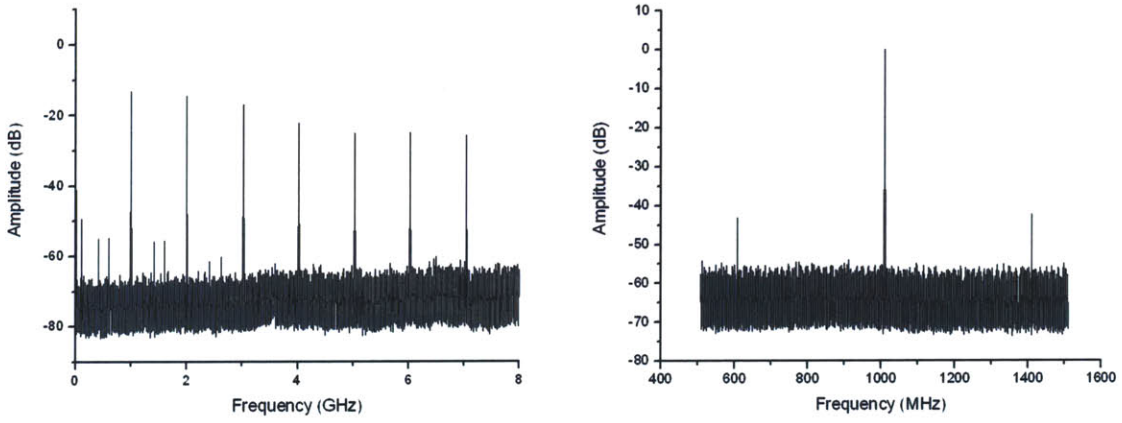

Figure 4-20 Long range RF spectrum (left) and Fundamental RF line (right) for 1 GHz laser with MIT VA86 SBR.

The right side of Figure 4-20 is an enhancement of the fundamental frequency with the sidebands visible in the scan window. The repetition rate is constant at 1.009 GHz and the sidebands are spaced exactly 400 MHz around the fundamental.

4.3.2.5.3 Output Power / Pulse Energy

The generation-two linear cavity, free-space SBR-coupled, erbium fiber laser also mode-locked with the MIT VA86 SBR. Given a pump power of 740 mW this laser output 6.50 mW of 1550 nm light for a pulse energy of 6.44 pJ and an efficiency of 0.9%.

4.3.2.5.4 SBR Burning

Unlike the BATOP mirrors, there are no layers of protective material in front of the sensitive mirror and absorbing layers of VA86. Therefore, the mirror is very sensitive to thermal and mechanical damage. Figure 4-21 is a microscope image of the mirror after attempts were made to mode-lock the laser.

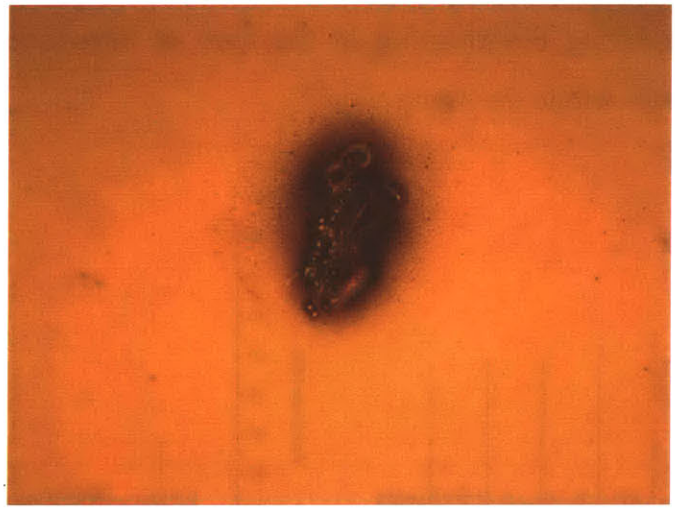

Figure 4-21 VA86 burn damage spots under 50X magnification in microscope.

These attempts all failed as the laser fell into a Q-switching state and the energy in those long pulses were enough to destroy the layers of the mirror and leave the circular spots seen in the image. There are many such spots because the mirror was translated around in the X and Y dimensions while searching for a mode-locking state. The laser did not always do this and on the (rare) occasions that it survived the Q-switching states it did mode-lock but we learned from this that the mirror will need some kind of protection against damage if it is to be a reliable part of this technology.

4.3.2.6 MIT VA86 PRC

With mirror protection in mind; and with the thought that perhaps the unabsorbed 980 nm pump light was thermally damaging the SBR, a protective dichroic optical coating

was deposited on some of the VA86 wafers. This coating, also described in Chapter 2, altered the VA86 characteristics as seen in Table 4-1.

4.3.2.6.1 Optical Spectrum

The addition of the pump reflective coating decreased the saturation fluence by 66% and increased the modulation depth by a factor of 3. This makes the VA86 PRC SBR more similar to the BATOP 14% SBR than the MIT VA86. Ultimately this resulted in a more rectangular pulse shape as seen in the BATOP mirrors. Figure 4-22 plots this spectrum.

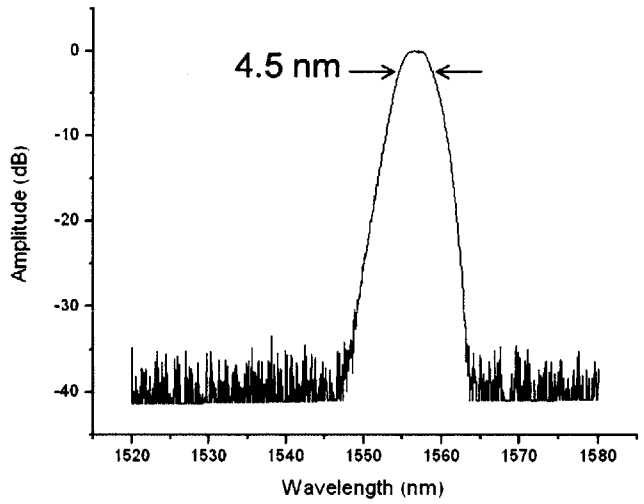

Figure 4-22 Optical Spectrum for 1 GHz laser with MIT VA86 PRC SBR.

The 4.5 nm 3 dB bandwidth centered at a wavelength of 1555 nm corresponds to a transform limited pulse duration of 565 fs. No autocorrelation traces were taken of this state.

4.3.2.6.2 RF Spectra

The long range RF spectrum is plotted on the left of Figure 4-23. Notable features of this plot include the relatively flat spectral envelope, and mild sidebands on the fundamental line. These weak sidebands suggest vector soliton behavior and should be removable through inducing birefringence in the fiber or introducing another means of polarization preference within the cavity.

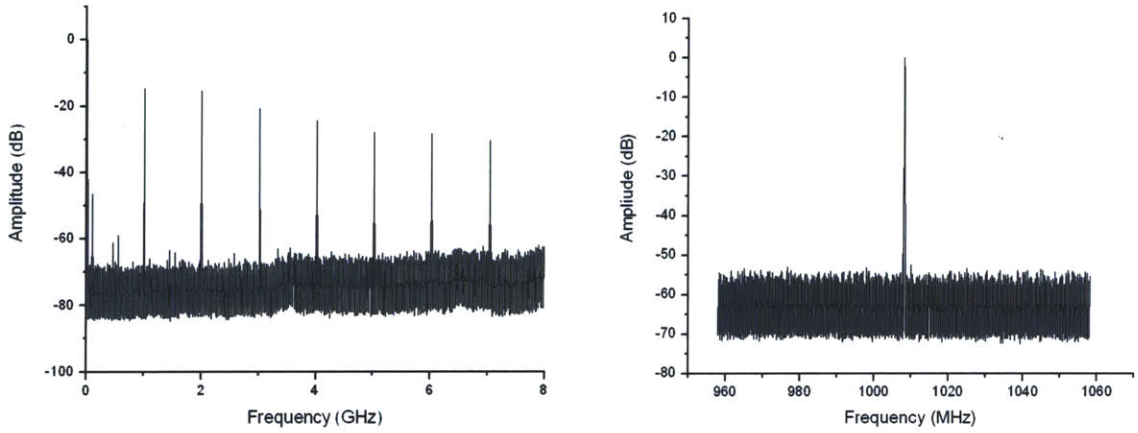

Figure 4-23 Long range RF spectrum (left) and Fundamental RF line (right) for 1 GHz laser with MIT VA86 PRC SBR.

The right side of Figure 4-23 is a zoom in of the fundamental frequency with no sidebands visible in the scan window. The repetition rate remains at 1.009 GHz.

4.3.2.6.3 Output Power / Pulse Energy

The generation-two linear cavity, free-space SBR-coupled, erbium fiber laser also mode-locked with the MIT VA86 PRC SBR. Given a pump power of 740 mW this laser output 5.00 mW of 1550 nm light for a pulse energy of 4.96 pJ and an efficiency of 0.7%.

4.3.2.7 MIT VA147 and VA148

Michelle Sander had developed some new SBR designs [8] based upon lessons we learned with our VA86 design and resulting tests. VA147 and VA148 are both new designs with two InGaAs absorbing layers and they were both tested in this cavity to see how they performed. Ultimately, the Q-switching states were too much and the laser was never able to enter a stable mode-locking regime before the mirror surfaces burned.

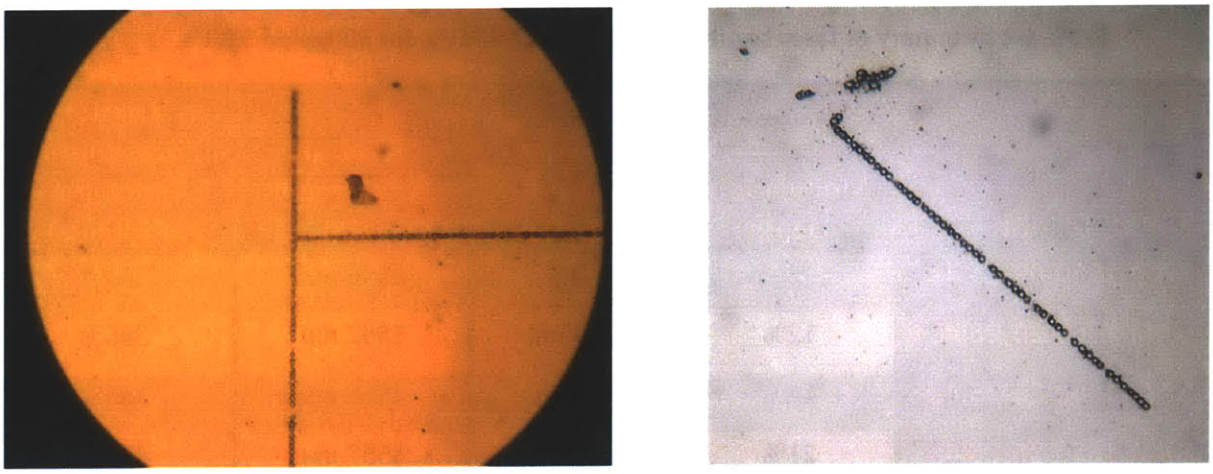

(a) (b)

Figure 4-24 Burn damage marks resulting from mode-locking attempts with (a) MIT VA147 and (b) MIT VA148

Figure 4-24(a) is a microscope photograph taken at 20X magnification demonstrating the results of attempts to translate the mirror along the X and Y directions searching for a stable state on VA147. We did not realize how rapidly the mirror was burning as the mirror was being translated so the nice "lines" of burn holes was the experimental result. Figure 4-24(b) is a microscope photograph taken at 30X magnification demonstrating the burn damage to VA148 as the mirror was moved around in a search for a mode-locking state.

Our conclusion for these double absorber mirrors is that without any protective coating layers there is no chance of obtaining mode-locking in the free space coupled SBR versions of the 1 GHz linear fiber laser.

4.3.3 Summary of Results

The following tables summarize the results reported in the above sections. Table 4-2 is a comparison of the maximum spectral bandwidths obtained and the corresponding pulse widths if the output were Fourier transform limited.

Table 4-2 Summary of laser bandwidth and pulse widths for all tested SBR's.

SBR Identifier	Modulation Depth	Spectral Bandwidth (3 dB)	Central Wavelength (*nm*)	Fourier Transform Limited Pulse Width (*fs*)
SAM-1550-09-25.4s	6%	4.50 *nm*	1556 *nm*	565 *fs*
SAM-1550-20-25.4s	12%	6.60 *nm*	1557 *nm*	386 *fs*
SAM-1550-23-25.4s	14%	6.98 *nm*	1556 *nm*	365 *fs*
SAM-1550-35-25.4s	21%	5.85 *nm*	1557 *nm*	436 *fs*
VA86	3.9%	4.42 *nm*	1556 *nm*	576 *fs*
VA86 PRC	12%	4.50 *nm*	1555 *nm*	565 *fs*
VA147	7.5%	N/A	N/A	N/A
VA148	4%	N/A	N/A	N/A

Table 4-3 is a summary of the power input and output from the laser given the various SBR's tests. Output pulse energies are also listed.

Table 4-3 Summary of laser power levels and pulse energies for all tested SBR's

SBR Identifier	Modulation Depth	Max Pump Power (*mW*)	Output Power (*mW*)	Pulse Energy (*pJ*)
SAM-1550-09-25.4s	6%	740 *mW*	2.08 *mW*	2.06 *pJ*
SAM-1550-20-25.4s	12%	336 *mW*	1.75 *mW*	1.73 *pJ*
SAM-1550-23-25.4s	14%	400 *mW*	2.80 *mW*	2.78 *pJ*
SAM-1550-35-25.4s	21%	214 *mW*	1.06 *mW*	1.05 *pJ*
VA86	3.9%	740 *mW*	6.50 *mW*	6.44 *pJ*
VA86 PRC	12%	740 *mW*	5.00 *mW*	4.96 *pJ*
VA147	7.5%	N/A	N/A	N/A
VA148	4%	N/A	N/A	N/A

4.3.4 Discussion

The objective of the second generation 1 GHz linear cavity erbium fiber laser was to reduce some of the losses of the first generation laser and identify the optimal saturable absorbing mirror to use for the shortest pulses. Eight different SBR's were tested and their results presented.

In this laser configuration, using the components listed in section 4.2.1, the SBR that yielded the shortest pulses was the BATOP SAM-1550-23-25.4s. This SBR had a large linear loss at 23% but the 14% modulation depth was necessary to generate the right cavity conditions to support a broad spectrum. The 14% BATOP SBR did not yield the greatest pulse energies, however. The highest pulse energies occurred, naturally, with the lowest loss SBR tested—the MIT VA86. However, the VA86 was not a reliable mirror due to its tendency to burn when being brought up to the mode-locking operating state. Efforts to protect the mirror structure with a pump light reflecting coating altered the properties of the mirror in such a manner as to restrict the bandwidth and reduce the output power of the laser.

4.4 Generation Two: Increase SBR Focal Spot Area

4.4.1 Cavity Design Changes

We next chose to test what would happen if the optimal SBR from the first set of tests was used with a different aspheric focusing lens in the laser. A lens with a significantly longer focal length would both a) lengthen the cavity by 12.19 mm and thus lower the repetition rate by 74 MHz and b) increase the size of the focal spot on the SBR thus reducing the optical fluence incident on the SBR.

The 3.1 mm focal length lens[44] was replaced with a 15.29 mm focal length lens[45]. Whereas the previous lens would focus the spot on a 3.84 μm diameter spot; the new lens would expand that to an 18.9 μm diameter spot. This lessens the incident fluence on the

[44] Thorlabs, Model: C330 TME-C 3.1 mm focal length aspheric lens
[45] Thorlabs, Model: C260 TME-C 15.29 mm focal length aspheric lens

mirror by a factor of 24 and should decrease the coupling losses seen from going fiber to mirror to fiber in this laser. That would in turn result in greater intra-cavity pulse energy and greater output power.

4.4.2 Results

The decreased fluence on the SBR was not so much as to eliminate the mode-locking effects and a continuum of states was observed for this laser configuration as well. At the upper edge of the single pulse mode-locking stability region, the laser found a particularly low loss state that resulted in the broadest spectrum and highest power yet seen from this fiber/SBR combination. This state is reported in the following sub-sections.

4.4.2.1 Optical Spectrum

Accepting the high linear loss of the 14% modulation depth BATOP SBR usually meant narrow spectral traces with little power in the high and low wavelength spectral "wings." Changing the spot size incident on the SBR and turning up the pump all the way resulted in something new—the broadest spectrum yet seen from this fiber. Figure 4-25 plots this broad, $sech^2$ shaped spectrum that sharply contrasts with the other spectral shapes produced with the BATOP family of SBRs.

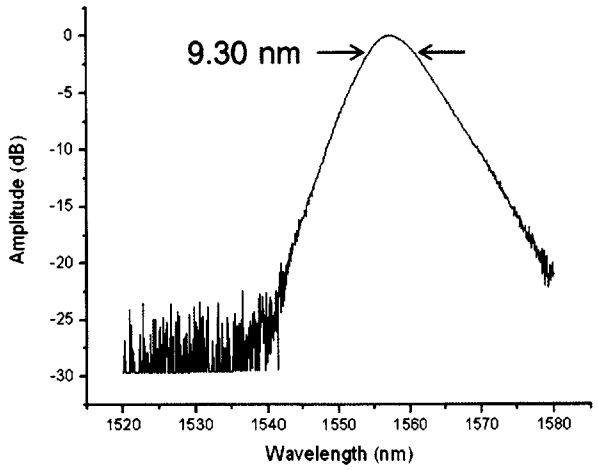

Figure 4-25 Optical Spectrum for the 935 MHz laser with BATOP 14% modulation depth SBR.

This state supported an uncharacteristically large 9.3 nm 3 dB bandwidth centered at a wavelength of 1557 nm. That spectral width corresponds to a transform limited pulse duration of 274 fs. No autocorrelation traces were taken of this state.

4.4.2.2 RF Spectra

The optical spectrum looks smooth but what about the RF traces? Figure 4-26 has the long range RF trace on the left and its envelope is typical of single pulse mode-locking with the small vector soliton beats around the first few harmonics.

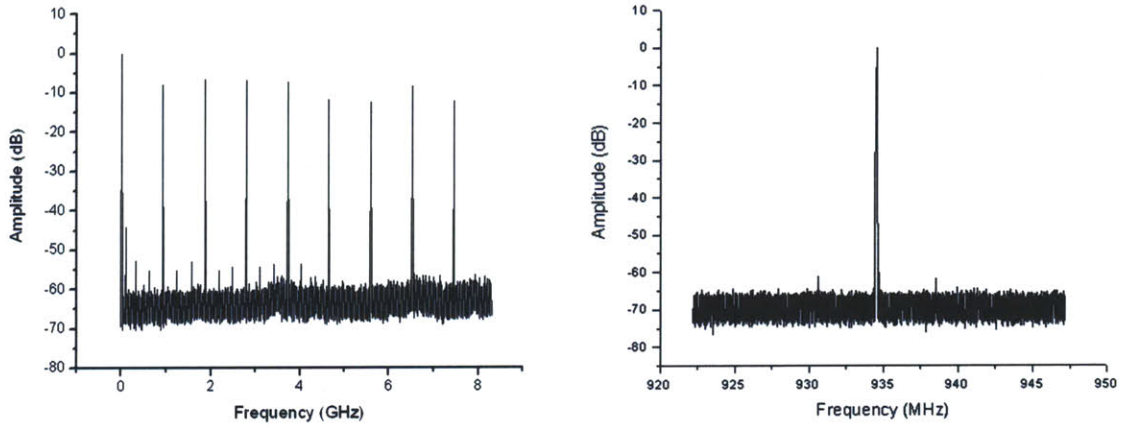

Figure 4-26 Full span RF frequency spectrum (left) and Fundamental RF line (right) for the 935 MHz laser with BATOP 14% modulation depth SBR.

Enhancing the fundamental frequency on the right side of Figure 4-26, we see that this laser cavity operates at a repetition rate of 935 MHz and has over 60 dB suppression of the vector soliton beats. Slight changes to the fiber birefringence may be able to completely eliminate those beats.

4.4.2.3 Output Power / Pulse Energy

Finding this broad laser state meant using the full stable output power of the pump diodes—measured to be 740 mW into the gain fiber. At this pumping level, this laser output 3.70 mW of 1550 nm light for a pulse energy of 3.96 pJ and an efficiency of 0.5%.

4.4.3 Discussion

The initial idea in replacing the focusing lens without changing any other laser components was to see if increasing the spot size incident on the SBR would assist or hinder mode-locking efforts in the cavity. Because of the mechanical design constraints and the challenge of cutting and polishing new fiber pieces, changing the lens meant also decreasing the repetition rate such that it was no longer technically a GHz laser.

Other than that caveat, this cavity performed very well. It found a state with broadband reflectivity and lower loss than any previous test with the BATOP 14% SBR. However, this state was at the extreme edge of the operation regime, it was very sensitive to cavity adjustments, and it was difficult to repeat.

The continuing search for a stable, repeatable, non SBR damaging laser system that had a broad bandwidth, short pulses, and high output power would continue as this variation of the cavity would not satisfy those criteria.

4.5 Generation Two: "L" Cavity

4.5.1 "L" Cavity Design

In a parallel effort to the development of a stable 1 GHz erbium fiber laser source, our group was working to determine the real cause of the saturable absorber mirrors burning within the laser cavities. Dave Chao and Jeff Chen performed a few experiments [private communication] where the mirrors were subjected to continuous wave and pulsed sources of both 980 nm and 1550 nm light. In those tests, no mirrors burned. No amount of excess pump light caused thermal failure of the test mirror layers. Yet, when put into a laser cavity, the mirrors fail at predictable and somewhat repeatable amount of pump energy.

So a new experiment was conceived that attempted to isolate the pump light from the signal light within a linear cavity laser. Previous efforts included coating the MIT VA86 absorber with a pump reflective coating (PRC) and while that should have in theory reflected all of the unabsorbed pump back into the fiber, the mirrors still burned in some

instances. The burning could be caused by the 1550 nm signal light, but we needed to completely eliminate the 980 pump incident on the SBR to be sure.

One known and proven way to do that is to pass the combined beam through a dichroic mirror. In this case, the pump light passes through the mirror while the signal is completely reflected. Taking full advantage of the collimated section of this laser design, the focusing lens and SBR are turned 90 degrees and one of the 980 nm transmitting, 1550 nm reflecting dichroic mirrors from the generation one laser was placed in the beam path. Figure 4-27 is the schematic of this experimental test cavity.

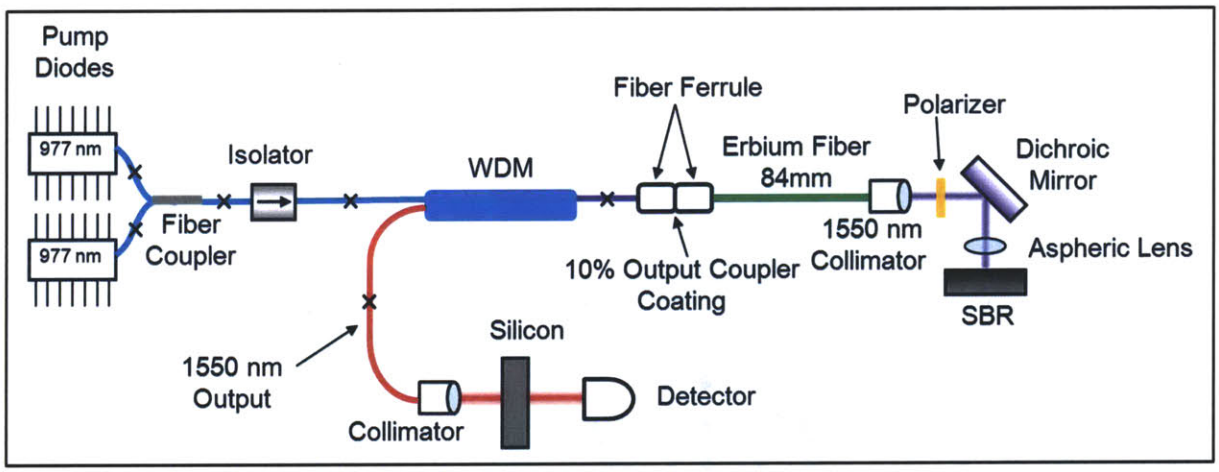

Figure 4-27 Schematic of the "L" cavity erbium fiber laser. The polarizer is optional and the dichroic mirror is the primary change between this and the previous linear fiber lasers.

The only other alteration this system has over the generation two design is the possibly of inserting a polarizer into the beam path. This might be desirable in that it can minimize the vector soliton behavior that is sometimes observed in these systems.

Figure 4-28 is the photograph of this cavity as built in the laboratory. Careful comparison of this image and that of Figure 4-10 reveals that the same components and stages are utilized to support and align this laser. It took a little time but eventually a procedure was found to align the optics and SBR in this cavity as well as they could be aligned in the straight line version.

Once everything was aligned, the pump power was turned on and the SBR's exchanged to explore both the burning issue and the feasibility of inserting a free space polarizing element into this already high loss cavity. The results are detailed in the following sub-sections.

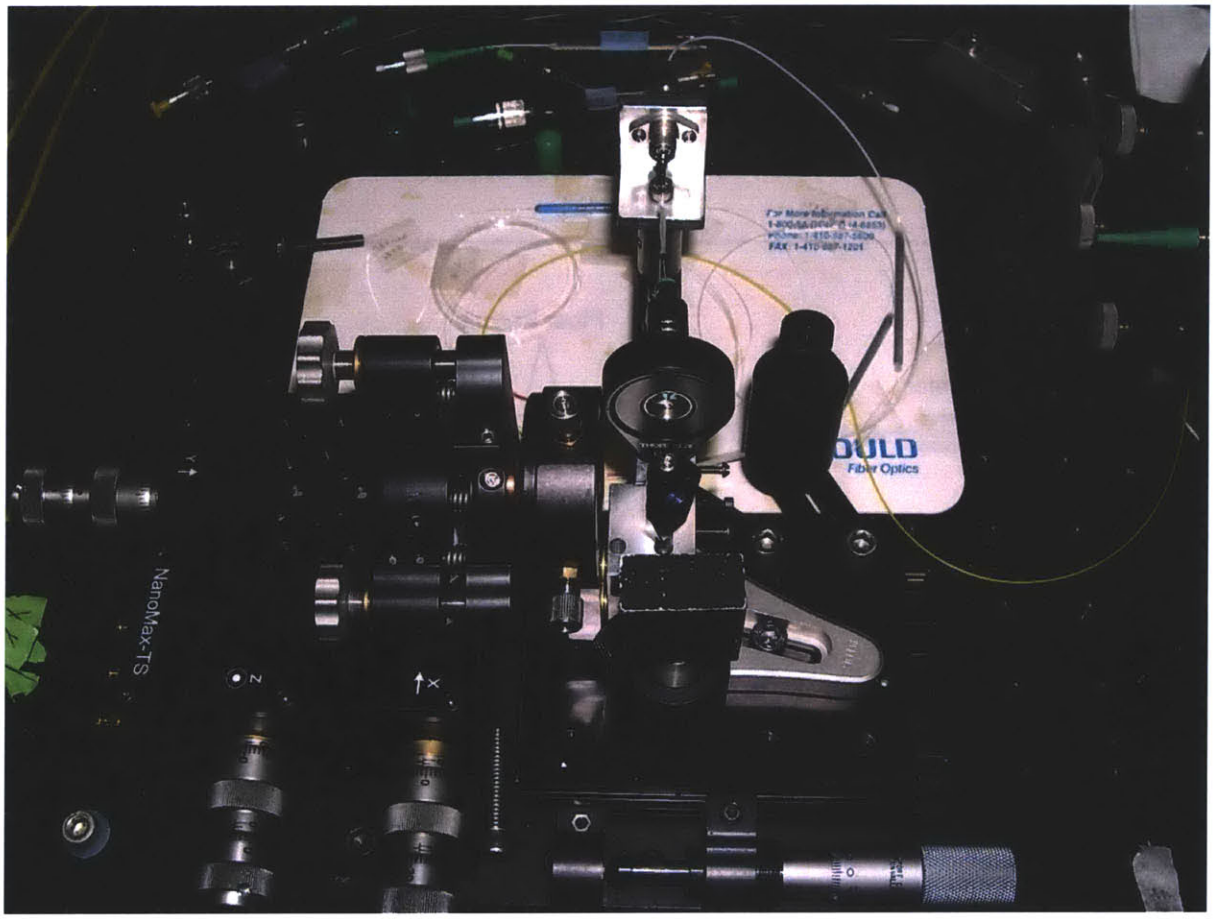

Figure 4-28 Photograph of the "L" cavity erbium fiber laser. There is no polarizer element in this photo.

4.5.2 "L" Cavity Results

The cavity rearrangement, while retaining the same length of erbium gain fiber, means the repetition rate of the laser will drop. In this case it reduced to 780 MHz. A longer cavity does mean fewer pulses per unit time and the intra-cavity pulse energy can be

increased thus aiding in the mode-locking effects of the SBR. Keeping this in mind, the following results were obtained:

- The BATOP 14% SBR mode-locked with vector soliton issues
- The BATOP 14% SBR mode-locked and the polarizer eliminated the vector solitons at the cost of bandwidth and power.
- The MIT VA86 SBR mode-locked very well and did not burn.
- MIT VA86 and polarizer did not mode-lock at all.
- MIT VA148 still burned with every attempt to pump it.

The recorded spectral and power data below elaborate on these results.

4.5.2.1 BATOP 14% SBR Results

4.5.2.1.1 Optical Spectra

The BATOP 14% modulation depth SBR produced the most reliable spectrum in the previous tests so it was chosen as the mirror to use in testing the polarizer. Both of these results occurred at the same pump diode power level.

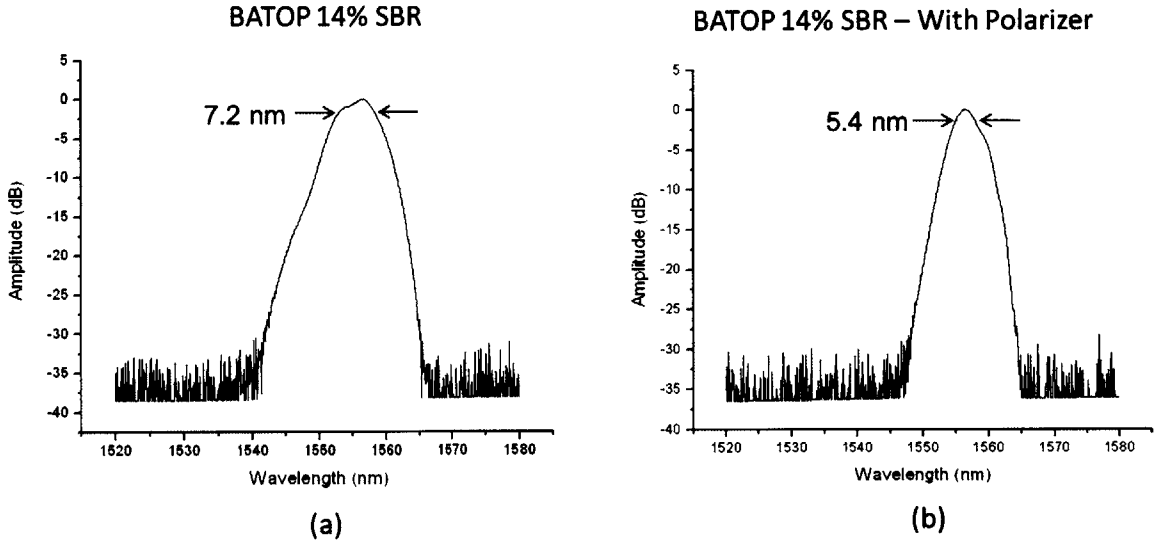

Figure 4-29 (a) optical spectrum of the 780 MHz "L" cavity with BATOP 14% SBR. (b) optical spectrum of the 780 MHz "L" cavity with BATOP 14% SBR and intra-cavity polarizer.

Figure 4-29(a) and Figure 4-29(b) demonstrate the spectral change that introducing a polarizer into the cavity produced. As can be seen by comparing the two figures, the bandwidth is narrower and the spectral shape altered by that additional loss element in the cavity.

Without a polarizer, we see a 7.2 nm 3 dB bandwidth centered at a wavelength of 1556 nm. This data corresponds to a transform limited pulse duration of 353 fs. With a polarizer, the reduced 3 dB bandwidth measures 5.4 nm also centered at 1556 nm. 5.4 nm corresponds to a transform limited pulse duration of 471 fs.

4.5.2.1.2 RF Spectra

Reducing the intra-cavity power and narrowing the spectrum is the consequence of adding the polarizer. The benefit is seen in the RF spectral data.

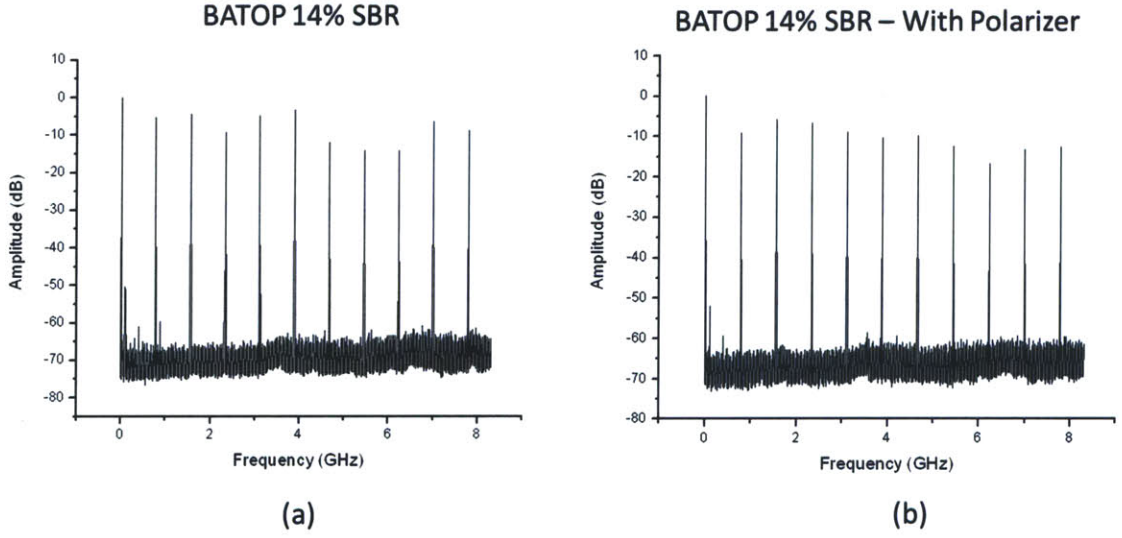

Figure 4-30 (a) RF spectrum of the 780 MHz "L" cavity with BATOP 14% SBR. (b) RF spectrum of the 780 MHz "L" cavity with BATOP 14% SBR and intra-cavity polarizer.

Figure 4-30(a) and Figure 4-30(b) are the full span RF scans demonstrating a (detector limited) flat spectral envelope for single pulse mode-locking operation in each case. There are some detected lines around the fundamental frequency in Figure 4-30(a); those are examined further in the zoomed-in data.

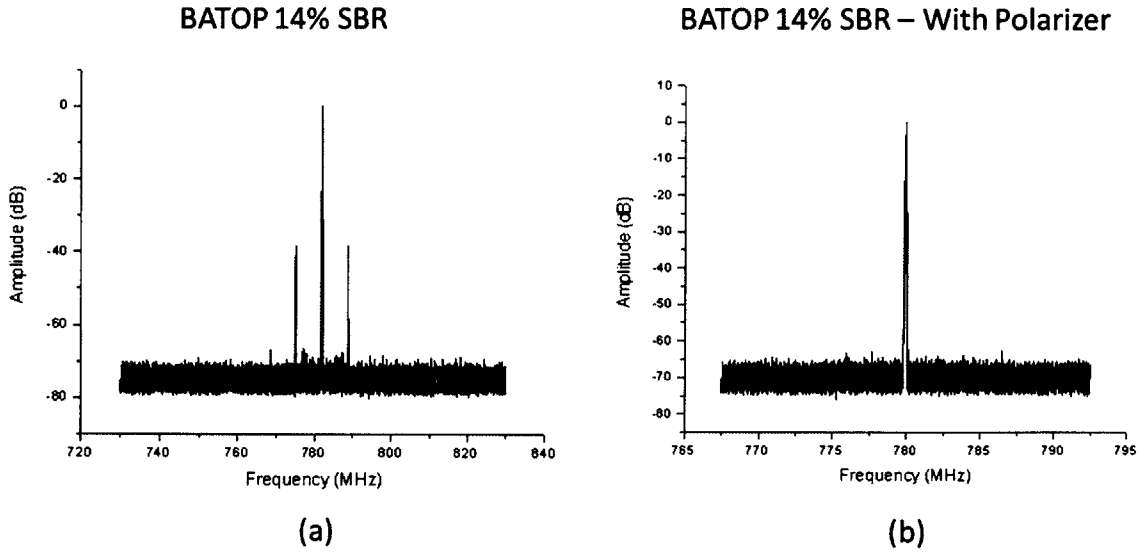

Figure 4-31 (a) RF spectrum of the fundamental line of the 780 MHz "L" cavity with BATOP 14% SBR. (b) RF spectrum of the fundamental line of the 780 MHz "L" cavity with BATOP 14% SBR and intra-cavity polarizer.

Figure 4-31(a) and Figure 4-31(b) are the close up traces of the detected fundamental RF frequencies. From these, we confirm that the repetition rate is now 780 MHz. More importantly, we see the desired benefit of the polarizer in the cavity. Figure 4-31(a) clearly has strong sidebands indicating undesirable vector soliton behavior while they are eliminated by the polarizer in Figure 4-31(b).

4.5.2.1.3 Output Power / Pulse Energy

For each test case, the full diode output of 740 mW was pumped into the cavity. The non-polarizer cavity produced 6 mW of output while the polarizer dropped the output to 3.7 mW. The corresponding pulse energies and efficiencies are 7.7 pJ at 0.8% and 4.7 pJ at 0.5%.

4.5.2.2 MIT VA86 SBR Results

4.5.2.2.1 Optical Spectrum

In previous tests, the commercial BATOP mirrors did not demonstrate the level of burn damage that the MIT ones did. So, as a way of testing if the excess pump light is

causing the burning, an uncoated VA86 mirror was aligned in this new cavity and the pump power brought up. Surprisingly, it did not burn but instead yielded a clean output. Figure 4-32 plots the recorded spectrum for this state.

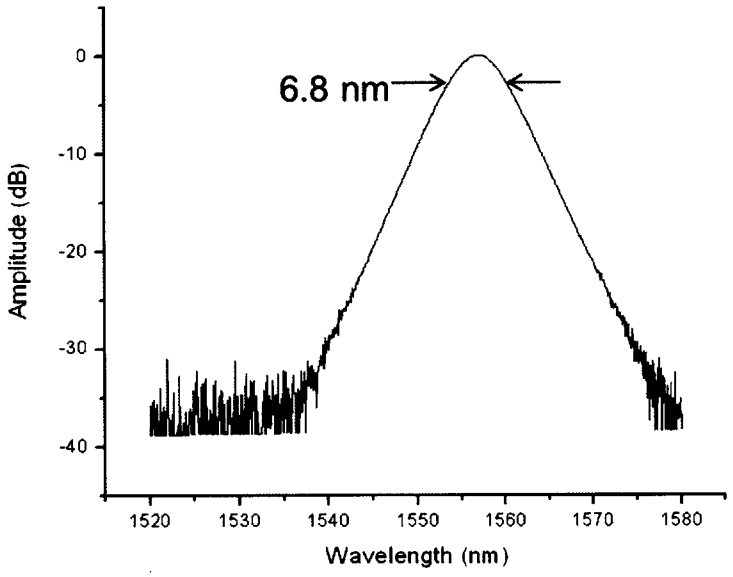

Figure 4-32 Optical spectrum of the 780 MHz "L" cavity with MIT VA86 SBR.

This state supported a broad 6.8 nm 3 dB bandwidth centered at a wavelength of 1556 nm. That spectral width corresponds to a transform limited pulse duration of 374 fs. There is no spectrum for VA86 with a polarizer because the increased losses in the cavity prevented any mode-locked pulses from forming.

4.5.2.2.2 RF Spectra

The clean harmonics seen in the long range RF scan on the left of Figure 4-33 further support the single pulse mode-locking state. The noise spikes around and below 500 MHz are associated with the detection equipment and are not from the laser cavity.

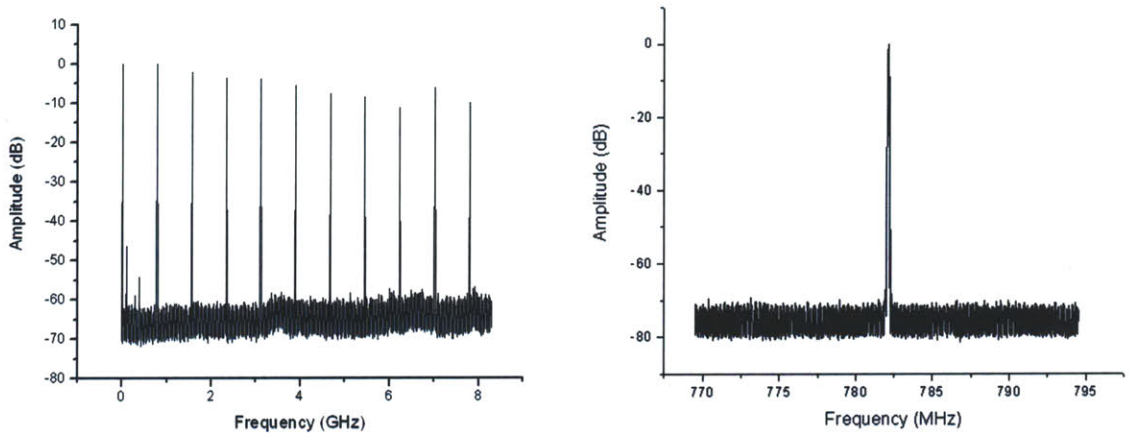

Figure 4-33 Full span RF frequencies (left) and Fundamental RF line (right) for "L" cavity laser with MIT VA86 SBR.

Confirmation that this state is free of vector solitons and that the repetition rate is 782 MHz is seen on the right in Figure 4-33.

4.5.2.2.3 Output Power / Pulse Energy

Given a pump power of 725 mW this laser output 8.60 mW of 1550 nm light for a pulse energy of 11.0 pJ and an efficiency of 1.1%.

4.5.3 Discussion

This experiment was designed to test two different variations to the free space coupled high repetition rate linear cavity erbium fiber laser. The first was to see if adding a polarizer to the cavity would eliminate the polarization sidebands without detrimentally affecting the mode-locking states. The second was to gather further information about the possible source of the burning observed on some of the SBR's when they are tried in the cavity.

We learned that adding a polarizer to the cavity will increase the intra-cavity losses, decreasing the output power and the available optical bandwidth. However, it will also suppress the vector soliton behavior as seen in Figure 4-31. If that trade-off is acceptable,

then adding a polarizer is a possible solution to the vector soliton issue in this type of fiber laser.

Regarding the mirror burning; the MIT VA86 and MIT VA147 SBR's were tested in the new "L" cavity to see if burns would still occur. VA86 did not burn but in fact settled into a good mode-locking state. This may have been due to the pump light being removed prior to hitting the SBR. Further tests will be needed to isolate the exact reason this mirror burns in the 1 GHz linear cavity but not in this slightly lower repetition rate system.

The MIT VA147 mirror, however, continued to burn with every test. The conclusion to this data is that the VA147's double absorber layers are absorbing very well and are being damaged solely by the 1550 light. One possible explanation is that the laser is passing through a Q-switch mode-locking state and this condition of long, high energy pulses is causing an excessing thermal load on the mirror structure and it delaminates and fails as a reflector.

4.6 Generation Two: 1.25 GHz

In an effort to continue to push the limits of this fiber laser technology and understand where the gain/loss balance tips out of mode-locking, shorter pieces of fiber were cut and polished into connectors. One piece still provided enough gain for mode-locked pulses and its results are detailed in this section.

4.6.1 1.25 GHz Cavity Design

For this experiment, the only change made to the generation-two laser was the length of the erbium doped gain fiber. Instead of 84 mm, a 62 mm piece was inserted into the cavity. Figure 4-34 details the entire layout of this laser. No set up photograph was available but it looked almost identical to Figure 4-10, just with a shorter piece of fiber.

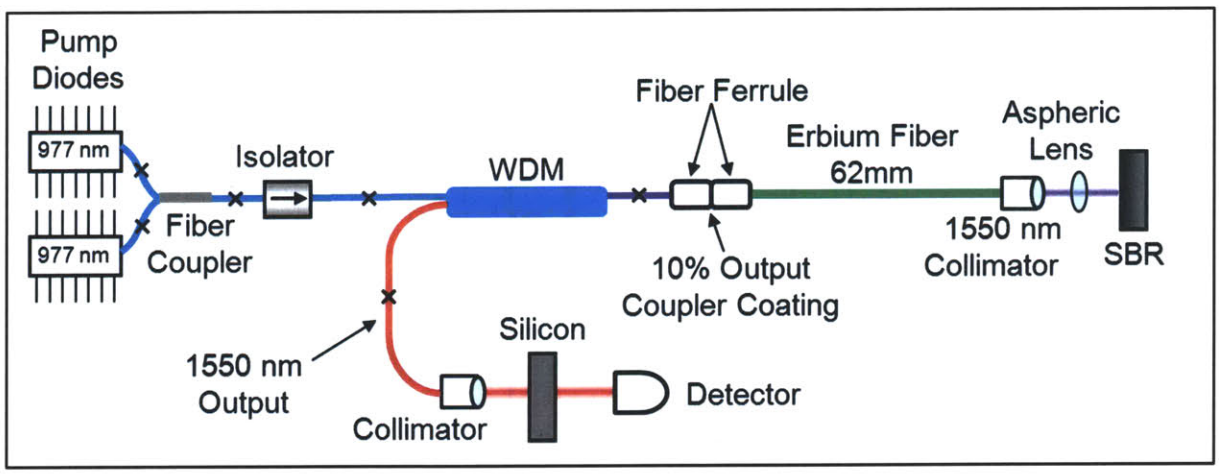

Figure 4-34 Schematic of 1.25 GHz linear cavity erbium fiber laser.

For this laser, the BATOP 12% modulation depth SBR demonstrated the broadest spectrum so the results shown use that SBR.

4.6.2 1.25 GHz Cavity Results

This test was meant to be a brief test to see if a 1.25 GHz laser could work. Once a positive result was obtained then my collaborator, Michelle Sander, would be able to try to develop it further for one of her ongoing experiments.

4.6.2.1 Optical and RF Spectra

Figure 4-35 plots the broadest optical spectrum achieved with this laser configuration on the left. The pulse shape is not symmetric and this is consistent with previous results using this SBR. This state supported a 5.9 nm 3 dB bandwidth centered at a wavelength of 1556 nm. That spectral width corresponds to a transform limited pulse duration of 431 fs.

The right plot of Figure 4-35 is the long range RF spectral plot for this state. Data for the enhanced view of the fundamental frequency was not available. This plot has enough detail to see that the vector soliton issue is suppressed and the envelope is flat to the extent of the RF analyzer can record.

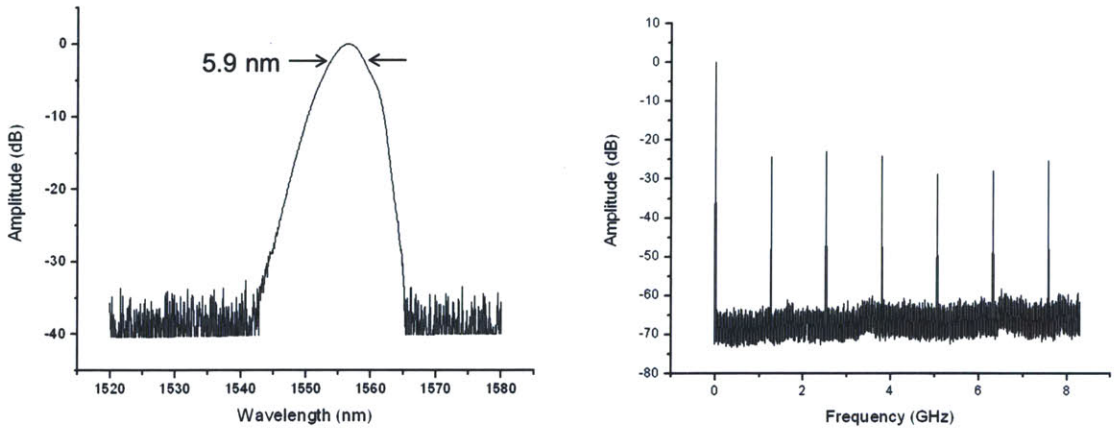

Figure 4-35 Optical spectrum (left) and full span RF spectrum (right) of 1.25 GHz linear cavity erbium fiber laser.

4.6.2.2 Output Power / Pulse Energy

The optimal state was found for a pump power of 390 mW. The 1550 nm output power was very weak – 0.78 mW. That corresponds to a pulse energy of 0.6 pJ and an efficiency of just 0.2%.

4.6.3 Discussion

Based upon the success of the 1 GHz linear fiber laser cavity, an experiment to see how high the repetition rate could be pushed while maintaining mode-locking pulses was undertaken. Different lengths of the specialty erbium doped gain fiber were constructed and one of them was able to support enough gain to lase. The shortest pieces corresponding to 1.5 or 2 GHz did not support mode-locking. However, a 62 mm long piece of fiber—which corresponded to a 1.25 GHz repetition rate—did weakly mode-lock when paired with the BATOP 12% modulation depth SBR. The results were not overwhelming but encouraging enough that further work could be done with this laser as the source of high repetition rate pulses.

4.7 314 MHz Custom SBR Test Laser

One reason this linear cavity erbium fiber laser was developed was to test new SBR mirrors for their performance in a high repetition rate environment. With this in mind, collaborator Shelia Nabanja designed and fabricated two alternate versions of the MIT VA86 mirror. These variations have oxidized layers of the semiconductor and this oxidation increases the index contrast between layers to greatly increase the reflectivity bandwidth of the mirror. The design and fabrication details of this mirror may be located in reference [9].

The part of these experiments relevant to this thesis are the test laser set-up and results with these experimental mirrors.

4.7.1 Linear Laser Cavity Design

The initial efforts at mode locking the 1 GHz laser cavity with the new mirrors failed. The reflectivity was too low and the modulation depth too shallow to form and sustain pulses in that short cavity. One solution to low pulse energy is to increase the length of the cavity so the pulses have more time to build up sufficient energy for the mode-locking effects of the saturable absorber and the soliton effects in the fiber to act to shorten the pulses.

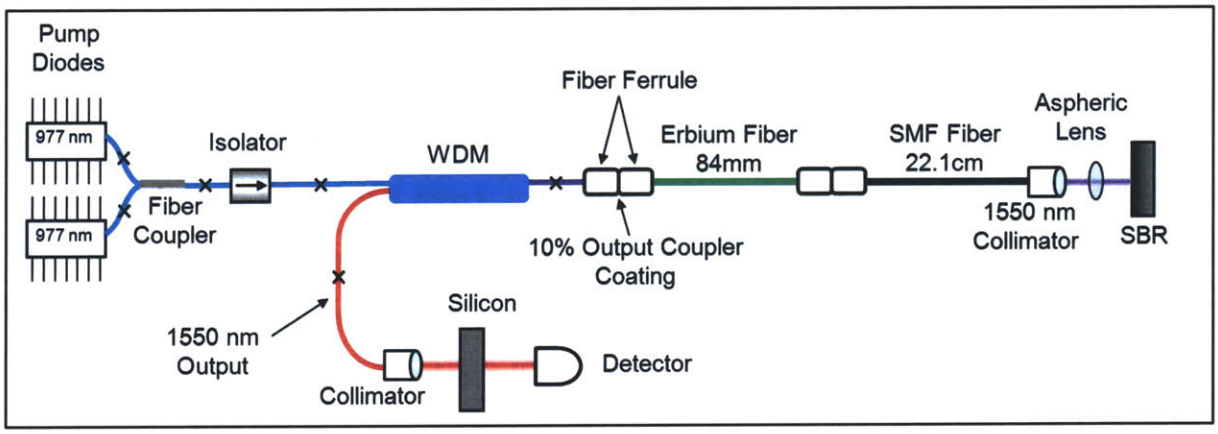

Figure 4-36 Schematic of 314 MHz VA176 Oxidized SBR test laser.

There are two experimentally straightforward ways to increase the repetition rate by lengthening the cavity—adding more fiber to the cavity or increasing the path length of the collimated free space section of the beam. We chose to add more fiber to the cavity to take advantage of increased soliton shortening effects. Figure 4-36 is the schematic of the test laser used for these experiments.

The only changes made between this cavity and the previously described second generation linear cavity fiber laser are the addition of 22.1 cm of single mode fiber and the experimental SBR mirror. The fiber length was chosen because that was the shortest piece of FC/APC connectorized SMF-28 fiber we could quickly locate in the laboratory. The mirrors were the devices under test for this system.

There were two different versions of a new mirror design tested in this experiment. Both are classified under the designator VA176. The first mirror consists of reflective "mesa" structures atop a substrate. These are 500 μm diameter columns of mirror layers arranged symmetrically on the substrate plane. The reason for this geometry is to permit physical access to the sides of the mirror stack so that during processing an oxidizing step can be employed whereby oxygen is diffused through the aluminum layers to create aluminum oxide. This oxidation alters their optical properties in a controllable fashion. Unfortunately, it means the mirror surface is not a uniform reflector, but an array of pillars on one of which the laser light will need to be carefully focused.

The second mirror design alleviates that concern. This time, a large array of small holes is patterned into the mirror layers. These 10 μm holes provide enough access for the oxygen to diffuse through the entire layer structure, given the proper conditions during fabrication. And since their spacing is 150 μm apart, there is plenty of mirror surface area for the laser beam to focus and reflect from, thus greatly simplifying this mirror's alignment in the cavity. Figure 4-37 is a photo demonstrating the holes and their proportions to each other on the mirror surface.

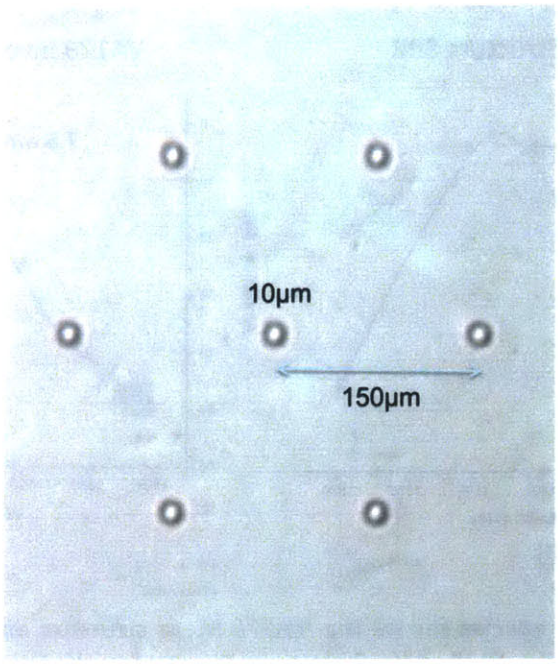

Figure 4-37 Microscope image and dimensions of the hole array found on MIT VA176 Inverted structure mirror.

Full descriptions of the design and fabrication of both mirror structures are found in Shelia's Ph.D. thesis [10]. The laser results that come from the use of these mirrors are found in the following sub-sections.

4.7.2 Linear Laser Results

When the 1 GHz linear cavity had 22.4 cm of fiber added to the length, it became a 314 MHz cavity. In this configuration, both versions of the MIT VA176 oxidized SBR's yielded mode-locking results. The design of the mirrors is such that the results should have been the same for both versions, and the results we see are very similar. Plotted below, in a side by side manner, are the outputs of these two fiber lasers.

4.7.2.1 Optical Spectra

First, the optimal optical spectra were recorded for both mirrors.

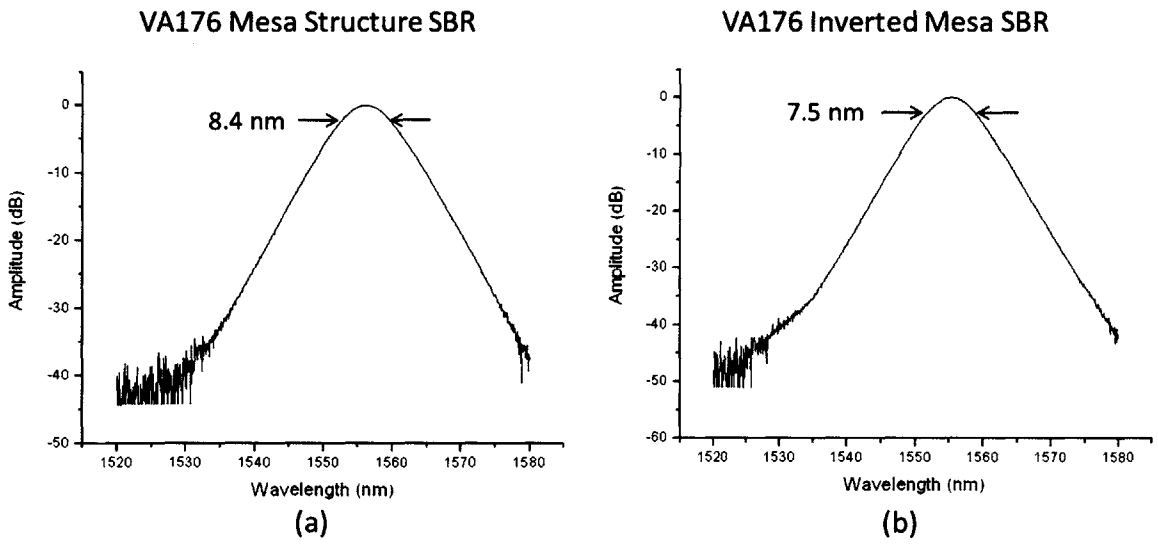

Figure 4-38 Optical spectra for (a) the VA176 Mesa structure and (b) the VA176 inverted mesa structure mirrors. Both plots show a similar state in the laser.

Figure 4-38 plots the widest optical spectrum recorded for each mirror. The reflective structures of the mirrors were designed to be the same so similar results were expected, and recorded. The mesa structure mirror resulted in a 3 dB bandwidth of 8.4 nm and that corresponds to a 303 fs transform limited pulse width. The inverted structure mirror performed nearly as well with a 7.5 nm 3dB bandwidth. 7.5 nm corresponds to 339 fs pulses in the transform limited case.

4.7.2.2 RF Spectra

The long range detected RF Spectra for these two lasers are plotted below. Both demonstrate a flat spectral envelope and sharp harmonic lines. Figure 4-39(a) plots the first four harmonics of the RF spectrum. Longer range scan data was unavailable for this state. Figure 4-39(b) plots the full 8 GHz span for the inverted mesa structure SBR.

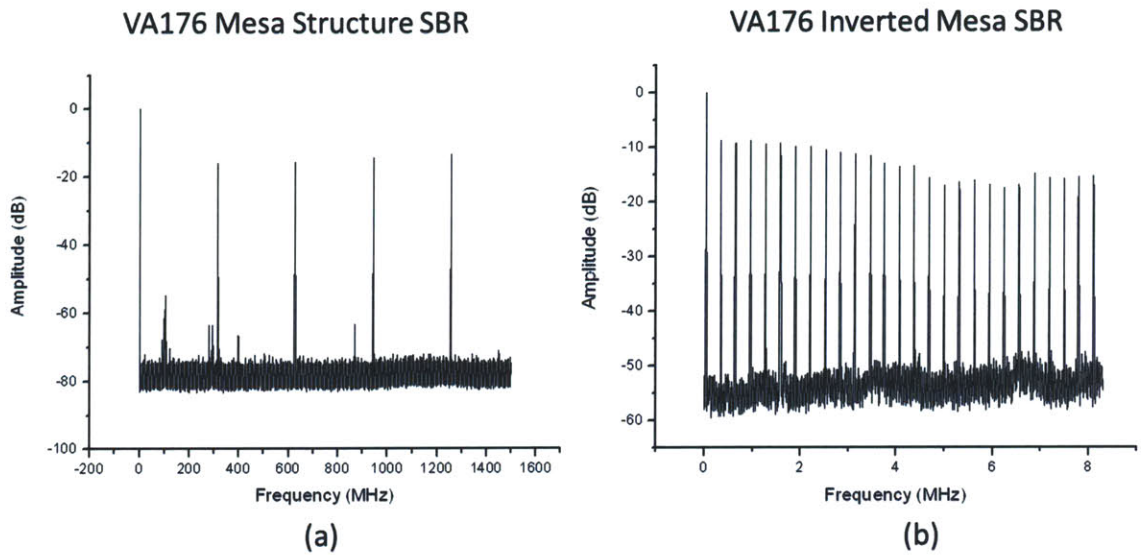

Figure 4-39 Long scan RF spectrums for (a) the VA176 Mesa structure and (b) the VA176 inverted mesa structure mirrors.

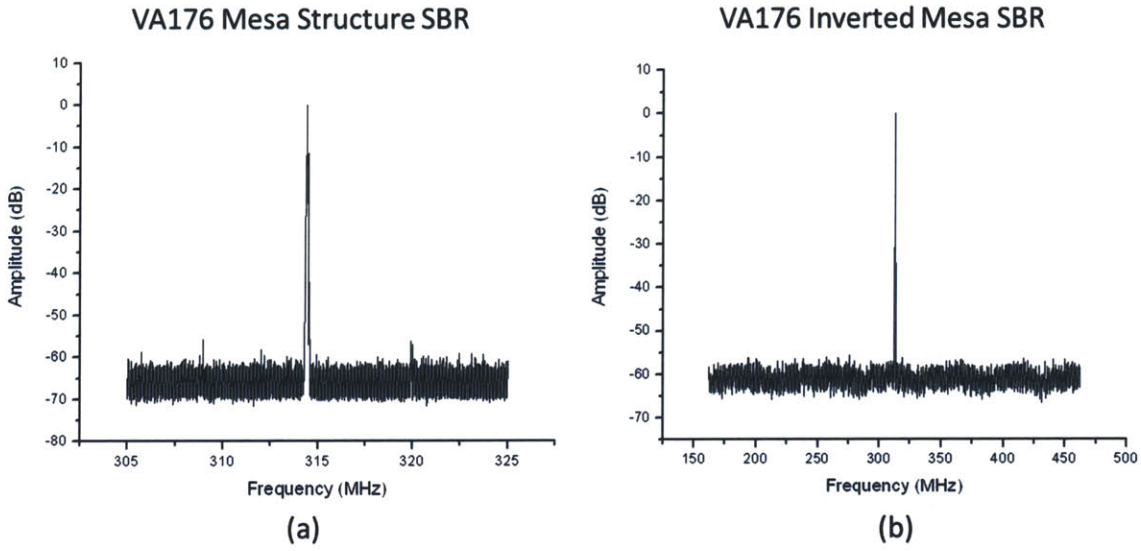

Figure 4-40 Fundamental frequency RF spectrums for (a) the VA176 Mesa structure and (b) the VA176 inverted mesa structure mirrors. Both plots show a similar state in the laser.

Zooming in on the fundamental frequency for the mesa structure mirror in Figure 4-40(a) indicates some slight vector soliton lines 5 MHz out. Figure 4-40(b) demonstrates that changing the SBR and modifying the cavity slightly can eliminate the sidebands. Both plots indicate a repetition rate of 314 MHz for this version of the linear laser.

4.7.2.3 *Output Power / Pulse Energy*

The optimal state for the laser with the mesa structure SBR was found at a pump power of 400 mW. The 1550 nm output power was pretty good at 4.11 mW. That corresponds to a pulse energy of 1.3 pJ and an efficiency of 1.0%. The optimal state for the inverted structure SBR laser required 490 mW of pump power and only produced 2.7 mW of output power. Those figures equate to a pulse energy of 0.86 pJ and an efficiency of 0.6%.

4.7.2.4 *SBR Burn Damage*

These mirrors were not designed to be protected against Q-switching or excess pump light impingement. Therefore, they were prone to burn damage and that is what we observed. Attempts to align and optimize these cavities for mode-locking behavior were fraught with burned spots on the mirrors. Figure 4-41(a) is a photograph of one of the mesa structures of the first VA176 run. Alignment in the cavity was difficult but as can be seen in the image, it was possible to get fairly close to the center of the mirror. Attempts to use too much pump power would burn the mirror and result in having to find a new spot to try again.

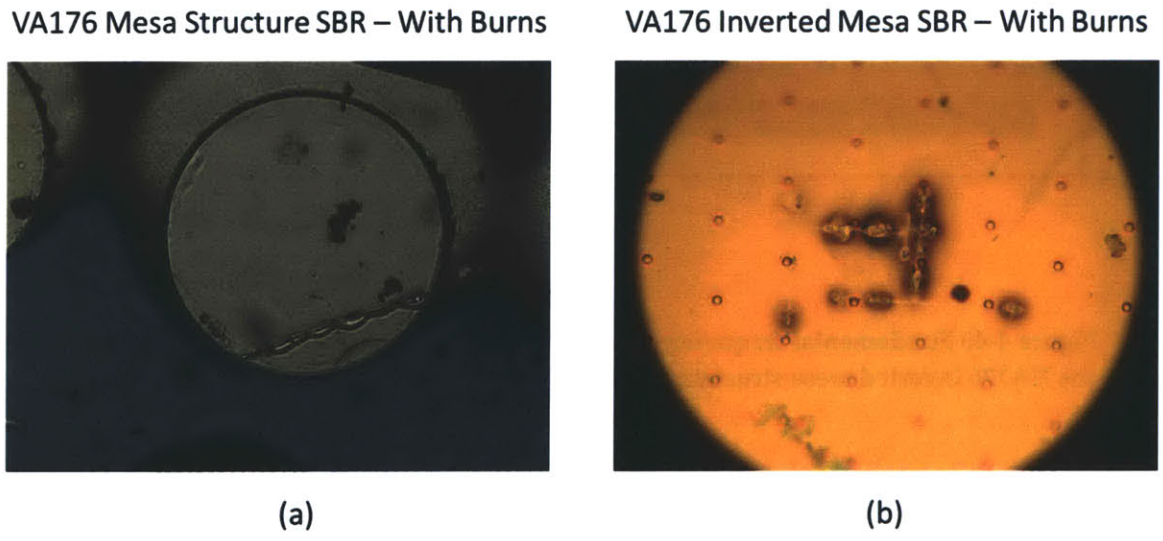

Figure 4-41 Photographs of the mirror structures and resultant burn spots from mode-locking tests. (a) An elevated mesa with burn marks. (b) The inverted mesa with burn spots.

Figure 4-41(b) clearly shows the mirror surface and hole pattern. The center of the image also shows a "T" shaped patter of burns that resulted from failed mode-locking efforts. Good states were found but if the pump power was increased too much the mirror would fail at that location and a new spot would need to be found by translating the mirror.

4.7.3 Discussion

As an experimental set up, the linear cavity erbium fiber laser has proven very versatile and useful. Though the VA176 SBR's would not work at a 1 GHz repetition rate, the simple addition of a length of single mode fiber produced some nice results.

Two different versions of the same mirror structure were fabricated and both tested in the cavity. The results were very similar and this encouraging result led to publications for the SBR's designer and fabricator, Shelia Nabanja. During testing, we learned more about how these systems respond when the intra-cavity power is too high and what the physical limits on the mirror surfaces were.

The higher loss of this type of laser cavity limited the advantages the oxidized mirror structure was supposed to bring—broader reflectivity bandwidth. One sacrifice to this broader bandwidth was the linear loss; VA176 had more linear loss than VA86 and that was enough of a difference to limit the mode-locking to a low power state. Further work would need to be undertaken to both reduce the mirror linear loss and harden the surface against burn damage before this mirror design could be reliably integrated into a high repetition rate fiber laser for regular use.

4.8 970 MHz Custom SBR Test Laser

The attempts to create a stable, repeatable 1 GHz linear cavity erbium fiber laser had all been stymied by the vector solitons that would sometimes creep up during what was otherwise a very good state. Some success at minimizing their effects had been seen in the end abutted fiber lasers being developed in parallel with this laser. Also, data gathered with the "L" cavity version of this laser demonstrated that a linear polarizer in the cavity was

successful (though with performance tradeoffs) in eliminating the vector soliton sidebands and their corresponding noise.

With this knowledge, one more try was made at building a free-space SBR-coupled linear cavity erbium fiber laser at 1 GHz with a polarizer in the free space section. This laser would be difficult to build to 1 GHz, and the increased loss introduced by the polarizer might prevent mode-locking from occurring at all. The new design and the results follow.

4.8.1 Linear Laser Cavity Design

As illustrated in Figure 4-42, the design change made to the standard second generation laser is trivial: insert a polarizer into the collimated free space section of the beam. This is easier said than done as dropping a polarizer in and maintaining the ability to rotate it to find the optimal state, of course, was not easy to accomplish. Because the first build of this laser was already very compact, there was very little space to work with. Several versions of opto-mechanical redesigns were necessary to realize this design. The changes were significant so it is useful to describe them here.

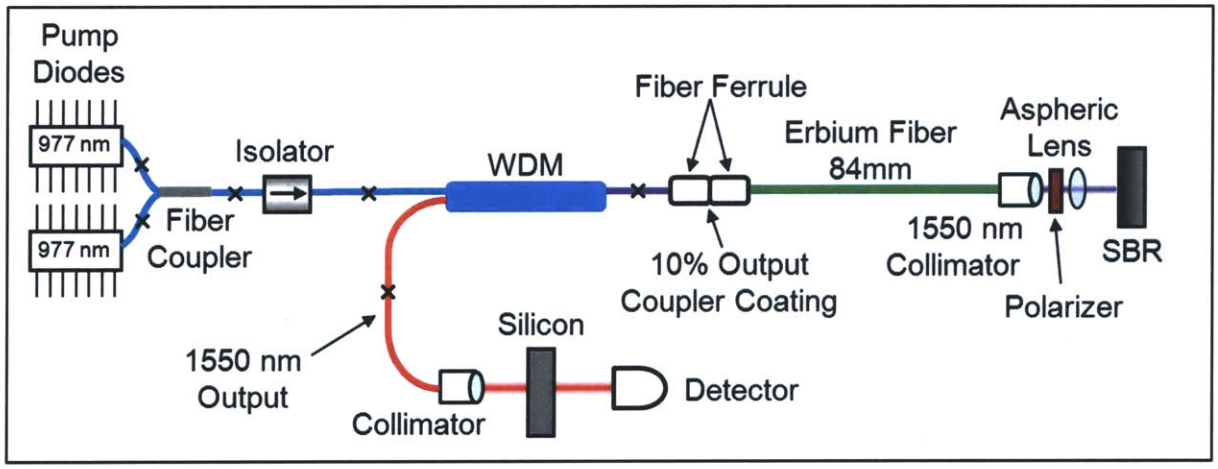

Figure 4-42 Schematic of 970 MHz linear cavity erbium fiber laser.

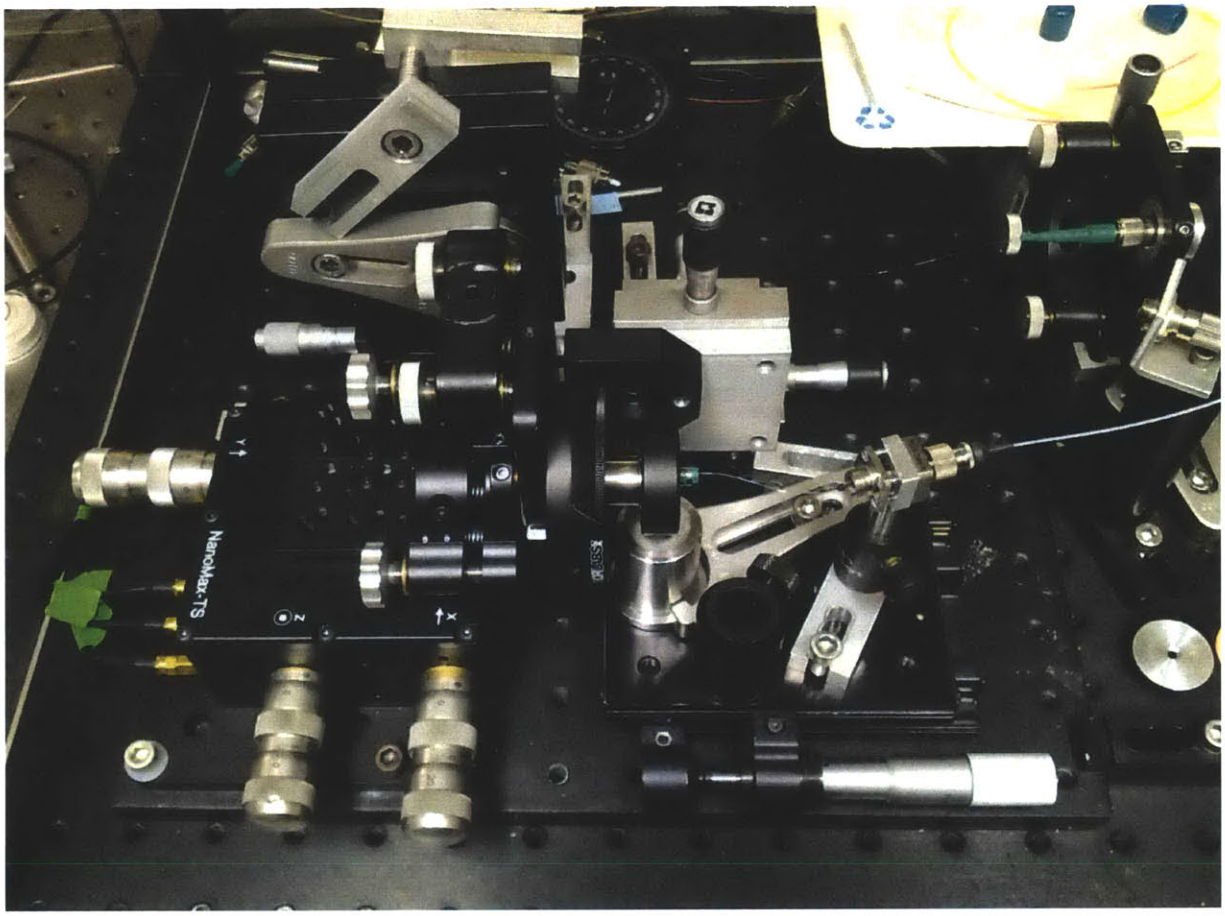

Figure 4-43 Photograph of 970 MHz linear cavity erbium fiber laser.

It would be informative to follow along in Figure 4-43, the photograph of the new laser. Beginning next to the SBR: the aspheric lens mount was thin, but it was much thicker than the lens itself. So, precious millimeters were saved by manufacturing a new mounting ring for that lens. An important consideration for this cavity design is the ability to remove the SBR and insert a different one without disturbing the alignment of the rest of the cavity. Previously, this was done by sliding the cavity far enough away from the SBR to allow fingers to reach in and change it. Alternately, a rear loading SBR mount could have been used but these mounts keep the surface of the mirror recessed and away from the focusing lens, a sub-optimal solution. Adding the polarizer mount meant a new way to remove the focusing lens was needed. This new way turned out to be mounting the lens in a tip/tilt

mount connected to a magnetic plate[46] attached to a precision XYZ stage in a vertical orientation. Now the entire mounting assembly of the focusing lens could be simply lifted away for SBR replacement.

Next follows the new polarizer rotation assembly. The first attempts to hold the polarizer in a fashion that allowed for rotation also rotated the focusing lens. It was learned through failures that this rotation moved the focal point of the lens too much on the SBR and made locating the optimal operating state impossible since it coupled two of the important degrees of freedom. The polarizer had to be completely independent and removable from the cavity. This was accomplished by using a solid rotation mount bolted to a fixed XYZ stage assembly. Now the fiber part of the laser could be backed away on the long range linear stage for polarizer insertion and removed without loss of alignment of the fiber or focusing lens.

Lastly, the fiber collimation package that was once held by the Z-ring in the lens mount is now simply bolted to the long range translation stage. This minor change retains the ability to fine tune the repetition rate of the cavity through the adjustment knob on the long range stage. Previously, that knob would only change the focal length of the SBR lens but now that degree of freedom is decoupled from this stage.

Overall, the extensive opto-mechanical overhaul of this laser resulted in no loss of adjustments or degrees of freedom within the laser. Every fine tuning alignment capability was maintained and the option of rotating a linear polarizer in the free space part of the beam was added. Regrettably, enough free space section was lost that the repetition rate dropped by 30 MHz. The only way to get back to a full 1 GHz would have been to fabricate a shorter fiber and that was decided to be an unnecessary step to take at this point in the experiment.

4.8.2 Linear Laser Results

Adding the linear polarizing element to the 1 GHz linear cavity free space SBR coupled fiber laser increased the intra-cavity losses. There appeared to be no truly low loss

[46] Thorlabs, Model: KB3X3 Kinematic base

mode of the laser corresponding to any linear polarization set by the polarizing element. There proved to be almost too much loss for the laser to mode-lock.

The only SBR that yielded any results was the MIT VA86 PRC. The uncoated VA86 burned when aligned in this system. The 20% coupling losses inherent with the fiber collimation process, the polarizer losses, and the linear losses of the coated SBR really held down the bandwidth of the optical spectrum.

4.8.2.1 Optical Spectrum

Figure 4-44 plots the narrow spectrum obtained for this laser configuration.

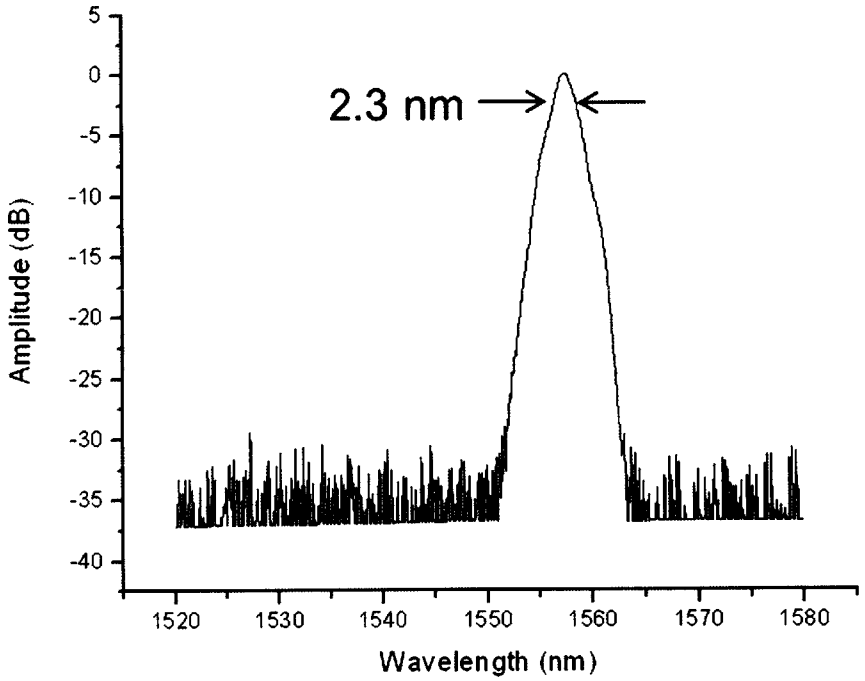

Figure 4-44 Optical spectrum of the 970 MHz linear cavity laser with VA86 PRC SBR.

This weak state supported a 2.3 nm 3 dB bandwidth centered at a wavelength of 1557 nm. That spectral width corresponds to a transform limited pulse duration of 1.1 ps. This doesn't even classify as a femtosecond laser anymore.

4.8.2.2 *RF Spectra*

For completeness, the detected RF spectra are plotted in Figure 4-45. The full span plot shows a nice flat spectral envelope for the harmonic lines but the fundamental beat line is actually a little noisy around the base. The fundamental does confirm the repetition rate to be 970 MHz. The mode-locking mechanisms are just barely able to form pulses and the noise seen in the RF scan is evidence of that.

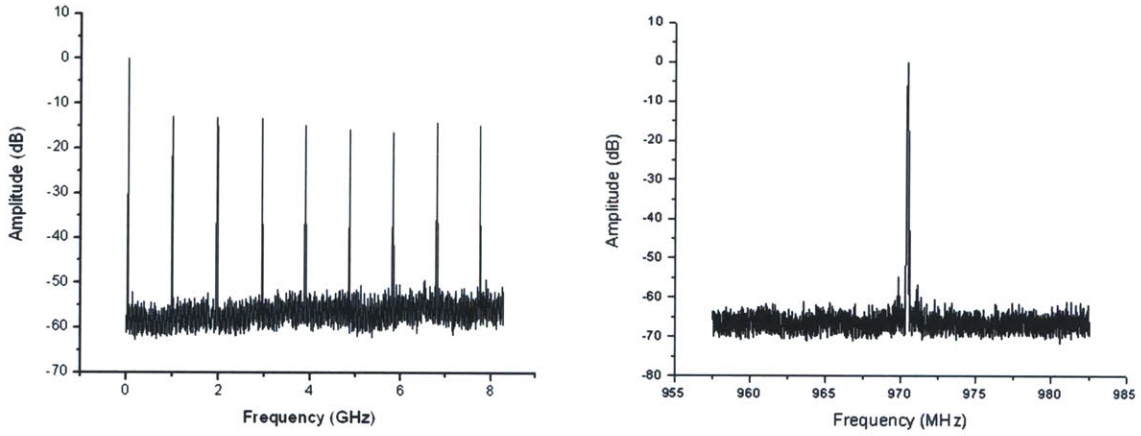

Figure 4-45 Full span RF spectrum (left) and Fundamental RF line (right) of the 970 MHz linear cavity laser with VA86 PRC SBR.

4.8.2.3 *Output Power / Pulse Energy*

The only operational state was found for full pump power of 780 mW. The 1550 nm output power was low for that level of pumping – 2.25 mW. That corresponds to a pulse energy of 2.3 pJ and an efficiency of 0.3%.

4.8.3 Discussion

Recent work on similar lasers in our group had shown that controlling the polarization of the light in the cavity was necessary to reliably eliminate the vector soliton behavior sometimes observed in this laser. Therefore, a serious effort was undertaken to remake this cavity with a rotating polarizer element while maintaining as high a repetition rate as possible.

The resulting setup turned out to be solid, useful, and retained all of the adjustments necessary to alighting and mode-locking the cavity with a SBR. Unfortunately, the increased loss introduced by the polarizer made stable mode-locking almost impossible and the only result that was obtained was very weak and not particularly useful as a course for future laboratory experiments.

4.9 Conclusions

This chapter described and explained six versions of an experimental laser with an erbium doped gain fiber, a linear cavity configuration, approximately GHz repetition rate laser, and a free space SBR coupling feature.

- The first generation - free space pumping and output coupling
- The second generation - fiber coupled pumping for SBR experiments
- "L" cavity fiber coupled pump rejection and polarizer test cavity
- Highest possible repetition rate - 1.25 GHz cavity
- Experimental Oxidized SBR test system at 314 MHz
- Second generation - Reengineered with intra-cavity polarizer

Each of these systems was diagramed, described, and analyzed. The first generation laser was intended as a "see if we can build it" experimental system. The output was a weak mode-locked pulse train. Primary weaknesses were identified such as the coupling losses into the fiber and a second generation system was built to address those issues.

This system was primarily used to test a variety of different saturable absorbing mirrors to ascertain their performance in a high repetition rate environment. The most reliable results came from the BATOP 14% modulation depth SBR which yielded 365 fs pulses at 2.8 mW of output power. The conclusions of this study, as often is the case, were more questions. So further tests were conceived and carried out.

To test the source of the mirror burning a cavity modification was made to integrate a dichroic mirror into the laser. This also opened up space for a polarizer to be placed in the cavity thus two separate tests could be made to the same laser. For the MIT VA86 mirror the new cavity did perform better and was much less prone to burning; however the MIT

VA148 double absorber mirrors still burned so we are able to conclude that the Q-switching process plays a part in the mirror burning issue. The polarizing element, when introduced into the cavity did attenuate the power but it did not prevent all mode-locking from occurring. Also, it accomplished the goal of eliminating the vector solitons seen in the laser prior to its insertion. Now that some answers were obtained, we could try to see how high the repetition rate could be and still support pulsed output.

For the fixed gain per unit length of the Liekki erbium doped gain fiber we found that about 60 mm was the shortest piece we could get to mode-lock in this cavity configuration. Including the glass and air of the free space section of the cavity the repetition rate maxed out at 1.25 GHz. Since this laser was operating just on the threshold of mode-locking, its output was not directly useful though amplification and filtering did make this laser a viable source for a few integrated waveguide experiments carried out by Michelle Sander [8].

When this laser had been established as a good SBR test system, another new SBR design could be tested. These SBR's were designed fabricated by collaborator Shelia Nabanja and their results were self-consistent enough for her to demonstrate that her process worked well. We built a slightly modified version of the test laser to have a lower repetition rate and that enabled these SBR's to have the necessary pulse shaping effects to enable mode-locking states. No further tests with these mirrors were undertaken.

In one final attempt to demonstrate that the free space SBR coupling method could produce a reliable, turnkey, femtosecond pulsed fiber laser source the entire cavity was redesigned to integrate a polarizing element. Ultimately, the system was unsuccessful in fulfilling the goals. The repetition rate demands required the fiber be relatively short which limited our available gain and the coupling and intra-cavity losses were ultimately too high to enable a useable mode-locking state.

Bibliography - Chapter 4

[1] D. Pudo, H. Byun, J. Chen, J. Sickler, F. X. Kartner, and E. P. Ippen, "Scaling of passively mode-locked soliton erbium waveguide lasers based on slow saturable absorbers," Opt. Express, vol. 16, no. 23, pp. 19221–19231, 2008.

[2] H. Byun, J. Sickler, J. Morse, J. Chen, D. Pudo, E. P. Ippen, and F. X. Kärtner, "Femtosecond passively mode-locked fiber lasers using saturable Bragg reflectors," in Ultrafast Phenomena XVI, vol. 92, P. Corkum, S. Silvestri, K. A. Nelson, E. Riedle, and R. W. Schoenlein, Eds. Berlin, Heidelberg: Springer Berlin Heidelberg, 2009, pp. 768–770.

[3] D. Chao, "Self-referenced 1.5 [mu]m fiber frequency combs at GHz repetition rates," Massachusetts Institute of Technology, 2012.

[4] H. Byun, D. Pudo, J. Chen, E. P. Ippen, and F. X. Kartner, "High-repetition-rate, 491 MHz, femtosecond fiber laser with low timing jitter," Opt Lett, vol. 33, no. 19, pp. 2221–2223, 2008.

[5] J. Chen, J. Sickler, E. Ippen, and F. Kaertner, "Fundamentally Mode-locked 3 GHz Femtosecond Erbium Fiber Laser," in Ultrafast Phenomena XVI, Proceedings of the 16th International Conference, Palazzo dei Congressi Stresa, Italy, June 9--13, 2008, 2008, pp. 727–729.

[6] J. Chen, "High repetition rate fiber lasers," Massachusetts Institute of Technology, 2009.

[7] H. Haus, "Theory of Mode Locking With A Slow Saturable Absorber," Ieee J. Quantum Electron., vol. QE-11, no. 9, pp. 736–746, 1975.

[8] M. Y. Sander, "High repetition rate fiber and integrated waveguide femtosecond lasers," Massachusetts Institute of Technology, 2012.

[9] S. Nabanja, M. Y. Sander, J. Morse, K. Shtyrkova, G. S. Petrich, L. A. Kolodziejski, F. X. Kartner, and E. P. Ippen, "Widely tunable large area SBRs for ultra-short pulse generation," in 2012 Conference on Lasers and Electro-Optics, CLEO 2012, May 6, 2012 - May 11, 2012, 2012.

[10] S. P. Nabanja, "The development of large area saturable Bragg reflectors for the generation of widely-tunable ultra-short pulses," Massachusetts Institute of Technology, 2012.

Chapter 5 1 GHz Linear Cavity Laser – End Abutted SBR

5.1 Introduction

One demanding possible application for femtosecond fiber lasers is as sources for optical frequency combs. Promising results in our group took Dave Chao down the research path to building a fully referenced and stabilized 1 GHz frequency comb centered around the 1550 nm wavelength. Details of his successful results are in reference [1], and a more complete description of the experiment and setup is located in his Ph.D. thesis [2]. While carrying out the amplification and filtering portions of his experiment, Dave noticed that the fiber laser source he was using had some interesting noise characteristics depending on which mode-locked state the laser was in. He iterated and discovered the lowest noise state for his experiment but this did raise some questions as to what was happening within the laser oscillator.

Therefore, a study was conceived that attempts to ascertain what the intracavity conditions were in each of these distinct mode-locking states. The experimental set up and results of that study constitute this chapter. Three mode-locking states were identified for testing. They are named for the approximate central wavelength of the optical spectra recorded for that state. Those wavelengths are 1560 nm, 1565 nm, and 1570 nm. Each state was sampled across the stable single pulse mode-locking regime to study how the output pulses evolved for changing intracavity energies. At each pumping power level, the complete laser performance was recorded including: output power, OSA trace, RF traces, autocorrelation, and phase noise. These data were subsequently run through the analysis procedures described in Chapter 2 to extract the repetition rate, time domain pulse shape, time domain pulse width, and RMS timing jitter.

5.2 Generation One: Free Space Pump and Output

The first fundamentally mode-locked linear cavity fiber laser to break the 1 GHz threshold in our laboratories evolved by adapting an existing 500 MHz laser [3]. Hyunil Byun and Michelle Sander continued that initial work and coaxed a pulsing state out of 10.4 cm of Liekki Er80–(8/125) erbium doped gain fiber. The best description of this first result is found in Hyunil's Thesis [2] and I summarize it in this section to properly segway into the fully fiber coupled devices.

5.2.1 Cavity Design

The design of this laser is structurally the same as the 491 MHz system detailed in reference [3], but with a shorter fiber to increase the repetition rate. The pump and output coupling section is also the same as described in Chapter 4 for the first generation free space coupled SBR laser. Figure 5-1 is a diagram of the basic essential parts to the system.

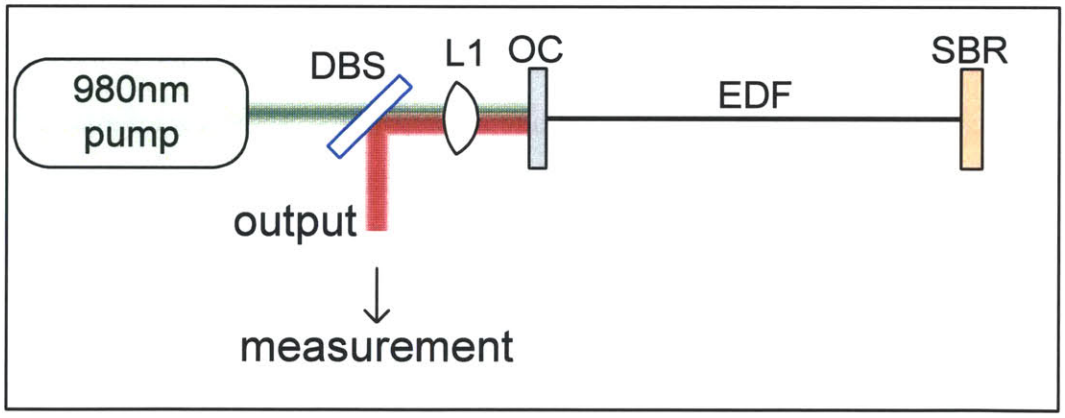

Figure 5-1 Rough schematic of the first generation linear cavity fiber laser design. (Figure courtesy of Hyunil Byun)

5.2.2 Results

The best performance achieved from this laser cavity is shown in Figure 5-2. The optical spectrum spanned a 3 dB bandwidth of 5.4 nm corresponding to a transform limited pulse width of 470 fs. The fundamental RF harmonic was detected at 974.6 MHz and there

are what we later recognized to be strong polarization-mode sidebands in the spectrum. This state was recorded quickly before the SBR suffered burn damage and the input and output power and pulse energy numbers were not readily available.

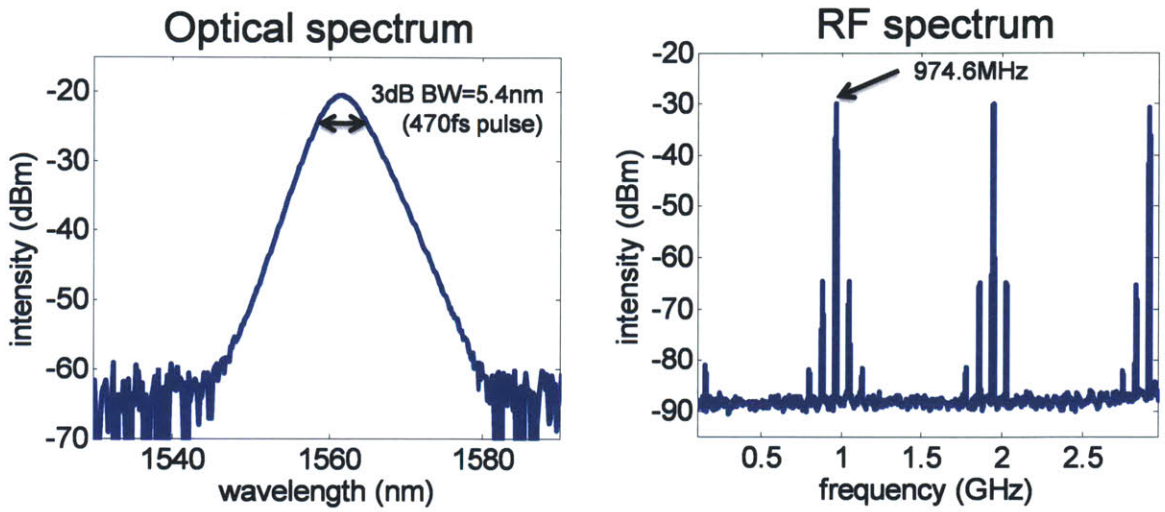

Figure 5-2 Optical and RF spectral results for the generation one linear cavity fiber laser. (Figure courtesy of Hyunil Byun)

5.2.3 Discussion

As a proof-of-concept laser, this system demonstrated that there was a path to take short fiber linear cavities up to and possibly beyond the 1 GHz repetition rate. The result was not clean but it did mode-lock and several ideas to solve the SBR burning and polarization sideband issues were investigated. Implementing some of these ideas resulted in the next generation linear cavity end abutted fiber laser.

5.3 Generation Two: Fiber Coupled Pump and Output

A through and complete study of the second generation version of this fiber laser as performed by Hyunil Byun and Michelle Sander can be found in several sources. Hyunil

describes the 976 MHz version of the laser in references [1] and [2]. A summary of this work is included here as an introduction to the output state study of the following sections.

5.3.1 967 MHz Cavity Design

The most significant advances from the first generation to the second were the pump and output coupling components. As a parallel to the free space SBR coupled lasers described in Chapter 4, WDM and coated fiber ferrule ideas were introduced to reduce the coupling losses and simplify the alignment. Figure 5-3 illustrates the design of the cavity.

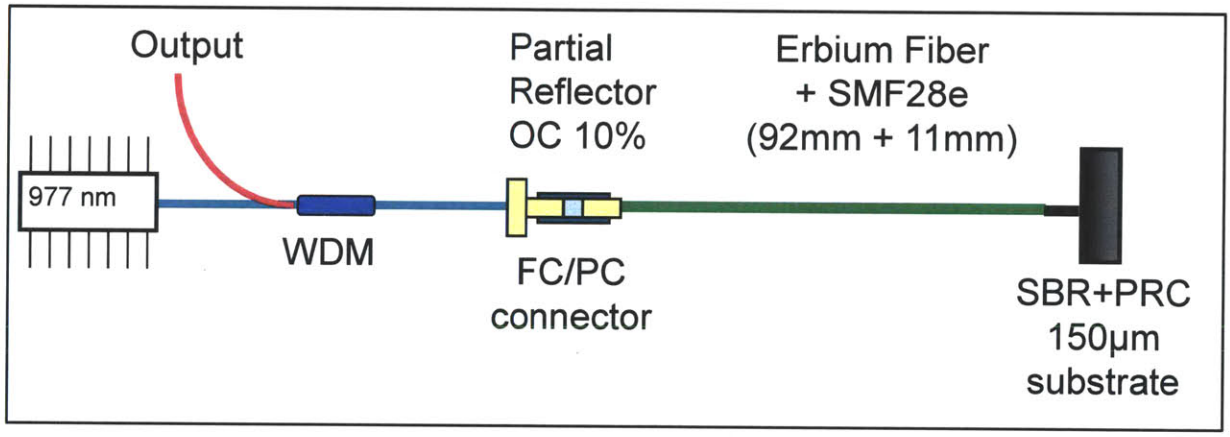

Figure 5-3 Schematic of 967 MHz linear cavity erbium fiber laser (Figure courtesy of Michelle Sander)

The laser is pumped with one 700 mW pump diode centered at the 977 nm wavelength. This pump was put through a 980/1550 WDM and passed into the gain fiber through the output coupling coating applied to the fiber ferrule. The coating was optimized as a 90% reflecting mirror for the 1550 nm wavelength, and 980 nm light passes through mostly unattenuated.

Ninety two millimeters of erbium doped fiber is fusion spliced to 11 mm of standard single mode fiber to form the 103 mm all-fiber cavity. A short piece of SMF is added to reduce the thermal load on the absorbing layers of the mirror. A full study into how to best manage the SBR thermal load is explained in reference [1] but is beyond the scope of this thesis and will not be described further.

Finally, the optical coating that functions as the cavity mirror and output coupler allows 10% of the cavity energy to escape each round trip. This light is coupled out through the WDM's 1550 nm fiber port for measurement.

After several iterations of mechanics to assemble the fiber to the SBR and reliably align the cavity, the following results were obtained.

5.3.2 967 MHz Laser Results

Figure 5-4 is a comprehensive plot of all relevant data for this laser's optimal operating state. A solid fiber to SBR coupling could be maintained that, coupled with an undamaged SBR mirror sample, resulted in a state that later proved difficult to replicate. This state's optical spectrum (Figure 5-4(a)) was centered at a 1573 nm wavelength and supported a 150 fs pulse with its 17.5 nm bandwidth. Interferometric autocorrelation measurements plotted in Figure 5-4(b) confirmed a 150 fs pulse width for the assumption of a sech pulse shape. The RF spectra in Figure 5-4(c) and Figure 5-4(d) confirm a clean single pulse mode-locked state at a repetition rate of 967 MHz. The output power was 27.4 mW given 380 mW of pump for an efficiency of 6.5%.

This laser is not only high repetition rate and reasonably high power, but its pulse to pulse timing jitter is low as well. Figure 5-5 plots the single sideband phase noise and the corresponding integrated RMS timing jitter for this state. For the span of 1 KHz to 10 MHz only 22 fs of timing jitter accumulates.

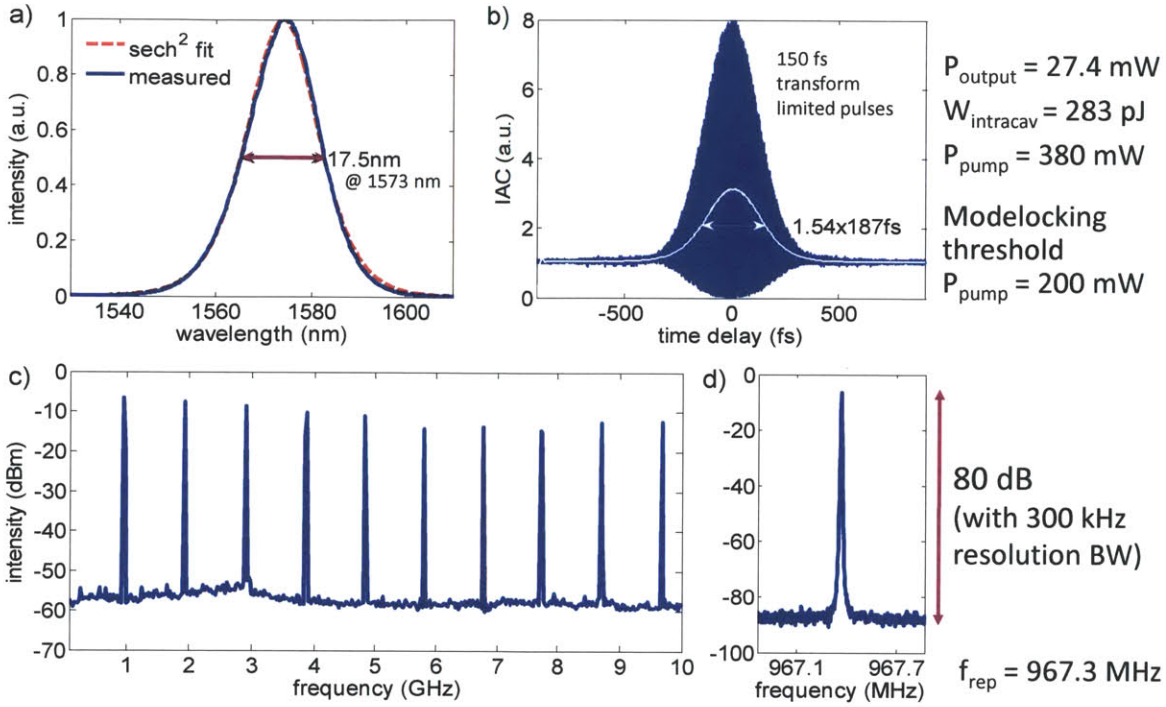

Figure 5-4 a) Optical spectrum and sech² fit. b) Interferometric autocorrelation measurement. c) Long range RF spectrum. d) Fundamental frequency RF spectral line to confirm repetition rate. (Figure courtesy of Michelle Sander)

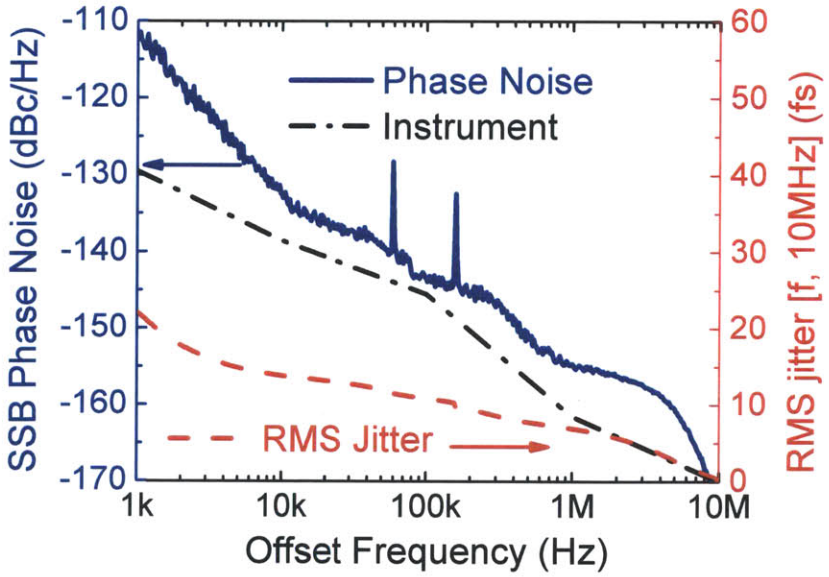

Figure 5-5 Phase noise and RMS timing jitter measurement of 967 MHz linear cavity fiber laser. (Figure courtesy of Michelle Sander)

5.3.3 967 MHz Laser Discussion

The lessons learned from the free space coupled end abutted fiber laser of section 5.2 were applied to create a successful 967 MHz linear cavity fundamentally mode-locked erbium fiber laser. This laser maintained a broad optical bandwidth supporting femtosecond pulses, high pulse energy and output power, and low timing jitter—exactly the attributes our group searches for in a next generation laser source. Therefore, a new version of this laser would be built to be used as a source in further experiments requiring femtosecond pulses and new questions would arise as a result of these experiments.

5.4 Output Pulse Characterization

The objective of this study was to complete a characterization of the 1 GHz linear cavity erbium fiber laser's performance through the different mode-locking states that we could force it into. To further that purpose, the design and one set of performance results are detailed to provide a baseline of comparison.

5.4.1 1.0367 GHz Cavity Design

This laser technology had greatly matured by the third generation version. The repetition rate was slightly above 1 GHz, the output pulses could be high energy and low jitter, and the laser itself was stable for long time periods if left undisturbed.

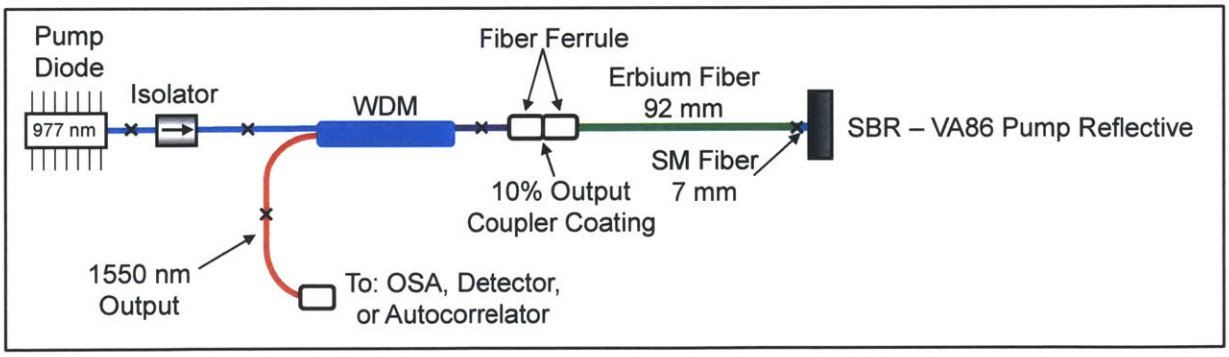

Figure 5-6 Schematic of 1 GHz linear cavity fiber laser as used for operating state testing.

Since this version of the laser is the source of this chapter's subsequent data; it is appropriate to fully diagram and carefully explain every component chosen. To begin, the system is diagramed in Figure 5-6.

The 980 nm pump diode manufacturers have been continuing to improve their product offerings and for this laser a 700 mW diode from EM4[47] was chosen. The polarization maintaining fiber from this pump is spliced to a FC/APC SMF fiber pigtail allowing for easily connecting and disconnecting the pump from various test systems. The pump isolator[48] is placed in the system to protect the diode from any back-reflections that may damage or destroy it. This isolator is also fiber connectorized on both ends for interchangeability.

The next component that changed from previous generations was the wavelength division multiplexer (WDM). This particular WDM[49] was chosen for the low dispersion fiber[50] used in its manufacture. Instead of Corning SMF-28e single mode fiber with a dispersion of +18 ps/(nm km), this OFS specialty fiber has a dispersion of -1.25 ps/(nm km) around 1550 nm. Low dispersion is important in keeping the laser output pulses from dispersing too much between the laser output coupler and the end of the output fiber.

To minimize loss, the combined input/output fiber of the WDM was fusion spliced to the SMF of the ferrule with the output coupler coating applied. This ferrule was then attached with a ceramic mating sleeve to the polished ferrule at the end of the gain fiber[51]. This gain fiber remains 92 mm long, as in the second generation system, but the piece of SMF spliced to it has been reduced in length from 11 mm to 7 mm to bring the laser repetition rate over the 1 GHz mark.

The end of the gain/SMF fiber piece is epoxied and polished into a standard 126 μm core FC/PC fiber connector and this connector is pressed against the SBR mechanically

---

[47] EM4, Model: 0700-0980-PM 700 mW 980 nm pump diode
[48] OFR, Model: IO-F-980 fiber coupled isolator
[49] AFW Technologies, Model: WDM-SM-2-9815-L-1-L-0 980/1550 WDM
[50] OFS, Model: "Lucent 980 Coupler" or BF05635-02, CL 980 16 Photonic Fiber
[51] Liekki, Model: Er80 – 8/125 erbium doped fiber

through the threads in the fiber coupler[52] and lens tube[53]. It is this connection that provides the necessary degree of freedom to change the laser's mode-locking states.

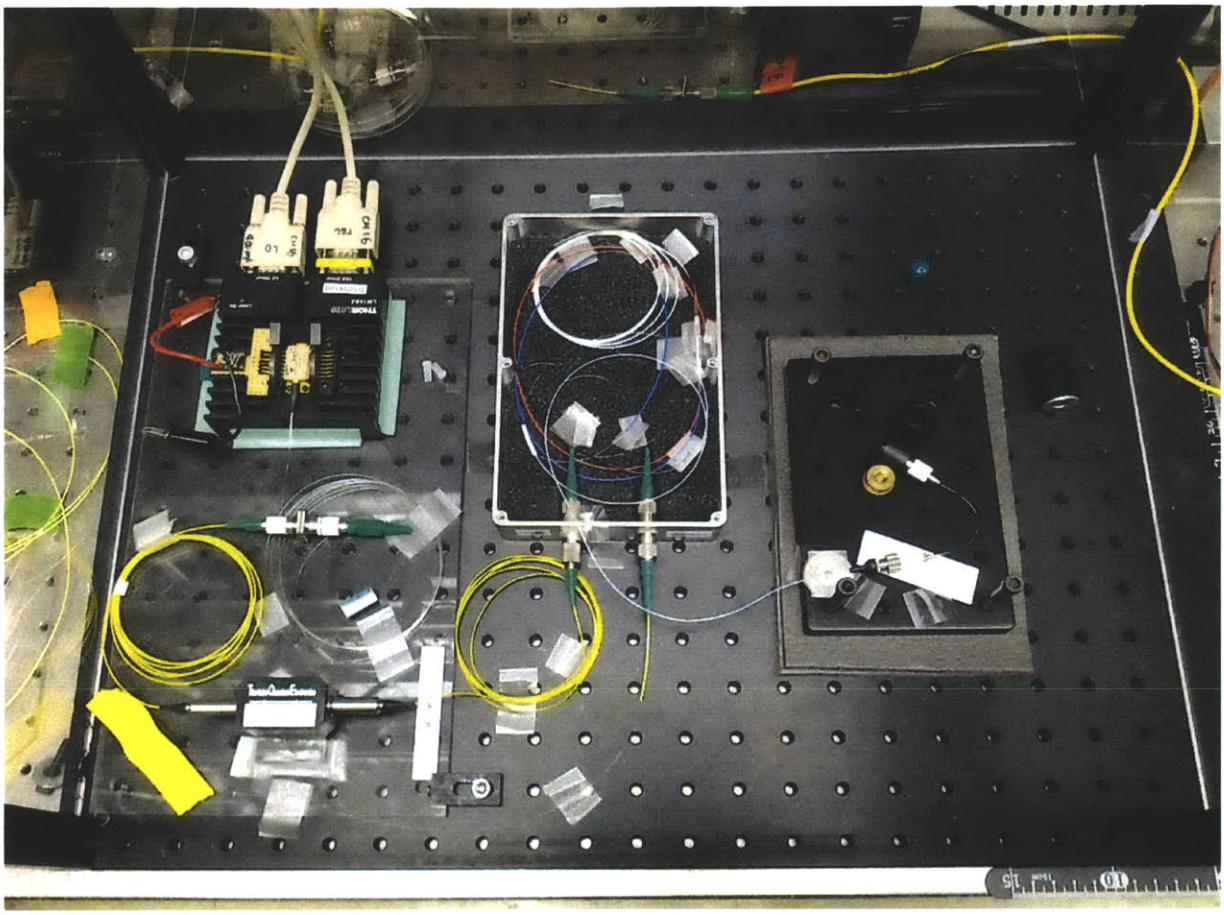

Figure 5-7 Photograph of 1 GHz linear cavity fiber laser. The pump and isolator are on the left, the WDM in the center, and the laser cavity on the black board to the right.

Figure 5-7 displays a photograph of the entire laser setup as it sat on the optical breadboard for testing. Several measures were in place to minimize the noise. First, the entire board was encased in a polycarbonate enclosure to eliminate any lab air movements. In addition, the fiber piece that composes the cavity sits on a separate aluminum board supported by alternating layers of lead and foam to further minimize any vibrations the air-floated vibration isolating optical table may fail to suppress. Not pictured is a foam covered

[52] Thorlabs, Model: SM05FC threaded fiber adaptor
[53] Thorlabs, Model: SM05L05 lens tube

cardboard box placed over the fiber board to further dampen air currents and maintain a more steady temperature during operation. These efforts do pay dividends when the optimal laser state yields a power level with only 5.75 fs of RMS timing jitter.

5.4.2 SBR Reflectivity

When the fiber is mechanically pressed against the SBR, the coupling may not be at an exact 90° angle. If it is not, the 125 μm diameter of the fiber means that an air gap of up to tens of microns between the fiber core and the mirror surface will form. This gap will introduce an index of refraction mismatch between the fiber glass and the PRC material altering the functional reflectivity of the mirror.

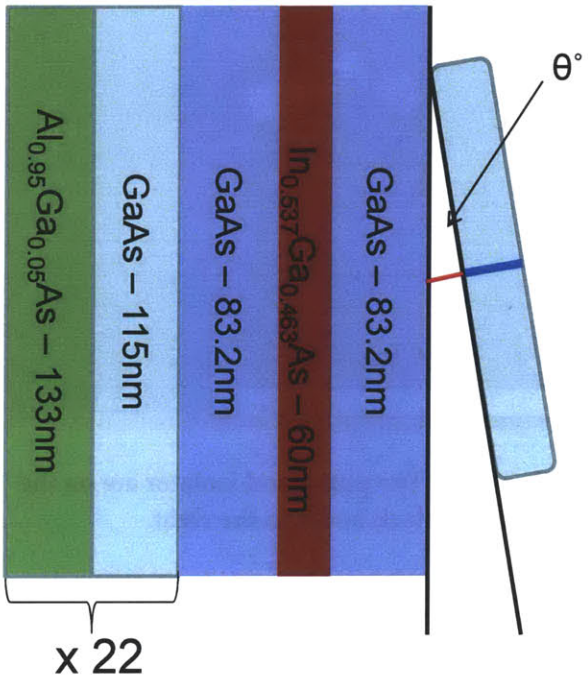

D = 1000 * sin(θ)

θ	Air gap (um)
0	0
0.2	3.5
0.4	7.0
0.6	10.5
0.8	14.0
1.0	17.5

Figure 5-8 Illustration of fiber to mirror air gap. Simulations also done for mirrors with pump reflective coating layers.

Hanfei Shen and Michelle Sander had investigated this phenomenon when designing the mirrors originally and, using MATLAB® code from Hanfei's Thesis [4] which calculates reflectivity based upon material indices and thicknesses, further simulations were

done to learn if this effect could be responsible for the different states we observe in the output spectra.

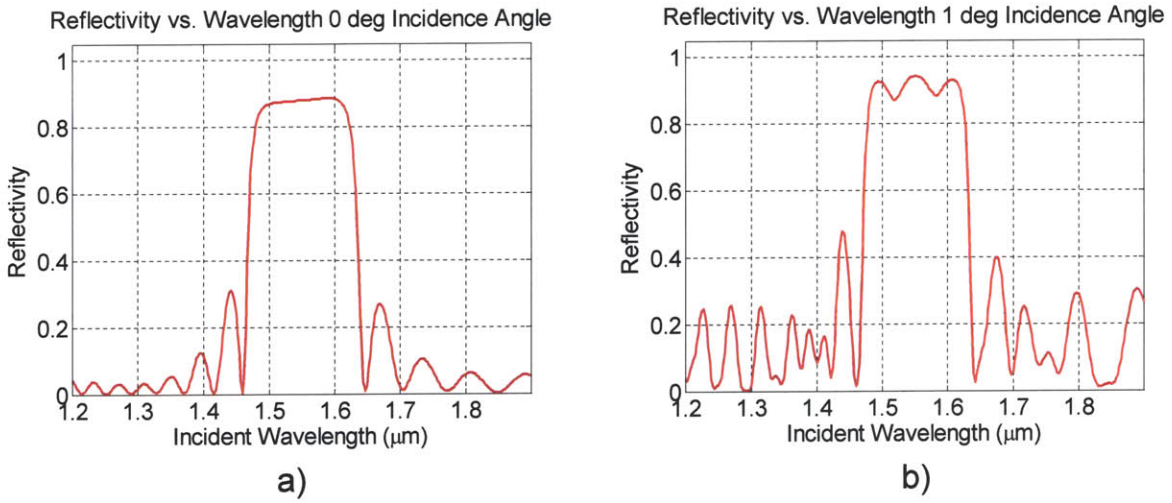

Figure 5-9 Calculated mirror reflectivity for a fiber incident at a) 0 degrees and b) 1 degree. The air gap introduced in b) causes the change in reflectivity.

As demonstrated in Figure 5-9a) and b), even a 1° tilt of the fiber to the mirror surface introduces ripples across the main pass-band of the reflectivity curve. These amplitude modulations will affect the optical pulse by shifting the center wavelength of the pulse slightly as the laser tries to settle into the lowest loss state. Based upon these simulation results, it is reasonable to assume that small changes in the fiber to SBR coupling will result in different mode-locking states within the laser cavity.

5.4.3 1.0367 GHz Laser "Best" Results

As a baseline with which to compare the three mode-locking states, the following data is presented because it represents the laser in the optimal state for seeding Dave Chao's frequency comb experiment. This state is spectrally centered around 1560 nm and it varies in 3 dB bandwidth from 4.3 nm to 7 nm. Figure 5-10 plots the evolving spectra as the pump power is steadily increased.

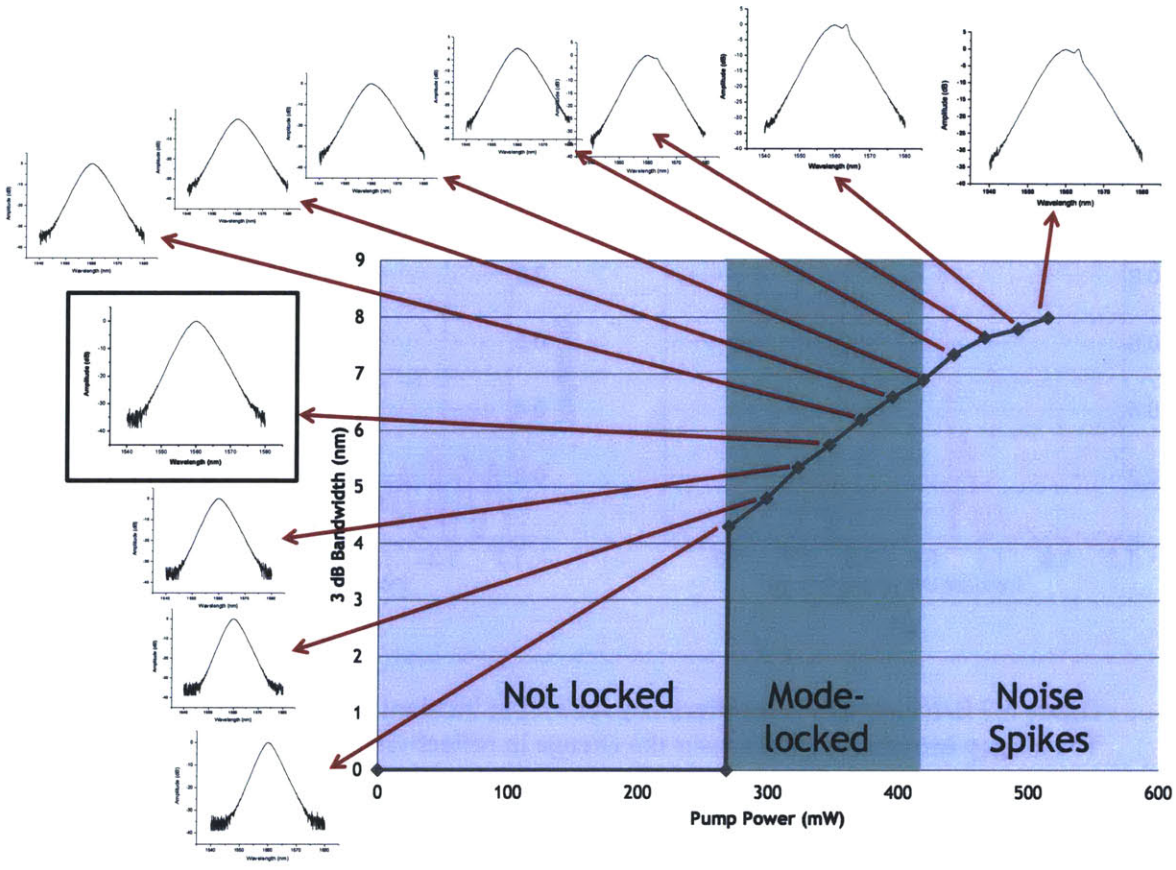

Figure 5-10 Spectral array displaying optical spectrum evolution for increasing pump power in the 1 GHz laser. The boxed spectrum represents the state used for frequency comb generation.

As highlighted in the green area, the clean mode-locking state exists for a range of approximately 100 mW of pump and the "best" state is in the center of the stability region. This state is considered best because it had the lowest timing jitter when the output pulses were filtered and amplified for use in the frequency comb. Its output power was a modest 7 mW from a pump of 350 mW for a 2% efficiency. The output pulse energies were 6.9 pJ and autocorrelation of the 6.15 nm 3 dB bandwidth yielded a 420 fs pulse width. Figure 5-11 plots the optical spectrum and the raw autocorrelation data from which the 420 fs number is extracted by assuming a sech pulse shape.

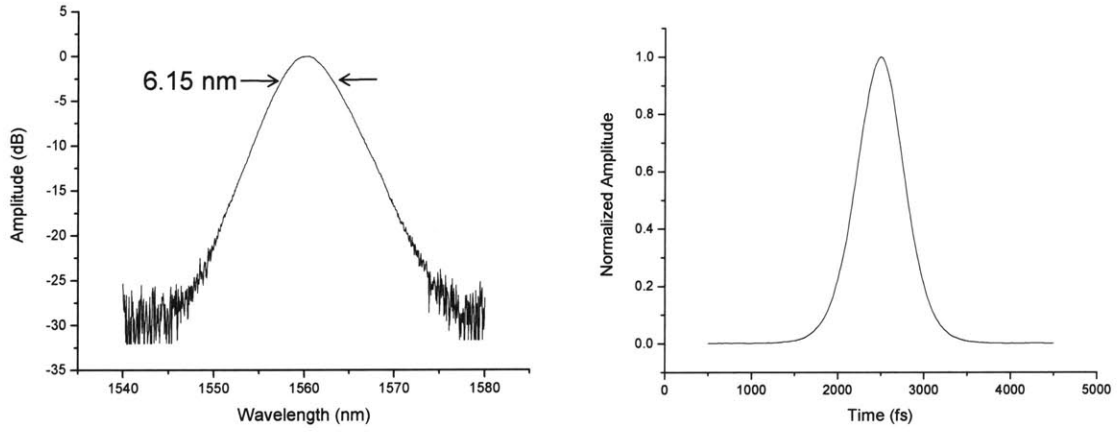

Figure 5-11 Optical spectrum (left) and autocorrelation trace (right) of 350 mW pump 1560 nm state.

As confirmation of a clean single pulse mode-locking state operating at a repetition rate of 1.0367 GHz we consult the RF spectrum analyzer data in Figure 5-12.

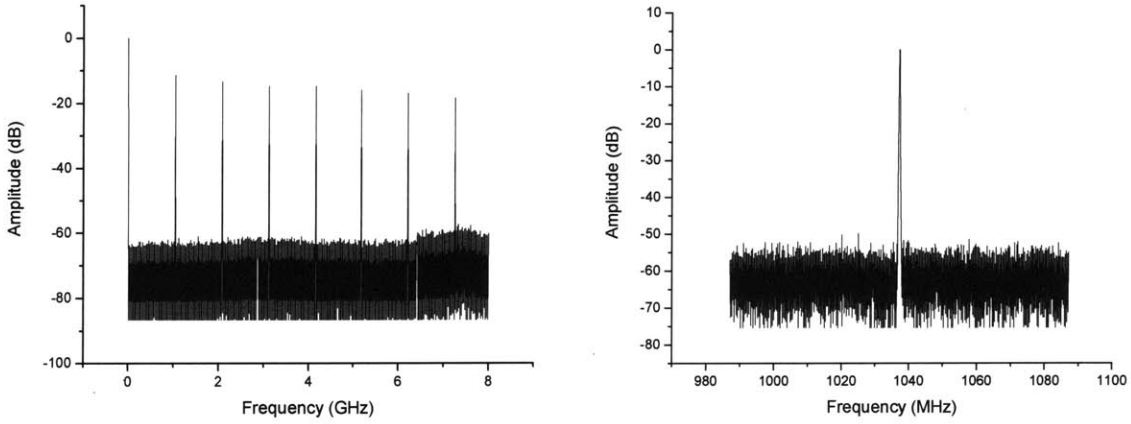

Figure 5-12 Full span RF spectra (right) and Fundamental RF line (right) for 350 mW pump 1560 nm laser state.

This is the "best" mode-locking state that Dave could obtain. The question as to why this was the best state is complicated and is partially answered by the results of the data analysis of the three states of the following sections.

5.4.4 1560 nm State

Centered around 1560 nm, this mode-locking state proved to be the lowest jitter operating mode the laser would settle into. The 1560 nm state does not have the most powerful output pulse energy or the broadest spectrum. This implies the mirror to SBR coupling is not as efficient and the cavity as a whole has higher losses. In addition, this is not the default state that a new construction of the cavity would naturally fall into when a SBR was screwed to the fiber and the power brought up. That coupling needed to be very carefully manipulated to get the angle such that a spectrum centered at 1560 would be the dominate cavity mode.

Once found and stabilized, the state was usually repeatable over several days and power cycles. It was our procedure to turn off the laser at the end of experiments rather than leave it running over night and the following day it would return to the same state by simply turning the pump current back on to the pump diode.

5.4.4.1 Optical Spectrum

This state is best visualized by Figure 5-13. Here the OSA plots of each input power level are plotted around a graph plotting spectral 3 dB bandwidth as the power level is increased from mode-locking threshold through cavity noise spikes breaking the clean single pulse state.

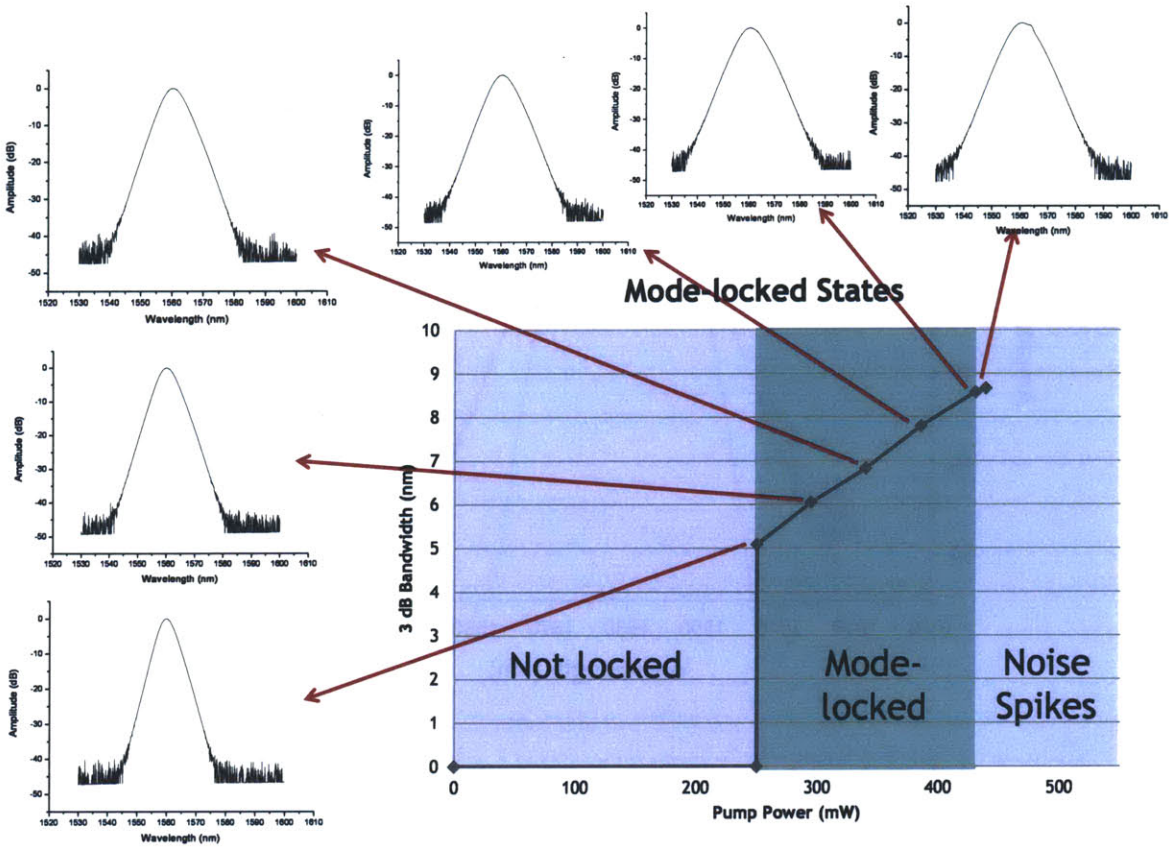

Figure 5-13 Spectral array displaying optical spectrum evolution for increasing pump power for the 1560 nm mode-locked state.

The difference between the two broadest bandwidth plots may look slight but that is due to the spectra being plotted in dBs to accentuate the details of the spectral wings. However, for both power levels there is a break through of a CW mode centered at 1570 nm that interferes with the primary mode and heavily influences the jitter. Visually this CW mode is more easily seen in the high power plots of Figure 5-10 as that figure shows more of the noise spiking spectra than Figure 5-13.

Let us choose the "best" state and examine it further. The closest state here to Dave Chao's state occurred for 385 mW of pump power.

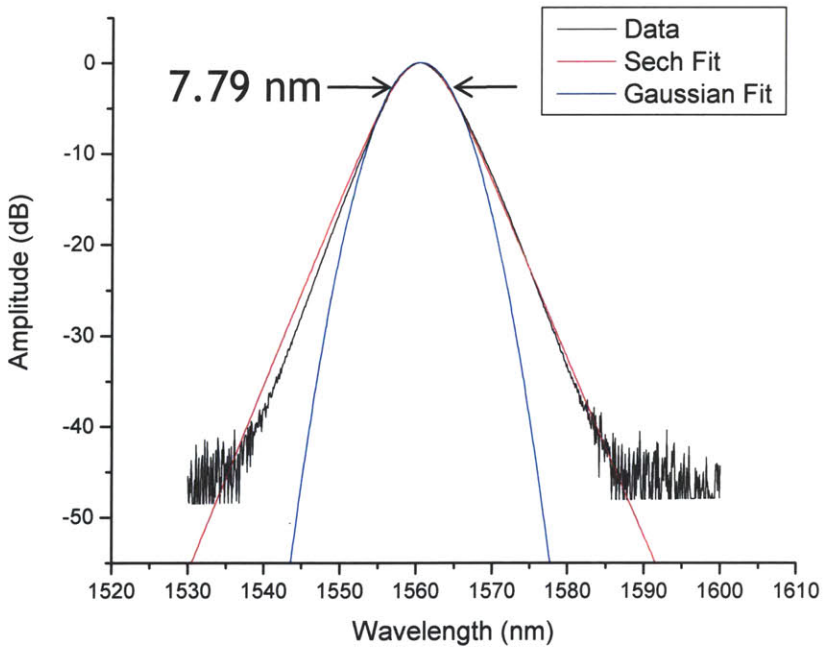

Figure 5-14 Optical spectrum with sech and Gaussian fits of the 385 mW pump 1560 nm state.

Figure 5-14 zooms in on the spectrum for the 385 mW pump power state. This state spanned a bandwidth of 7.79 nm and that corresponds to a transform limited pulse width of 328 fs. The spectrum fits a sech pulse shape very well as expected from a soliton laser. The Gaussian fit is plotted to demonstrate that the pulse shape is sech.

5.4.4.2 Autocorrelations

Autocorrelation data were taken via the free space path method and the resulting trace for the 385 mW state is plotted and fitted for both a sech and Gaussian pulse shape in Figure 5-15.

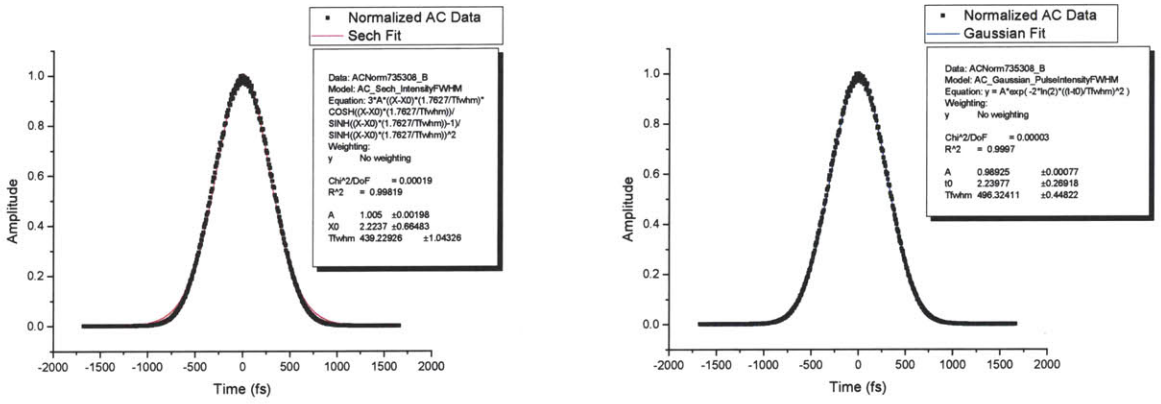

Figure 5-15 Normalized autocorrelation data for the 385 mW 1560 nm laser state. A sech pulse shape fit is plotted in red (left plot) and a Gaussian pulse shape fit is plotted in blue (right plot). The boxes are the fitting function results and are not intended to be readable.

Recall that the optical spectrum predicts a 328 fs pulse. Ultimately, a sech fit (red line) deconvolution yields 439 fs and a Gaussian (blue line) deconvolution fits to a 496 fs pulse width. This difference in inferred pulse widths is a consequence of the measurement process and the shape of a hyperbolic secant pulse verses a Gaussian pulse shape. It also continues across every power level of the 1560 nm state.

Figure 5-16 plots the same autocorrelation data with the same fits on a dB vertical scale. It is seen from this plot that the data fit a Gaussian shape down to 27 dB and a sech shape only down 10 dB. This trend also continues across every power level of the 1560 nm state and while not readily explained, must be a result of pulse propagation in fiber to the measurement apparatus and/or to filtering in the measurement itself.

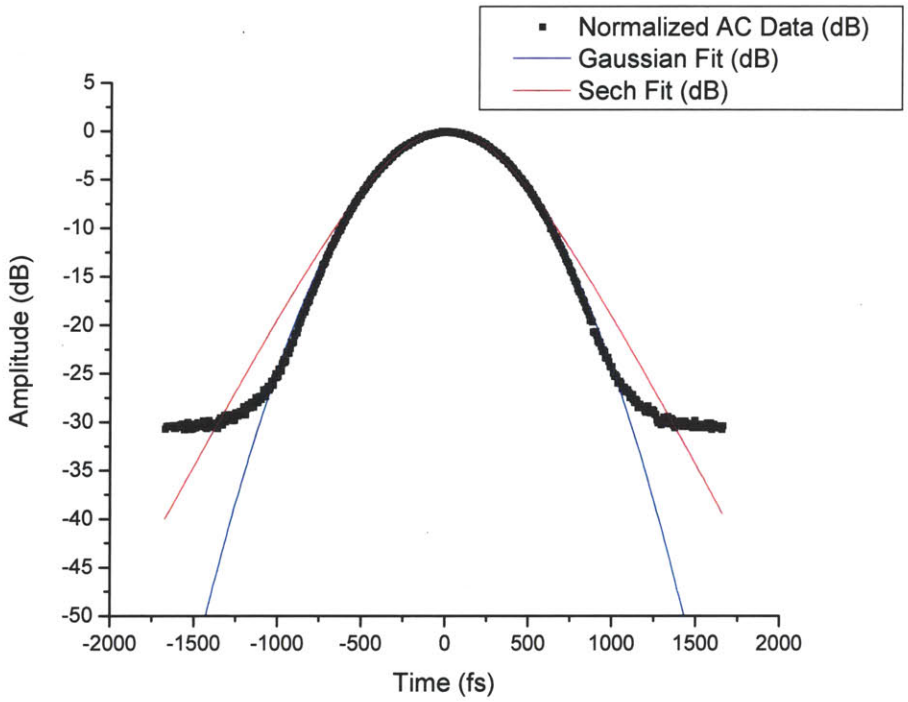

Figure 5-16 Normalized autocorrelation data and sech and Gaussian pulse shape fits plotted in dB for the 385 mW pump 1560 nm state.

5.4.4.3 RF Spectra

Figure 5-17 plots the RF spectra for the 385 mW pump state. The full span plots show clean lines and a relatively flat envelope. The fundamental frequency line is detected at 1.0367 GHz and since the fiber length does not change this repetition rate is steady and repeatable across all power levels of the 1560 nm laser.

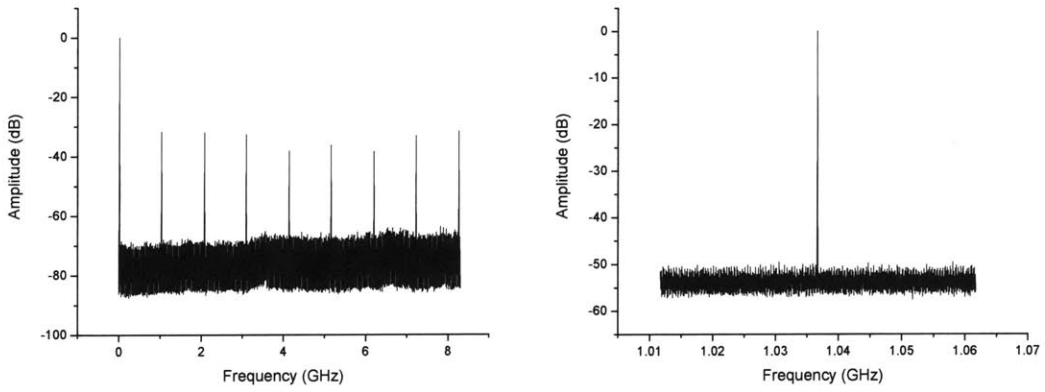

Figure 5-17 Full span RF spectra (left) and Fundamental RF line (right) for 385 mW pump 1560 nm laser state.

Notable for their absence, the polarization side bands due to vector solitons have been eliminated through purposeful manipulations of the cavity fiber's birefringence. The photograph of Figure 5-7 shows the strong bend the fiber is held in; that is the optimum position we found to eliminate the sideband behavior and suppress their noise contributions.

5.4.4.4 Timing Jitter

Regarding noise, the 1560 nm state of this laser had by far the lowest pulse to pulse timing jitter. Figure 5-18 plots the recorded phase noise and the integrated RMS jitter calculated from each power level of the 1560 nm laser state. Note that Figure 5-18(c) is the very lowest noise state at 5.75 fs of jitter. The data independently confirms that this laser state at this power level results in the lowest possible jitter. It is not coincidence that 350 mW of pump power into the 1560 nm state alignment is the laser configuration used by Dave Chao to create his frequency comb [5].

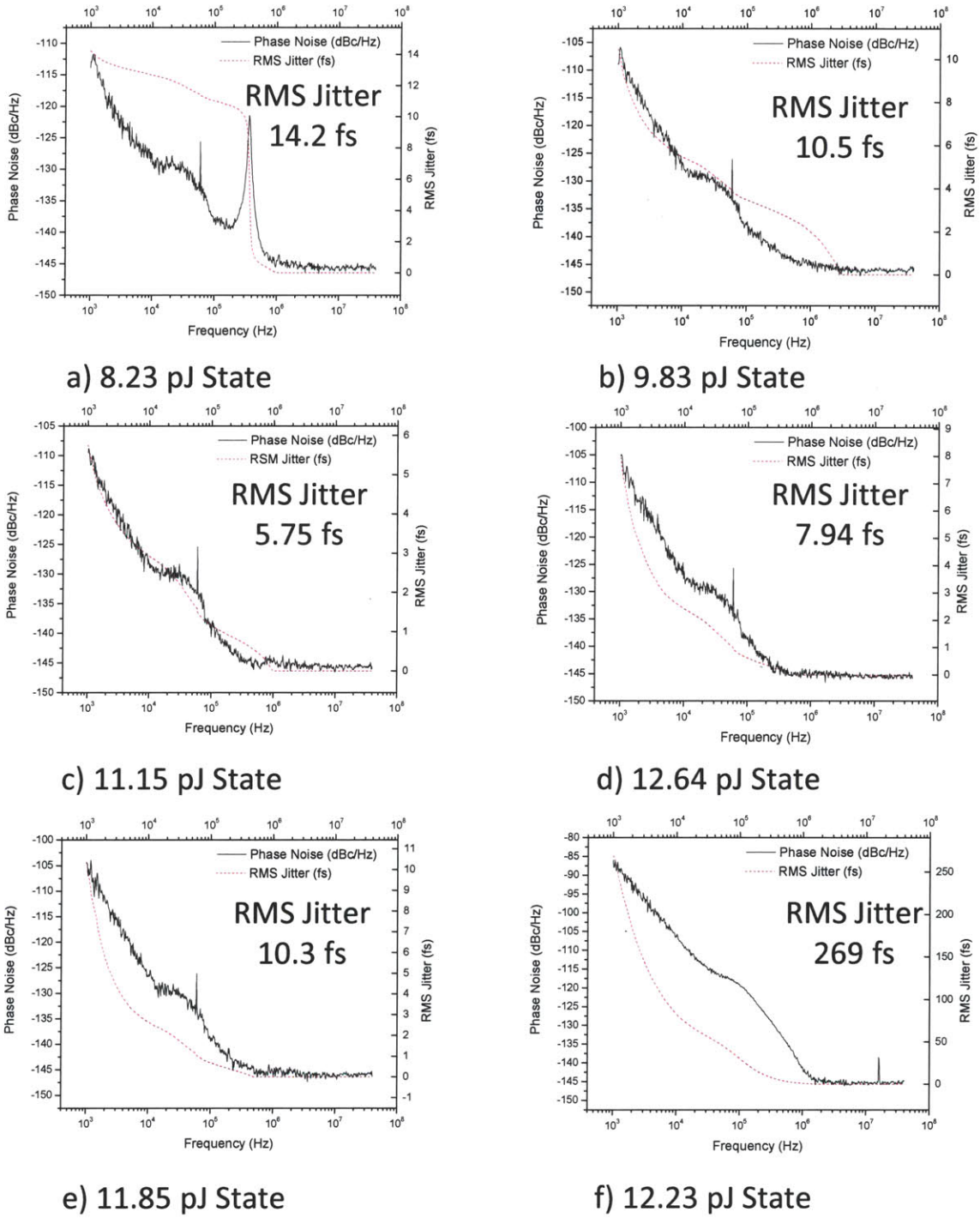

Figure 5-18 (a-e) Phase noise and integrated RMS timing jitter plots for six recorded power levels of the 1560 nm state.

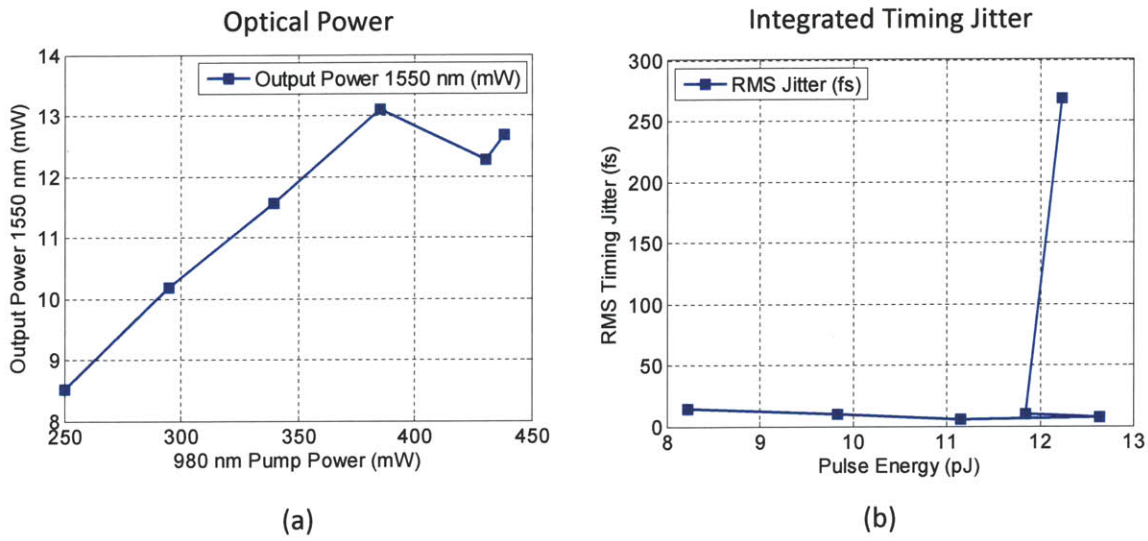

Figure 5-19 (a) Output power for increasing pump powers of the 1560 nm state. (b) Integrated RMS timing jitter for the recorded power levels of the 1560 nm laser state.

For a more comprehensive look at the laser's performance, note the interesting dip in power illustrated by Figure 5-19(a). This dip in output power occurred when the intracavity mode-locking state jumped from its most stable single pulsing condition to a state also supporting the 1570 nm CW modes. As that CW spike becomes visible in the optical spectral data (top right plot of Figure 5-13), the timing jitter explodes from 10.3 fs to almost 270 fs. Figure 5-19(b) then makes much more sense in the context of this CW state jump. The forth recorded pump power level resulted in the highest pulse energy but the jitter remained low for one more power level before breaking down and because the jitter is plotted by pulse energy and not pump power the plot takes on that staggered look.

5.4.4.5 Pulse Width Analysis

The purpose of this laser state study is to determine how well each state agrees with soliton mode-locking theory and, if it deviates, how and why. Chapter 2 explained some of the mathematical techniques and formulas used to extract information from the raw spectral and autocorrelation data.

This short cavity fiber laser operates via SBR initiated soliton mode-locking. Soliton mode-locking theory postulates that the pulses will conform to a hyperbolic secant (sech)

pulse shape [6]. Within the cavity the pulse broadening anomalous dispersion fiber and the anomalous dispersion of the pump-reflection-coated MIT VA86 SBR balance the pulse shortening self-phase modulation effects of the fiber to produce a clean soliton pulse train. These pulses pass through 2.7 meters of single mode fiber before being free space coupled into to any measurement devices and that fiber needs to be allowed for in pulse width measurements. Figure 5-20 plots measured, calculated, or predicted pulse widths at a given pulse energy for the assumption that the laser is outputting sech shaped pulses.

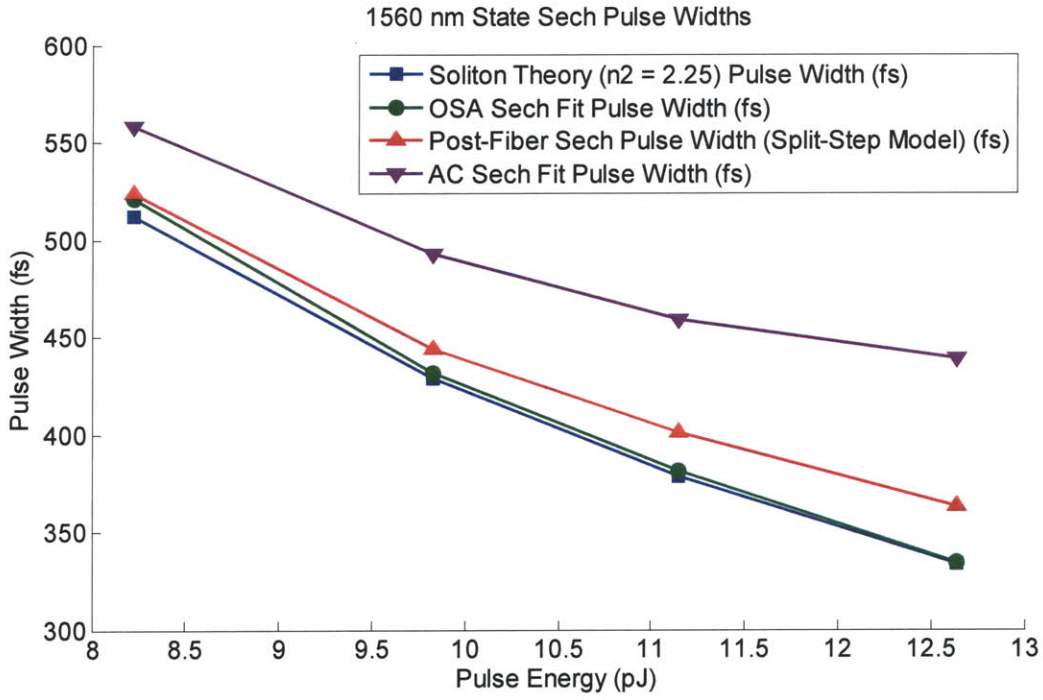

Figure 5-20 Data and simulations of the output time domain pulse width of the 1 GHz laser's 1560 nm state given increasing output pulse energies. This data assumes a hyperbolic secant pulse envelope shape.

The baseline plot is the soliton area theorem predicted pulse widths shown with blue squares in Figure 5-20. This calculation assumes that the average polarization state in the cavity is somewhere between linear and circular. Recall that, as explained in Chapter 2, we know that the effective n_2 for circular polarization is 2/3 that for linear polarization. Setting the n_2 at 2.25 instead of 3.2 results in pulse width calculations that agree very well with

spectral data and split step simulation results. Notice how the blue line of the soliton theory and the green line of the transform limited sech fits of the OSA trace data basically overlap.

The data from the OSA fits are input to a split step simulation of passing through the WDM and output fiber and the calculated pulse widths are plotted in red triangles. These pulses are broadened slightly by passing through the fiber.

As can be seen, the soliton theory, the spectral measurements, and the fiber simulations all roughly agree on pulse widths varying from 520 fs down to 350 fs at the maximum available pulse energies. The final plot showing the longest pulse widths are the real autocorrelation traces curve fitted and deconvolved assuming a sech pulse shape. These pulse widths are all about 50 fs longer than the other curves predict. However, they follow the same basic sloping trend as the pulse energy is increased implying that the underlying assumptions are correct but there must be a variable in the measurement itself that is slightly increasing the measured pulse widths.

The conclusions to draw from all of this information are that this laser state is in fact outputting sech shaped pulses conforming to SBR soliton mode locking theory and the autocorrelation measurements confirm a shortening pulse for increasing pulse energy—just with a small offset likely due to an experimental factor.

5.4.5 1565 nm State

This is what the author considers to be the "default" state of this laser cavity. The coupling loss is the lowest of all the states because the output powers are highest for this state. If a different sample of SBR or fiber is tried, the first time the mirror is physically screwed into the mount and pump power applied, the first state to demonstrate mode-locking is centered around 1565 nm. This state is also stable and repeatable. Any laser constructed with the fiber and SBR in a position favorable to support the 1565 nm modes could hold that for weeks as long as the box was not removed and the fiber manipulated.

5.4.5.1 *Optical Spectrum*

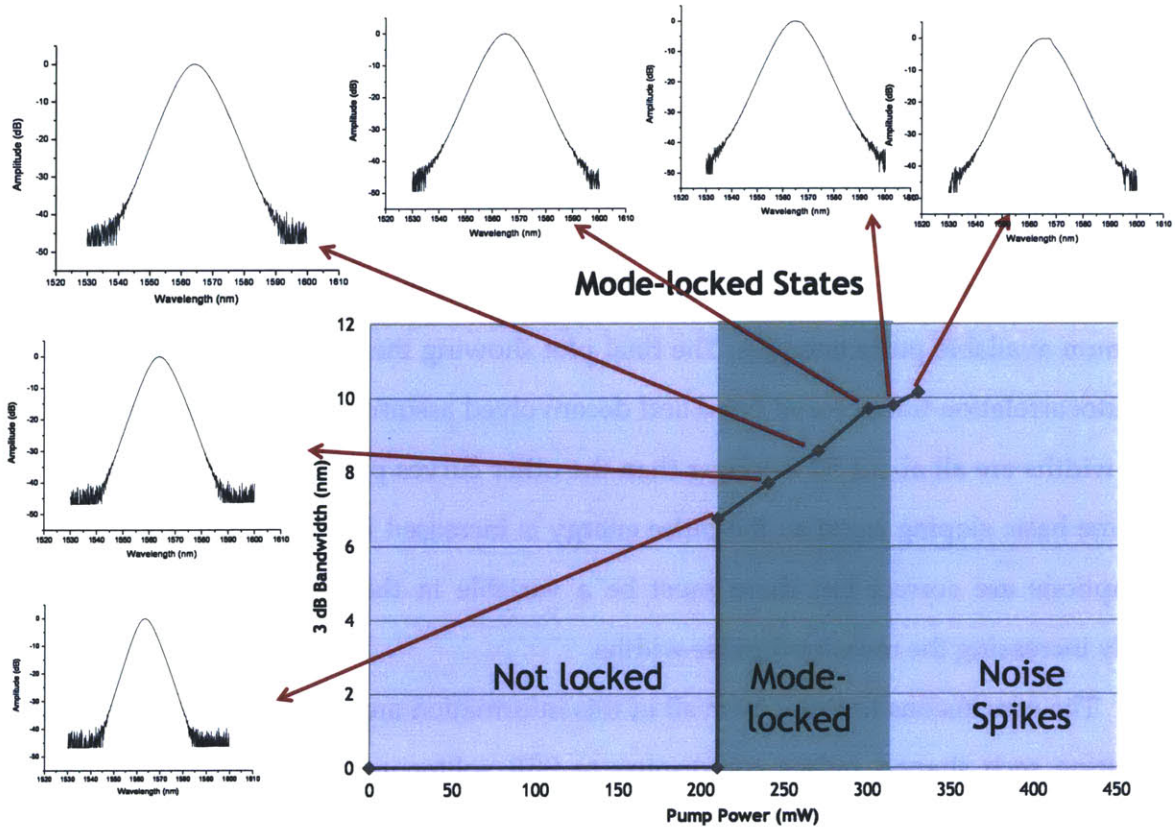

Figure 5-21 Spectral array displaying optical spectrum evolution for increasing pump power for the 1565 nm mode-locked state.

The 1565 state is visualized by Figure 5-21. Here the OSA traces of 6 input power levels are plotted around a graph plotting the spectral 3 dB bandwidth as the pump power level is increased from mode-locking threshold through cavity noise spikes. When this data was collected an effort was made to obtain 5 clean spectral traces and one trace just into the noise spiking mode-locking regime. The clean spectral states were only obtainable for a 100 mW pump power window from 210 mW to about 310 mW. As seen by the dip in increasing bandwidth from 300 mW of pump to 315 mW, the laser had actually already dropped into the noise spiking state at this power level. The timing jitter results confirm this observation. So there are four clean power levels recorded and analyzed for the 1565 nm laser state. The

"best" power level was for 300 mW of pump power and results for that laser are detailed here.

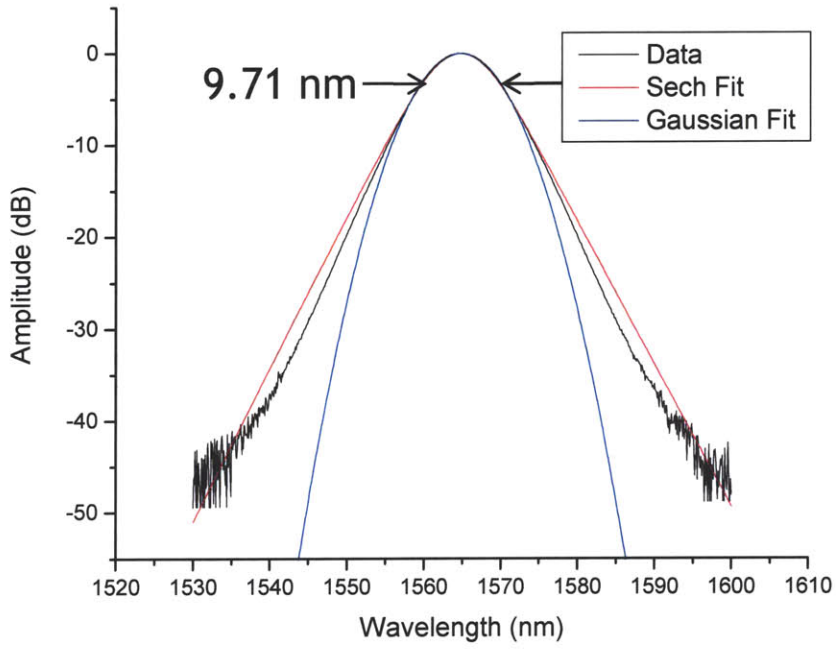

Figure 5-22 Optical spectrum with sech and Gaussian fits of the 300 mW pump 1565 nm state.

Figure 5-22 plots the recorded optical spectrum of the laser pumped with 300 mW of 980 nm light. The 3 dB spectral bandwidth of 9.71 nm corresponds to a transform limited sech pulse width of 265 nm. Sech and Gaussian pulse shape fits are plotted as well, and it is clear that the spectral shape fits the red sech line better than the blue Gaussian one. This is the case for all six recorded power levels of this state.

5.4.5.2 Autocorrelations

Autocorrelation data were taken via both the dispersion compensating fiber and the free space path methods and the resulting free space path trace for the 300 mW state is plotted and fitted for both a sech and Gaussian pulse shape in Figure 5-23.

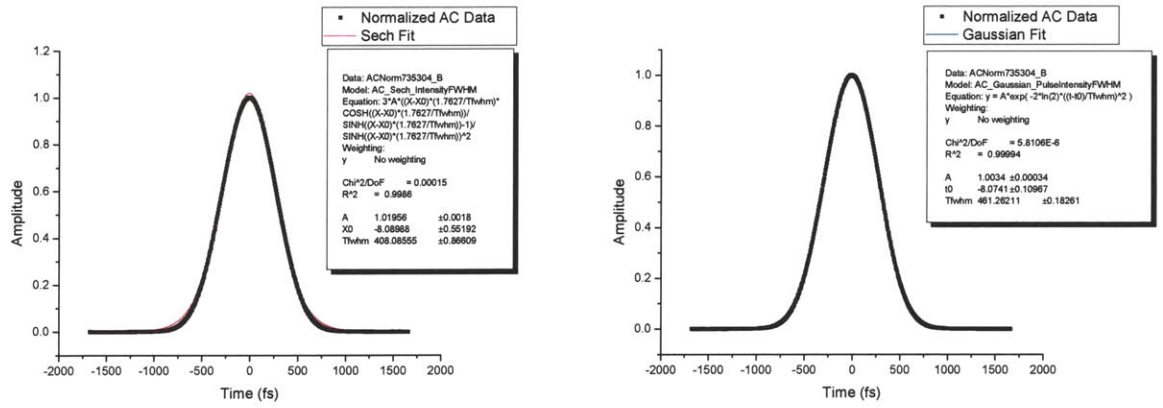

Figure 5-23 Normalized autocorrelation data for the 300 mW 1565 nm laser state. A sech pulse shape fit is plotted in red (left plot) and a Gaussian pulse shape fit is plotted in blue (right plot). The boxes are the fitting function results and are not intended to be readable.

The optical spectrum predicts a 265 fs pulse. Ultimately, a sech fit (red line) deconvolution yields 445 fs and a Gaussian (blue line) deconvolution fits to a 503 fs pulse width. These large pulse width differences continue across every power level of the 1565 nm state.

Figure 5-24 plots the same autocorrelation data and fits on a vertical scale in dB. It is seen from this plot that the data fit a Gaussian shape down to 33 dB and a sech shape only down 10 dB. This trend also continues across every power level of the 1565 nm state as indicated above for the 1560 nm state.

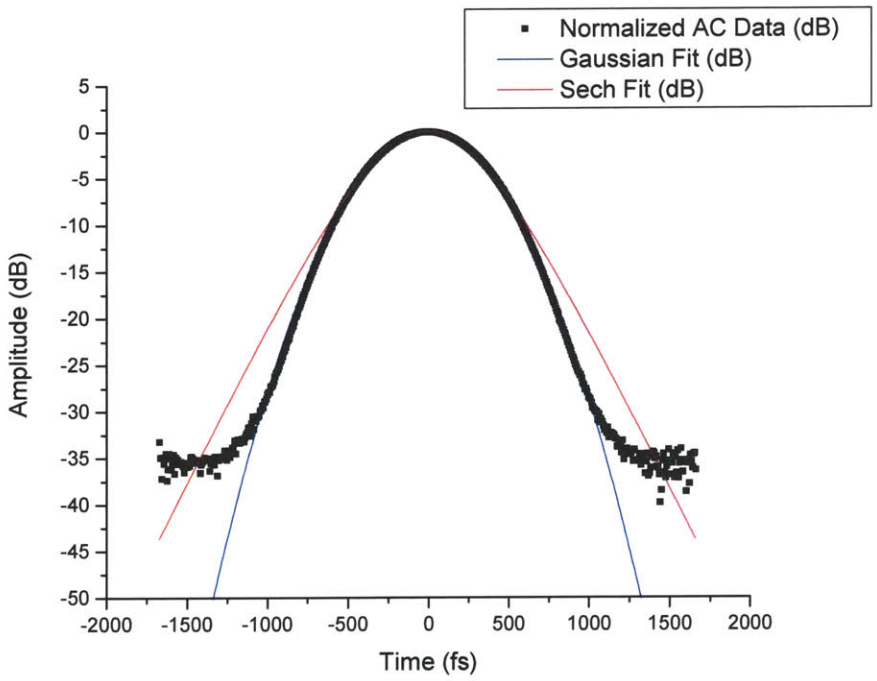

Figure 5-24 Normalized autocorrelation data and sech and Gaussian pulse shape fits plotted in dB for the 300 mW pump 1565 nm state.

5.4.5.3 RF Spectra

Figure 5-25 plots both recorded RF spectra for the 300 mW pump state. The full span plot on the left shows clean lines and a relatively flat envelope. The fundamental frequency line on the right is always detected at 1.0367 GHz across all power levels of the 1565 nm laser.

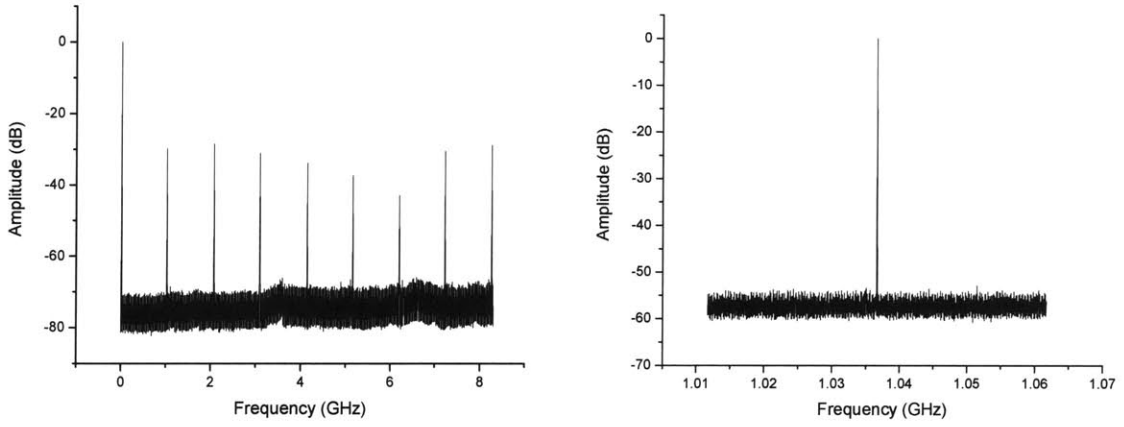

Figure 5-25 Full span RF spectra (left) and Fundamental RF line (right) for 300 mW pump 1565 nm laser state.

Elimination of the polarization sidebands (note their absence on both plots) is also achieved through fiber positioning introducing birefringence, exactly as in the 1560 nm laser state. This helps to ensure the laser is in a low noise state for the jitter measurements.

5.4.5.4 Timing Jitter

Regarding noise, the 1565 nm state of this laser had fairly low and consistent pulse to pulse timing jitter (below 100 fs) as long as it remained in the stable single-pulse mode-locking regime. Figure 5-26 plots the recorded phase noise and the integrated RMS jitter recorded from each power level of the 1565 nm laser state. Note that for this state Figure 5-26(a) demonstrates the lowest noise at 23.7 fs of jitter.

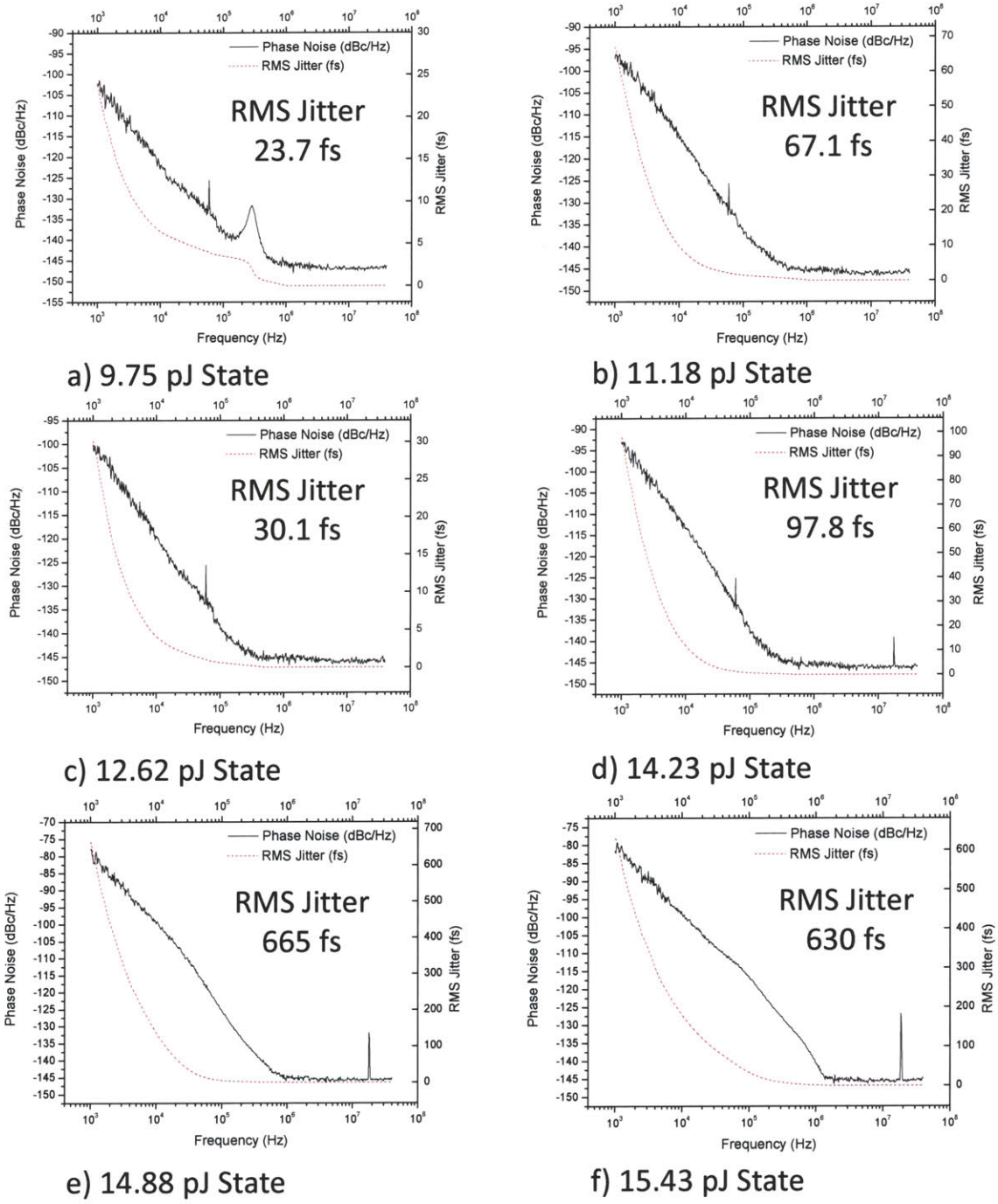

Figure 5-26 Phase noise and integrated RMS timing jitter plots for six recorded power levels of the 1565 nm state.

It is notable just how much the jitter jumps in this laser state as well when the 1570 nm CW noise spike starts to dominate the cavity. Figure 5-27 attempts to make the

difference between the two recorded operating modes clear. Figure 5-27(a) plots the nicely linear increase in output power given increasing pump power. Figure 5-27(b) plots the jitter associated with each of those power levels. Although the output power was monotonically increasing—giving no indication of changing cavity states—the timing jitter markedly increases at the 315 mW pump power level.

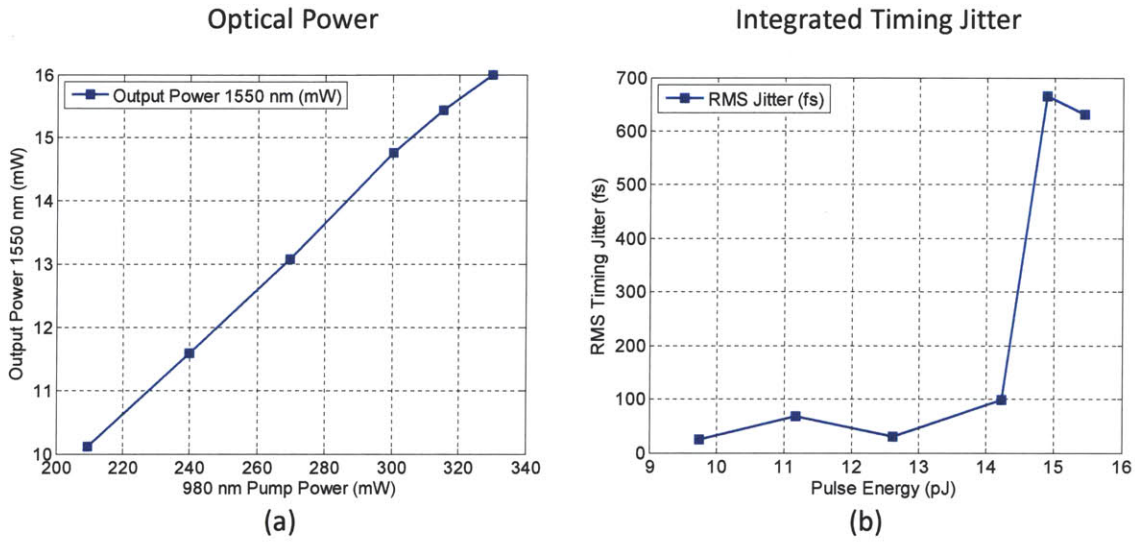

Figure 5-27 (a) Output power for increasing pump powers of the 1565 nm state. (b) Integrated RMS timing jitter for the recorded power levels of the 1565 nm laser state.

This is further evidence that 310 mW of pump was the maximum pumping the clean and stable single-pulsing mode-locking state could absorb before breaking into other, high noise cavity modes.

5.4.5.5 Pulse Width Analysis

Keeping in mind that the core of this study are the pulse width numbers, the same data were assembled for this laser state as was done for the 1560 nm state. Plotted below is a summary of the relevant results of the pulse width calculations and measurements.

The 1565 nm state of this short cavity fiber laser still operates via SBR initiated soliton mode-locking. Figure 5-28 plots the measured, calculated, or predicted pulse widths

at a given pulse energy for the assumption that the laser is outputting these sech shaped pulses.

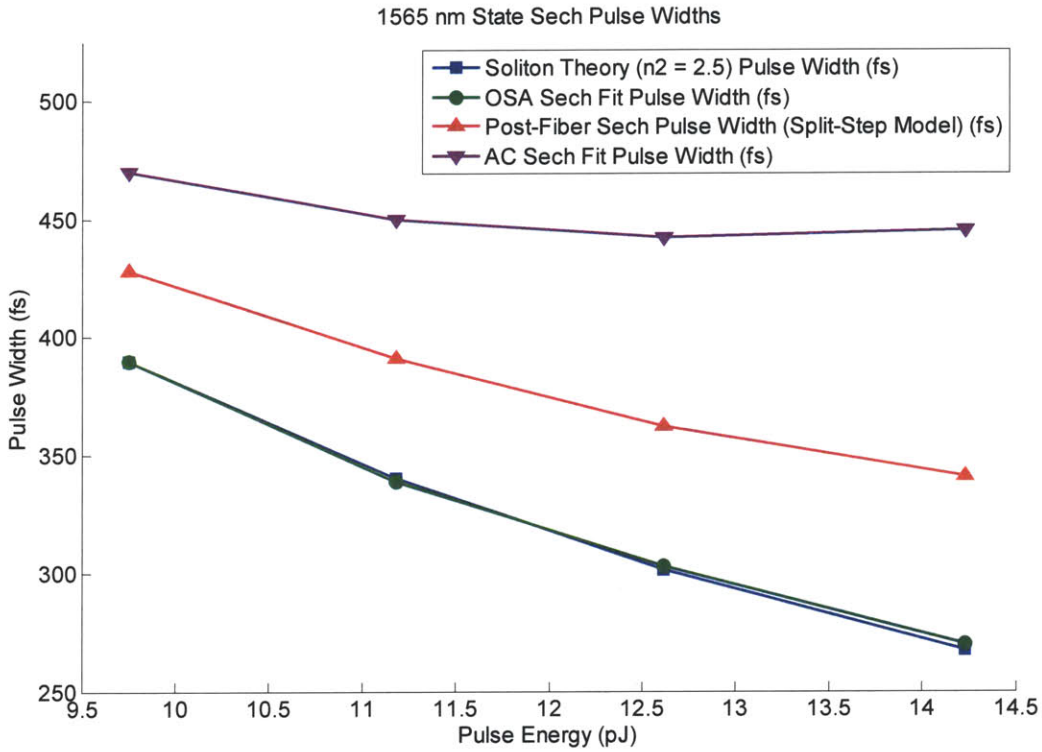

Figure 5-28 Data and simulations of the output time domain pulse width of the 1 GHz laser's 1565 nm state given increasing output pulse energies. This data assumes a hyperbolic secant pulse envelope shape.

The soliton area theorem predicted pulse widths for the measured pulse energies are shown with blue squares in Figure 5-28. As done for the 1560 nm state, the blue line is for the assumption that the polarization state is elliptical but with larger n_2. For this laser setting the average n_2 at 2.5 results in pulse width predictions that agree very well with spectral data. Due to this state's higher output powers and broader spectra than the 1560 nm state, the pulses should spread more if traveling through the same length of fiber. The split step simulation pulse widths were indeed proportionally longer than their 1560 nm counterparts. Remember, to create the red triangles of the split step simulations the data from the green OSA fit plot is run through the simulation assuming transform limited pulses initially. It is

notable that the general slope of these fiber broadened pulses still trends downward at about the same rate as the spectral bandwidth increase.

The measured data, calculations, and simulations are all consistent with theory up to this point in the experiment. The final numbers to compare are the sech pulse widths extracted from the autocorrelation traces. Every autocorrelation was curve fitted assuming a sech pulse input and the resulting pulse width extracted from the fitting equation. These data are plotted as the "AC Sech Fit Pulse Width" line in purple down arrows. For the 1565 nm state, the autocorrelation data does not match the theory or simulations. The pulse measurements are too long by 100 fs at low powers and over 250 fs at the highest pump powers.

Essentially, the pulses that are measured through the autocorrelation technique are not shortening despite the increased energy in the pulses. Within a few tens of femtoseconds the pulse widths are the same across the entire single pulse mode-locking regime for the 1565 nm laser state. This could be due partially to the increasing pulse spreading effects of the output fiber for the higher pulse energies. This could also be related to the large jump in timing jitter within the cavity at the higher pulse energies and increased deviation from the transform limit. The data from the next state will help establish a trend regarding this deviation from soliton theory in the pulse width measurements.

5.4.6 1570 nm State

A third distinct state that could be obtained from the SBR-to-fiber coupling manipulations produced much broader bandwidths and was spectrally centered around the 1570 nm wavelength. However, the output powers were similar to the 1560 nm state indicating that the cavity losses are higher and the SBR coupling losses were likely the cause. The first versions of this laser, as detailed in section 5.3.2, displayed almost twice the output power for a similar 3 dB spectral bandwidth of 17 nm.

The reasons for this difference have to do with the number of times the components have been used in experiments. Those second generation results were obtained by Michelle Sander immediately after the spliced and polished fibers were fabricated. Also, fresh and

new pieces of the VA86 PRC mirrors were used. This meant the best possible coupling results could be recorded because there was no burning or damage to the fibers or the mirrors yet. Over time, we have observed that the ends of the fibers will accumulate damage that cannot be cleaned off. The end must be repolished—a tedious task that carries risks of breaking the fiber completely.

Also, the SBR's begin to look like the lunar surface when viewed under the microscope due to mechanical and optical damage to the material layers. This is illustrated in Figure 5-29. It is still possible to manipulate the mirror into a highly reflective area; it is just more difficult.

These factors combined to make actually recording this 1570 nm state challenging. The gain fiber sample that was used for the previous two states developed visible burn damage and was unusable during continuing attempts to isolate a stable 1570 nm state. Fortunately, one other sample of the fiber was available and it had less damage to it and was yet able to couple well enough for mode-locking; just at a reduced power level.

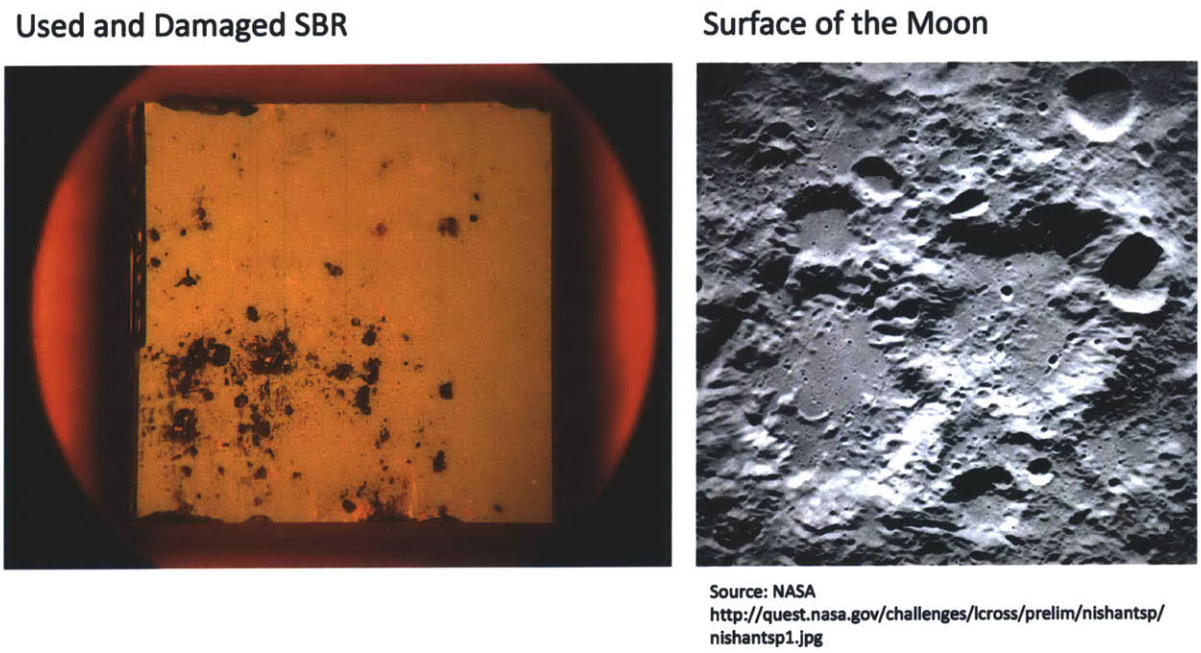

Figure 5-29 SBR mirror damage after many uses and realignments in cavity (on left). For visual reference, the lunar surface (on right).

This laser state was stable, but very sensitive to alignment and prone to component damage. The following state was recorded despite the CW mode trying to break out because it was the only version of this state that could be found with the components and time available for the study. Removal of the CW spike might be possible through delicate fiber manipulations but attempts to do that ended up losing the state and it was not recoverable. Therefore, this version of the 1570 nm mode-locked state data is presented in the following sections.

5.4.6.1 Optical Spectrum

The 1570 state is visualized by Figure 5-30. Here the OSA traces of 5 input power levels are plotted around a graph plotting the spectral 3 dB bandwidth as the power level is increased from mode-locking threshold through pulse break up. Compared to the previous two states, the 1570 nm state mode-locks over a broad range of input power levels—from less than 200 mW to over 350 mW.

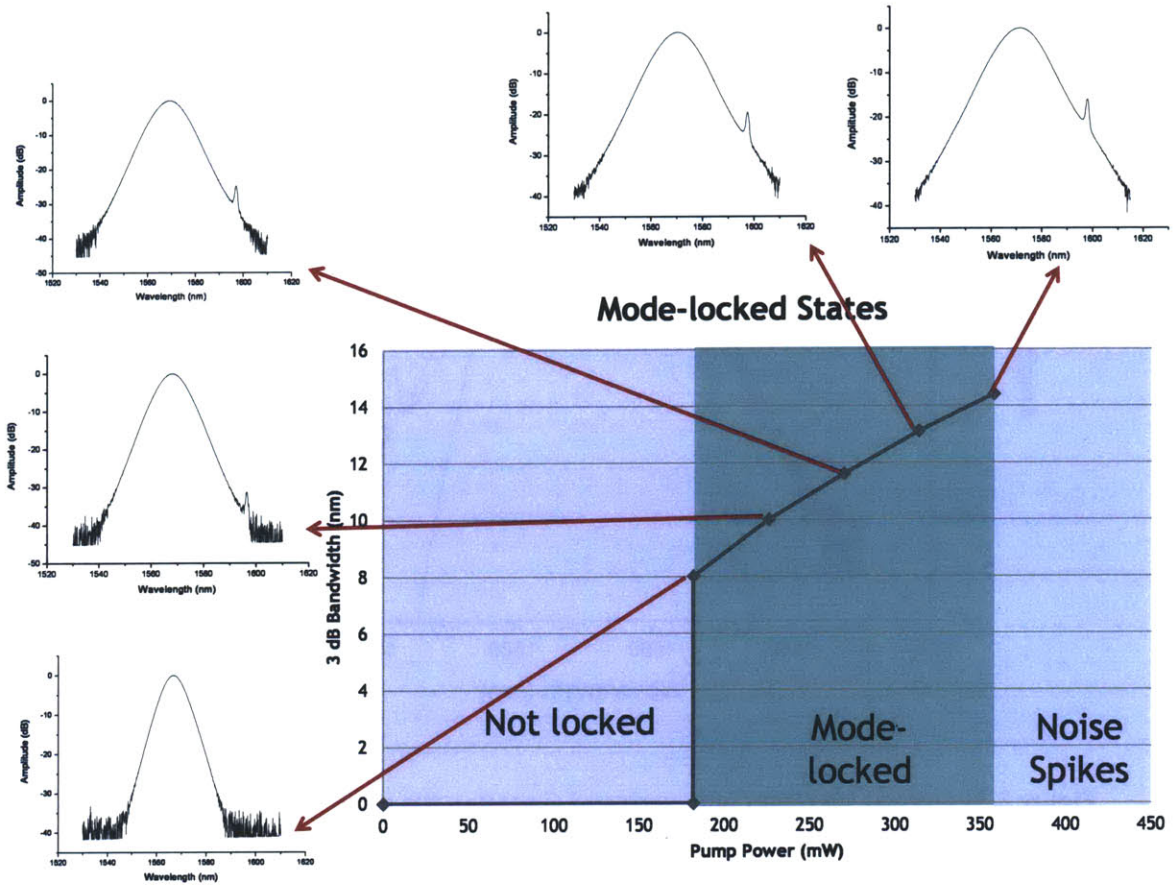

Figure 5-30 Spectral array displaying optical spectrum evolution for increasing pump power for the 1570 nm mode-locked state.

As mentioned previously, there is a small CW mode centered at 1600 nm that is present in the cavity and it remains at 1600 nm as the pulse broadens around it. Ultimately, this mode causes instabilities that result in large timing jitter for the pulses in the cavity.

For the purpose of equal comparisons, the power level in the middle of the stable mode-locking regime is detailed in the follow sections. Figure 5-31 plots the optical spectrum and both sech (in red) and Gaussian (in blue) curve fits. In this plot, as with every OSA trace for this state, the sech fit is better than the Gaussian and contributes evidence to the theory that the pulses are sech shaped in the cavity.

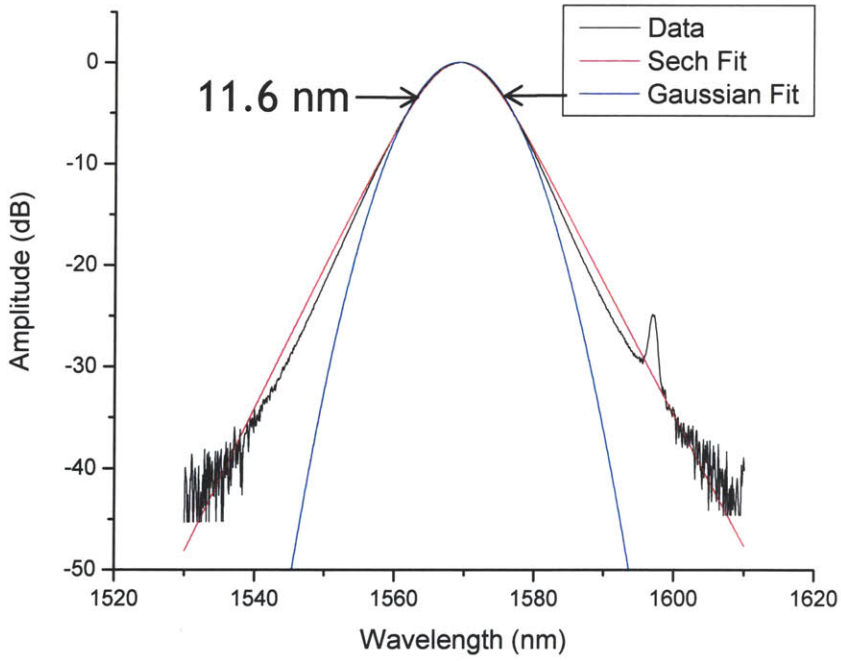

Figure 5-31 Optical spectrum with sech and Gaussian fits of the 270 mW pump 1570 nm state.

Assuming a sech shape, the 3 dB bandwidth of 11.6 nm corresponds to a 223 fs transform limited pulse. Pulse width measurements, ultimately, did not find pulses that short however.

5.4.6.2 Autocorrelations

Autocorrelation data were again taken via the free space path method to reduce fiber nonlinearities and the resulting trace for the 270 mW state is plotted and fitted for both a sech and Gaussian pulse shape in Figure 5-32. The optical spectrum predicts a 223 fs pulse. A sech fit (red line) deconvolution yields 496 fs and a Gaussian (blue line) deconvolution fits to a 550 fs pulse width. These are quite different numbers and the analysis in the pulse width sections attempts to explain this situation.

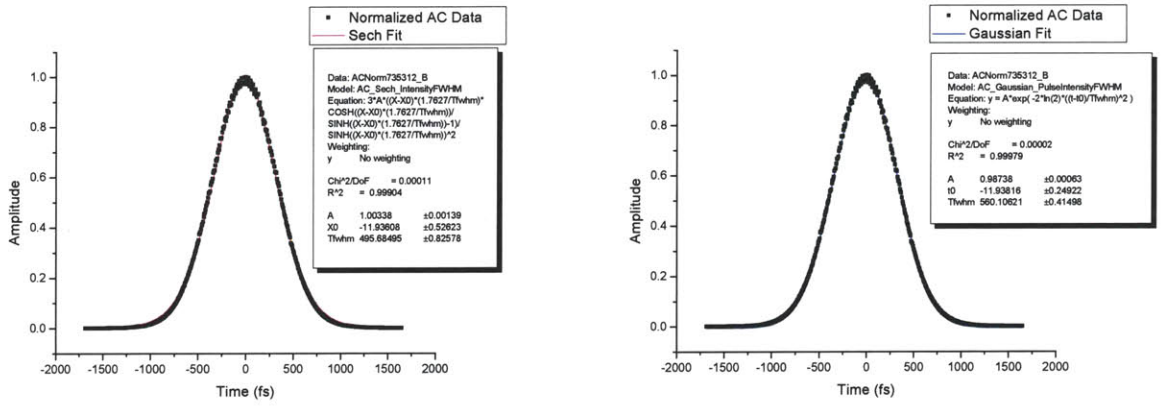

Figure 5-32 Normalized autocorrelation data for the 270 mW 1570 nm laser state. A sech pulse shape fit is plotted in red (left plot) and a Gaussian pulse shape fit is plotted in blue (right plot). The boxes are the fitting function results and are not intended to be readable.

To get a better visual idea which pulse shape better describes the data, Figure 5-33 plots the autocorrelation data and curve fits on a vertical scale in dB. This pulse shape data shows a new trend. It is seen from this plot that the Gaussian and the sech fits both approximate the data equally well down to about 15 dB before deviating one way or the other. For the two lower power level data states taken the Gaussian fits are better than the sech, as in the 1560 nm and 1565 nm states. However, for the two higher power level data states, the sech fits better trace the autocorrelation data and that is a new phenomenon not seen in any other states. The implications of this information are discussed in the pulse width section of this state.

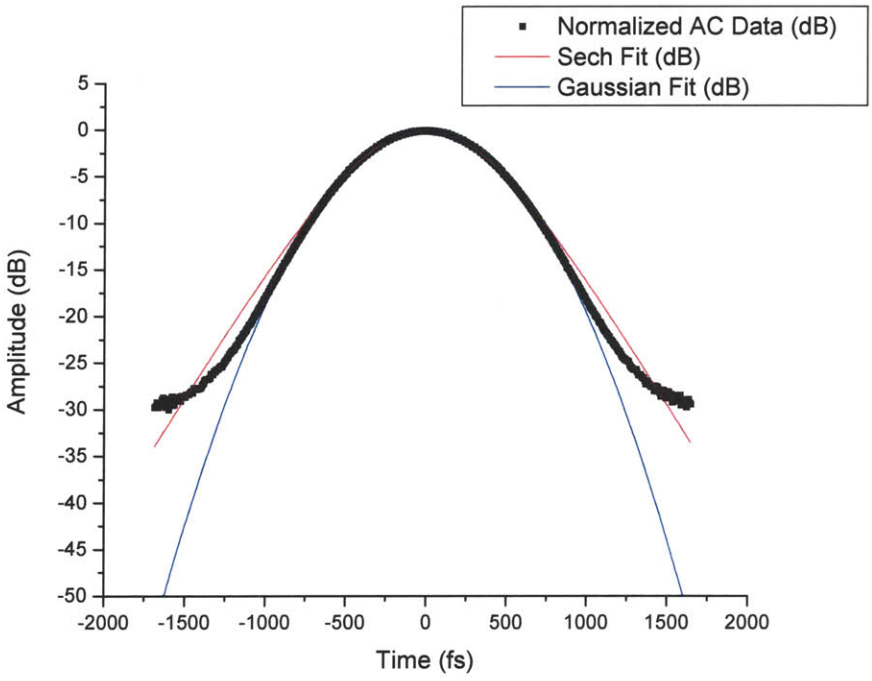

Figure 5-33 Normalized autocorrelation data and sech and Gaussian pulse shape fits plotted in dB for the 270 mW pump 1570 nm state.

5.4.6.3 RF Spectra

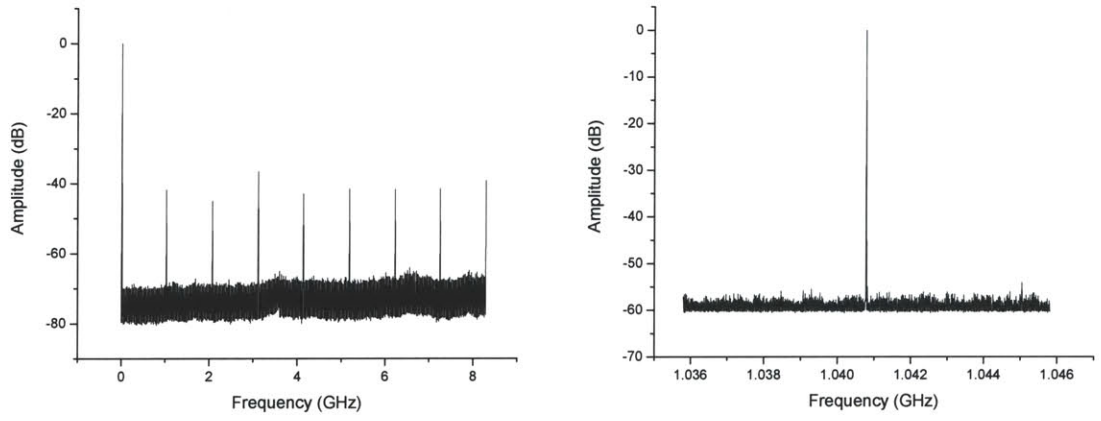

Figure 5-34 Full span RF spectra (left) and Fundamental RF line (right) for 270 mW pump 1570 nm laser state.

Figure 5-34 plots both recorded RF spectra for the 270 mW pump state. The full span plot on the left shows clean lines and a relatively flat envelope. A small variation in the exact length of the fiber package resulted in a different repetition rate for this laser sate. Plotted on the right of Figure 5-34, the fundamental frequency is now detected at 1.0408 GHz across all power levels of the 1570 nm laser.

A different fiber does not change the issues introduced by vector solitons however, Elimination of the polarization sidebands (note their absence on both plots) is still achieved through fiber positioning introducing birefringence, exactly as in the other two laser states. This should help to ensure the laser is in a low noise state for the jitter measurements, however for this laser the vector solitons did not appear to be the primary source of pulse to pulse timing jitter.

5.4.6.4 Timing Jitter

Regarding jitter, the 1570 nm state of this laser had rather high pulse to pulse timing jitter when compared to the other recorded states. Even in the stable single-pulse mode-locking regime the 1600 nm CW spike was the probable cause of the excessive jitter.

Figure 5-35 plots the recorded phase noise and the integrated RMS jitter recorded from each power level of the 1570 nm laser state. Note that for this state Figure 5-35(a) demonstrates the lowest noise at 141 fs of jitter and it gets progressively noisier as the power is increased.

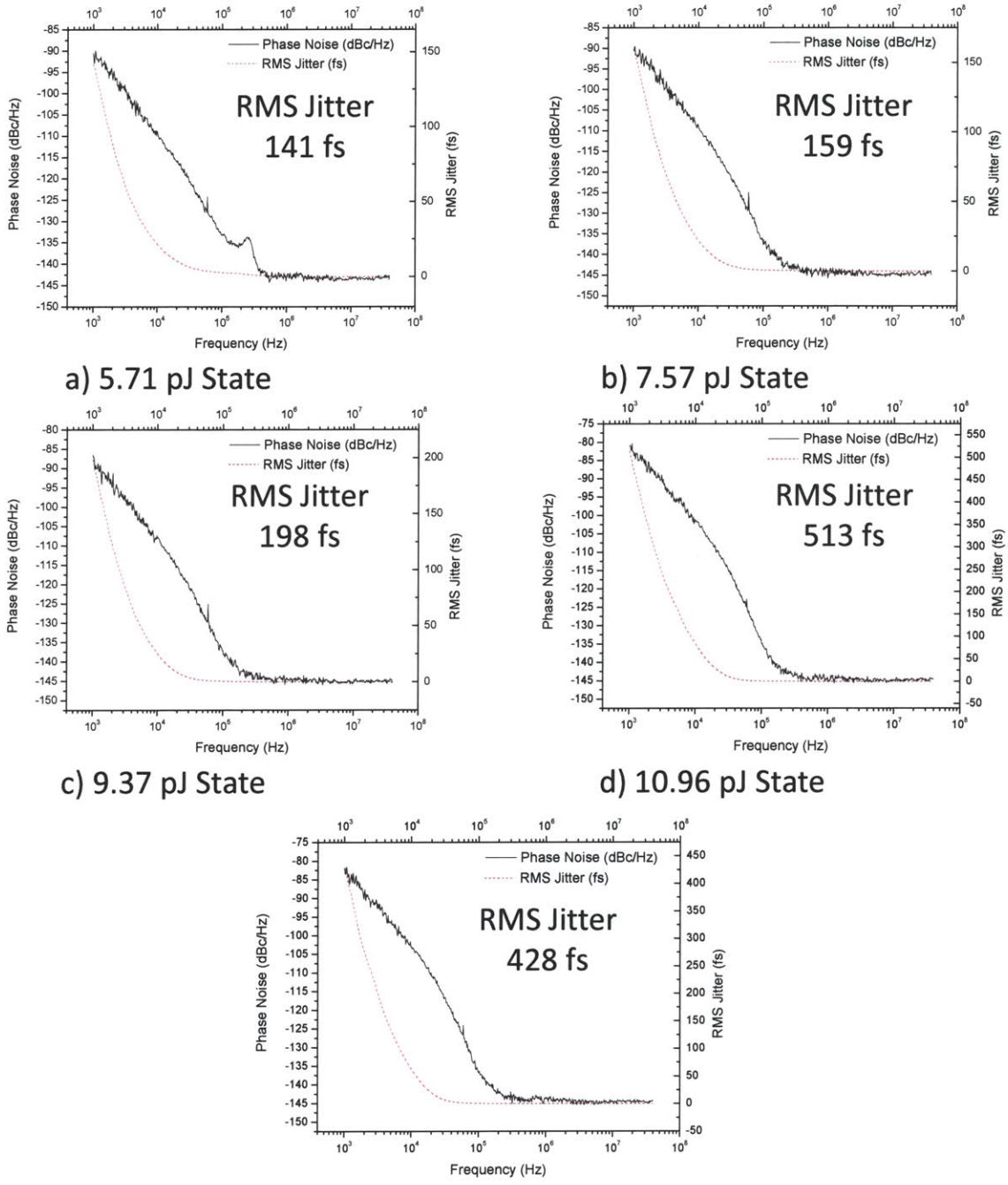

Figure 5-35 Phase noise and integrated RMS timing jitter plots for six recorded power levels of the 1570 nm state.

Figure 5-36(a) plots the reasonably linear increase in output power given increasing pump power. Figure 5-36(b) plots the jitter associated with each of those power levels.

Although the output power was monotonically increasing—giving no indication of changing cavity states—the timing jitter markedly increases for the 314 mW and 358 mW pump power levels.

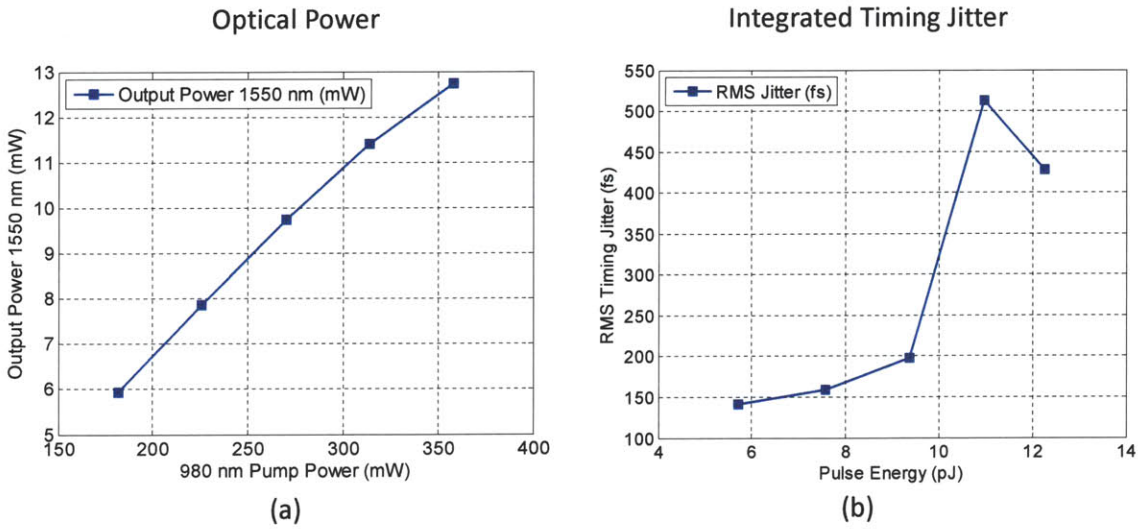

Figure 5-36 (a) Output power for increasing pump powers of the 1570 nm state. (b) Integrated RMS timing jitter for the recorded power levels of the 1570 nm laser state.

5.4.6.5 Pulse Width Analysis

This state did not really agree with soliton mode-locking theory. Plotted below is a summary of the relevant results of the pulse width calculations and measurements.

The 1570 nm state of this short cavity fiber laser should still operate via SBR initiated soliton mode-locking. Figure 5-37 plots the measured, calculated, or predicted pulse widths at a given pulse energy for the assumption that the laser is outputting these sech shaped pulses.

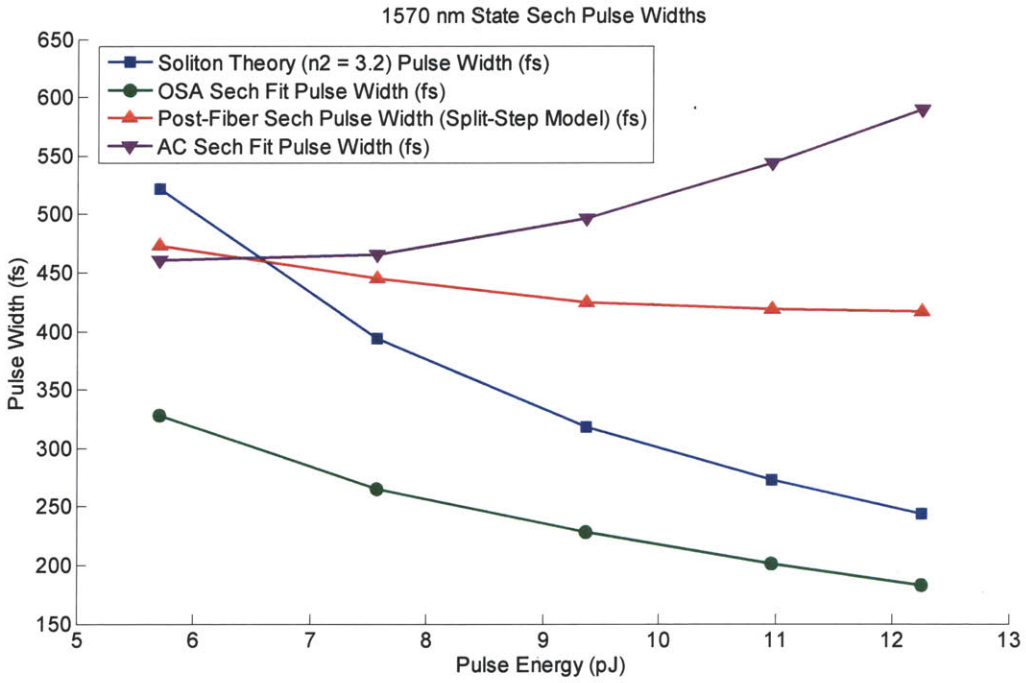

Figure 5-37 Data and simulations of the output time domain pulse width of the 1 GHz laser's 1570 nm state given increasing output pulse energies. This data assumes a hyperbolic secant pulse envelope shape.

The measurements and curve fits for this laser state were different from the previous two. First, as the pump power was increased and the optical bandwidth increased the measured pulse widths also increased. One would expect they should have been decreasing or at least remaining about the same as in the previous state. Also, the soliton area theorem does not appear to be valid for the optical spectral measurement of this state. The only uncertainty in the calculations was the fiber nonlinearly, n_2, and the largest value that can reasonably assumed for a perfect linear polarization state is 3.2 [7]. Thus, assuming that perfectly linear polarization state in the cavity (likely not valid because the fiber was contorted in the usual birefringence inducing position) the soliton theory predicted pulse widths for an n_2 of 3.2 is plotted in blue squares. Using a smaller (more reasonable) value of n_2 would only move the curve up and indicate an even worse fit.

Since the spectral widths, fitted assuming sech pulses and plotted as green circles, yield pulse durations much shorter than the soliton theory widths (plotted as blue squares),

it is assumed some other mechanism must also be affecting this cavity. Despite this, for completeness, the optical spectral widths were still input to the split step simulations to see what output pulse widths might be expected after propagating through the 2.7 m of output fiber. Results of those simulations are plotted as red triangles in Figure 5-37. For these broader bandwidths and moderate power levels, the nonlinearities of the fiber were significant enough to theoretically broaden the pulses by as much as 200 fs. Interestingly, the broadening spectrum and the increasing power influences that should have been decreasing the pulse widths were evenly balanced by the nonlinear response of the fiber to basically keep the simulated pulse widths at the same value through the entire range of input powers. Would the autocorrelation measurements in the lab confirm this prediction?

Plotted in purple down arrows, the sech fitted autocorrelation data recorded continually increasing pulse widths for increasing pump power. We do not have a satisfactory explanation for these results but we can point to the CW modes in the cavity and perhaps greater pulse broadening effects from the fiber or other measurement components in the autocorrelation system as possible causes of this behavior.

5.4.7 Gaussian Pulse Shape

The other common pulse envelope shape that is possible from a mode-locked laser is the Gaussian. A Gaussian pulse, for the same 3dB bandwidth, will be broader near the peak and narrower down in the wings of the pulse than a sech shape. Curve fitting optical spectra or autocorrelation traces will typically yield a broader pulse width for the Gaussian fit than for the sech and thus the sech fits are more commonly reported in the literature. However, despite the optical spectra for every recorded power level of all three laser states curve fitting a sech pulse shape, the autocorrelation data for almost all recorded power levels of all three laser states fitted a Gaussian pulse shape. Therefore, in an attempt to see if perhaps the laser is outputting Gaussian pulses the pulse width analysis was also carried out assuming a Gaussian pulse shape and the results for the 1560 nm state are plotted in Figure 5-38.

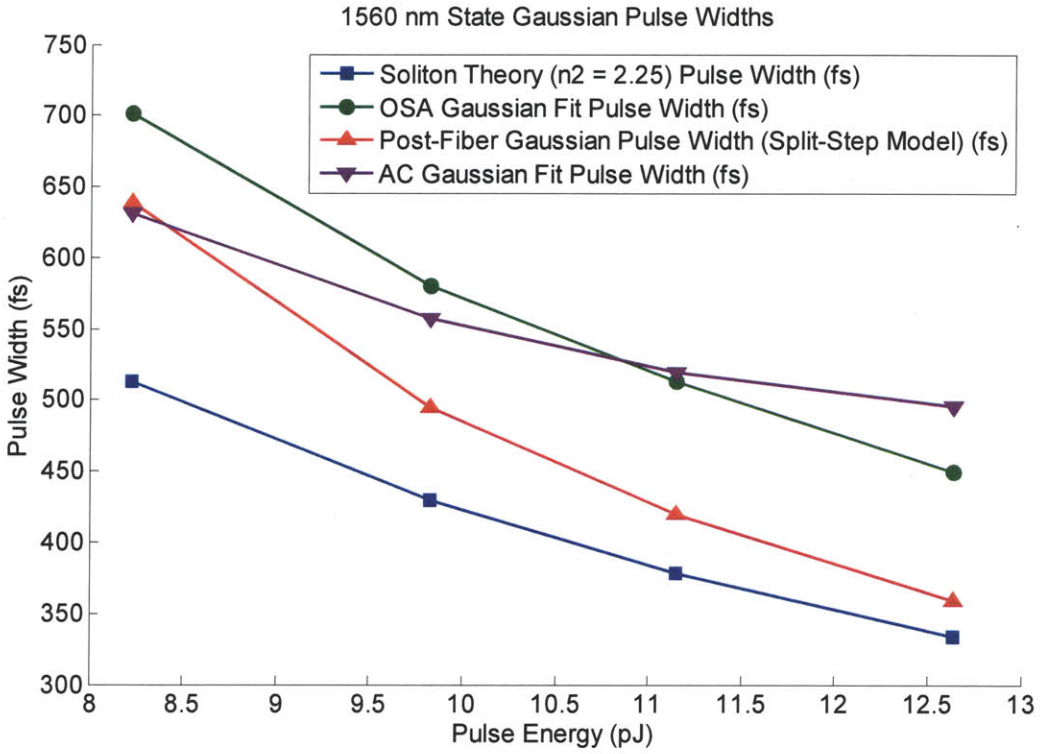

Figure 5-38 Data and simulations of the output time domain pulse width of the 1 GHz laser's 1560 nm state given increasing output pulse energies. This data assumes a Gaussian pulse envelope shape.

For the sake of visual comparison and reference, the same soliton theory line from Figure 5-20 is plotted in blue squares. These data points are really not valid for a Gaussian pulse shape assumption so it is not an issue if the other Gaussian data points do not match. The green circle line plots the ideal transform limited pulse widths calculated from a Gaussian fit of the optical spectrum. Recall from Figure 5-14 for example that the Gaussian fit was not as good as the sech but it was a decent fit for about 10 dB so it is used as the starting number for the simulations while keeping in mind this caveat.

Next, with the OSA Gaussian fitted pulse widths as the seed pulse, and assuming that linear dispersion is not the only process shaping the pulses in the fiber, the OSA pulse widths are input along with their corresponding pulse energies and central wavelengths into the split step simulations. Surprisingly, for these power levels the nonlinear effects of the fiber were significant enough to theoretically shorten the pulses by as much as 10% as

they traveled down the 2.7 meters of fiber. Those results are plotted in red triangles. Interestingly the pulse width predicted by this method nearly matched the measured autocorrelation data pulse width (for a deconvolved Gaussian assumed curve fit) for the lowest pump power state.

This trend did not continue as the autocorrelation measurements (plotted in purple down arrows) trended along a different slope than the spectral and theoretical data generally followed. As the pulse energy increased, the measurements stopped getting shorter like they were expected to. Basically, since the data trend for the 1560 state or any other state (calculated but not included here) does not match the slope trend or any of the spectral or simulation pulse width results the assumption that this laser was outputting Gaussian pulses does not appear valid.

5.4.8 Discussion

The purpose of this laser state study was to determine how well each state agreed with soliton mode-locking theory. We can say that Gaussian and sech curve fit results of the optical spectra confirm to the soliton mode-locking theory postulate of sech shaped soliton pulses. This was consistent across all collected data sets as in every case the sech fit was much more accurate to the data down to the noise floor than the Gaussian.

We can also say that the three laser states all followed the trend of greater intra-cavity powers and higher energy solitons yielding correspondingly broader bandwidths. These broadening bandwidths should have led to a steady decrease in the measured output pulse widths. This was not always the case however.

The data indicate that the pulse to pulse timing jitter correlated with the pulses widths reaching a minimum beyond which they would not shorten. This situation was not so evident in the 1560 nm state data because the pulses were somewhat longer. The timing jitter within this stable mode-locking regime was very low. At the same time as pulses corresponded less to the transform limit, jitter increased. These observations are all consistent with possible filtering and nonlinear phase effects that result in increased shedding tot the continuum.

Also, the fitted pulse shape of the autocorrelation data conformed better to a Gaussian than a sech. Since sech pulses do not just transform to Gaussian shapes while propagating through fiber or being frequency doubled in a nonlinear crystal some other pulse shaping effects have taken effect during the autocorrelation measurement process. Further experiments would need to be designed and implemented to conclusively know the exactly reasons for this pulse shape transformation.

5.5 Conclusions

The 1 GHz repetition rate end-abutted SBR linear cavity erbium doped fiber laser technology developed here at MIT is a positive advance in compact, turnkey, low jitter fiber source development. The first generation version of the laser taught valuable lessons about the critical points of the system to improve. The input/output coupling and the importance of the fiber to SBR interface being the important upgrades necessary to reducing losses and improving the pulse quality.

Once those improvements were implemented in the second generation system, more subtle issues began to become evident. The RF sidebands on the fundamental frequency and its harmonics pointed toward polarization related vector soliton behavior over many round trips in the cavity. Techniques were developed to minimize and eliminate those modes via fiber birefringence control [8]. The SBRs developed issues with burning when the laser was being powered up and a series of solutions were implemented for that issue. Applying a 980 nm pump light reflective coating to the mirror, insulating the mirror from the erbium fiber by splicing a short piece of undoped single mode fiber, thinning the wafer substrate, and mounting the SBR with thermally conductive silver paste all contributed to reducing the thermal load on the mirror and preventing burn damage.

Despite these refinements, the laser still demonstrated some interesting behavior. It would favor not just one center wavelength for mode-locking; several independent stable states could be isolated if the SBR to fiber coupling was manipulated carefully. Hyunil and Michelle had demonstrated the 1570 nm state to have the broadest output spectrum. Dave Chao discovered through his thesis work that the state centered on 1560 nm was by far the

lowest timing jitter. A comprehensive pulse width study was initiated to attempt to characterize and understand these different laser states and their output characteristics.

The purpose of the pulse width laser state study was to determine how well each mode-locking state agreed with soliton mode-locking theory. Overall, several lessons were learned regarding the important connection between jitter and pulse width. Basically, the less transform limited the pulses are the more jitter there is. If the oscillator is very quiet, the spectrum broadens and pulses shortened with increasing energy at the rate expected from the spectral data and the soliton theory. As pulse shortening deviates from theory, jitter increases.

Therefore, to increase the usefulness of this high repetition rate laser source technology the following points are important in locating and maintaining a stable, low jitter state.

- Eliminate CW mode break through
- Eliminate RF spectral sidebands
- Careful control over fiber to SBR state coupling

There were two different types of continuous wave (CW) modes that could manifest themselves on the optical spectrum trace. One would be a mode separated in wavelength from the main pulse that would appear throughout the mode-locking regime. The other is a mode that only appears as pulse energy is increased too far. The only way to avoid the excess energy spike is to not pump the laser beyond the maximum soliton energy the cavity can support. The primary way to avoid the off-wavelength CW spikes was careful cavity polarization management.

Fortunately, polarization management is the same approach required to eliminate the vector soliton behavior. Tuning the cavity polarization through fiber birefringence can synchronize the multi-round trip polarization rotation frequency with the repetition rate and eliminate the beat frequencies that appear in the RF data traces.

Lastly, to optimize the laser state and minimize the timing jitter, careful control over the SBR to fiber coupling is required. For this laser package to be truly useful it would need to be packaged in a robust manner and that means the mechanics securing the fiber to the

mirror would need to be reengineered from what we have built in the lab. The lab device is capable of obtaining the low jitter state but maintaining it is delicate and not possible if the fiber is moved around. The fiber position also requires careful positioning and mechanics in order to hold the lowest jitter mode-locking states. Polarization maintaining fiber throughout could solve this problem.

Overall, this 1 GHz repetition rate fiber laser represents a solid advance in the field of 1550 nm femtosecond pulse laser sources and it has already been put to use as the source laser of experiments ranging from frequency comb generation [5] to on-chip pulse interleaving [9] to optical analog to digital converters [10]. With further engineering refinement it could find further real world applications as a compact, portable, turnkey, GHz femtosecond fiber laser.

Bibliography - Chapter 5

[1] H. Byun, M. Y. Sander, A. Motamedi, H. Shen, G. S. Petrich, L. A. Kolodziejski, E. P. Ippen, and F. X. Kartner, "Compact, stable 1 GHz femtosecond Er-doped fiber lasers," *Appl. Opt.*, vol. 49, no. 29, pp. 5577–5582, 2010.

[2] H. Byun, "Integrated high-repetition-rate femtosecond lasers at 1.55 [mu]m," Massachusetts Institute of Technology, 2010.

[3] H. Byun, D. Pudo, J. Chen, E. P. Ippen, and F. X. Kartner, "High-repetition-rate, 491 MHz, femtosecond fiber laser with low timing jitter," *Opt Lett*, vol. 33, no. 19, pp. 2221–2223, 2008.

[4] H. M. Shen, "Novel broadband light sources and pulse generation techniques at 1.5 [mu]m," Massachusetts Institute of Technology, 2009.

[5] D. Chao, M. Y. Sander, G. Chang, J. L. Morse, J. A. Cox, G. S. Petrich, L. A. Kolodziejski, F. X. Kärtner, and E. P. Ippen, "Self-referenced Erbium fiber laser frequency comb at a GHz repetition rate," in *2012 Optical Fiber Communication Conference and Exposition and the National Fiber Optic Engineers Conference, OFC/NFOEC 2012, March 4, 2012 - March 8, 2012*, 2012.

[6] H. Haus, "Theory of Mode Locking With A Slow Saturable Absorber," *Ieee J. Quantum Electron.*, vol. QE-11, no. 9, pp. 736–746, 1975.

[7] G. P. Agrawal, *Nonlinear fiber optics*, vol. 3rd. San Diego: Academic Press, 2001.

[8] M. Y. Sander, "High repetition rate fiber and integrated waveguide femtosecond lasers," Massachusetts Institute of Technology, 2012.

[9] M. Y. Sander, S. Frolov, J. Shmulovich, E. P. Ippen, and F. X. Kartner, "10 GHz femtosecond pulse interleaver in planar waveguide technology," *Opt. Express*, vol. 20, no. 4, pp. 4102–13, Nov. 2011.

[10] C. W. Holzwarth, R. Amatya, M. Araghchini, J. Birge, H. Byun, J. Chen, M. Dahlem, N. A. DiLello, F. Gan, J. L. Hoyt, E. P. Ippen, F. X. Kartner, A. Khilo, J. Kim, M. Kim, A. Motamedi, J. S. Orcutt, M. Park, M. Perrott, M. A. Popovic, R. J. Ram, H. I. Smith, G. R. Zhou, S. J. Spector, T. M. Lyszczarz, M. W. Geis, D. M. Lennon, J. U. Yoon, M. E. Grein, R. T. Schulein, S. Frolov, A. Hanjani, and J. Shmulovich, "High speed analog-to-digital conversion with silicon photonics," in *Silicon Photonics IV, 26-28 Jan. 2009*, 2009, vol. 7220, p. 72200B (15 pp.).

Chapter 6 Conclusions and Future Work

The work presented in this thesis details steps taken along the evolving path toward increasing the repetition rate of erbium-doped femtosecond fiber lasers while maintaining strong output powers and low timing jitter. A stable, 1 GHz, low jitter, femtosecond pulse linear cavity erbium-doped fiber laser is demonstrated. The improvements were made through a combination of careful design and the use of new components (highly doped erbium gain fibers, powerful single mode pump diodes, custom SBR's). As a review; the following presents the primary lessons taken from each laser design.

- **Chapter 3 – High Repetition Rate, High Average Power, Femtosecond Erbium Fiber Sigma Lasers**

  A modification to the P-APM fiber laser was introduced and scaled to 300 MHz. GHz repetition rates will be difficult to achieve with a P-APM system.

- **Chapter 4 – 1 GHz Linear Cavity Laser – Free Space SBR**

  A 1 GHz repetition rate SBR performance study reveals that soliton pulse shaping effects influence the pulse as much as the SBR effects. Also, the SBR's require protection from heat and Q-switched operation to avoid burn damage and total failure.

- **Chapter 5 – 1 GHz Linear Cavity Laser – End Abutted SBR**

  Three distinct mode-locking states of a 1 GHz repetition rate mode-locked fiber laser with an end abutted SBR were investigated. The cavity was sensitive to the SBR-to-fiber coupling mechanics, and one state shows markedly less jitter than the others.

An understanding of the optimum operating conditions for a high repetition rate, low jitter, femtosecond fiber laser begins to emerge. Overall, a great deal has been learned by these studies, however many questions remain and further investigation into how Q-switching is affecting the SBR burning, what the dispersion balance within the short cavity

is doing to the soliton pulse shaping, and exactly why the autocorrelation pulse shapes fitted a Gaussian shape better than the expected sech shape could provide interesting clues to why these systems performed the way they did.

Future directions the linear cavity erbium doped femtosecond fiber laser technology could be taken primarily include the use of better fibers and further optimized absorbing mirrors. The fibers would need to be polarization maintaining and doped more heavily to enable higher gain in less length. The mirrors will need to be more thermally resilient and the protective coating's contributions to the pulse shaping fully understood. Finally, engineering techniques to fuse the mirror to the fiber in a repeatable fashion to always ensure operation in the low jitter 1560 nm state would open the door to integrating the 1 GHz laser system in a commercial package that could be utilized as a femtosecond source in real-world applications.